university
of south africa

SYNTHESIS AND CHARACTERIZATION OF HYBRID ION EXCHANGE RESINS EMBEDDED WITH HYDROUS FERRIC OXIDE NANOPARTICLES FOR THE REMOVAL OF METAL IONS FROM ACID MINE DRAINAGE

by

ZIZIKAZI SODZIDZI

STUDENT NUMBER: 58564101

Thesis in fulfilment of the requirement for the degree

(MTech)

in

CHEMICAL ENGINEERING

in the

DEPARTMENT OF CIVIL AND CHEMICAL ENGINEERING, COLLEGE OF SCIENCE, ENGINEERING AND TECHNOLOGY

of the

UNIVERSITY OF SOUTH AFRICA

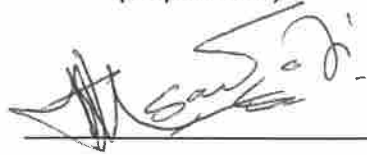|	
Supervisor:	**Dr LA De Kock**
Co-supervisor:	**Prof TAM Msagati**

DECLARATION

I hereby declare that this dissertation, which I herewith submit for the research qualification

MASTER'S OF TECHNOLOGY IN CHEMISTRY

To the University of South Africa is, apart from the recognised assistance of my supervisors, my own work and has not previously been submitted by me to another institution to obtain a research diploma or degree.

_____   on this __16_ day of _October 2020_

(Candidate)

_____   on this _19_ day of __October 2020__

(Supervisor)

_____   on this _19_ day of _OCTOBER 2020_

(Co-supervisor)

DEDICATION

This work is dedicated to my mother Nomfundiso Matakana-Sodzidzi for all the love she gives freely without boundaries. I would have not made it without her sacrifices.

My father Ntobeko Sodzidzi for believing in me even when I fail to, which has given me hope throughout my studies.

To my son Someleziwe Sodzidzi for bringing so much joy into my life.

ACKNOWLEDGEMENTS

I would like to extend my sincere thanks to the following people and organisations for their contributions towards the success of this work:

ABSTRACT

Acid mine drainage (AMD) is a serious water pollutant that contaminates freshwater sources such as rivers, lakes, ground water and even sediments with heavy metals which include Cr(VI), Cd(II) and Pb(II). In this study a novel remediation strategy for the remediation of Cr(VI), Cd(II) and Pb(II) was developed.

Hybrid anionic and cationic exchange resins embedded with hydrous ferric oxide nanoparticles were synthesized and then subjected to batch adsorption tests to determine the factors influencing the adsorption of Cr(VI), Pb(II) and Cd(II). Lastly, the hybrid cationic resin, HCIX-HFO was used to determine the adsorption of metal ions from a real AMD water sample.

The hybrid anion exchanger (HAIX-HFO) was used for the remediation of Cr(VI). The optimum pH for the removal of Cr(VI) was found to be pH 4. The adsorption of Cr(VI) with and without sulphate was a better fit to the pseudo-second order kinetic model, with an equilibration time of 360 minutes. In the absence of co-competing sulphate the experimentally determined adsorption capacity for Cr(VI) was 4.9 mg.g^{-1}. In the presence of 3000 mg/L sulphate the adsorption capacity for Cr(VI) decreased to 2.2 mg.g^{-1} while percentage of Cr (VI) adsorbed was 50.8 % in the presence of sulphate. The isotherm studies for Cr(VI) in the absence of sulphate was found to be a better fit to the Langmuir isotherm model, and with the Temkin isotherm model in the presence of sulphate.

The hybrid cationic ion exchange resin (HCIX-HFO) was used to adsorb both Cd(II) and Pb(II). The pH for the optimum adsorption both the two metallic species (Cd(II) and Pb(II)) was found to be pH 4. Like in the case for Cr (VI), the kinetic studies for Cd(II) and Pb(II) in the presence of sulphate followed the pseudo-second order kinetic model and equilibrium was achieved in 360 minutes. The experimentally determined adsorption capacities for Cd(II) and Pb(II) were 1.45 mg.g^{-1} and 2.27 mg.g^{-1} respectively. The isotherm adsorption data for both Cd(II) and Pb(II) were a good fit to the Freundlich model. In a competitive study with both Cd(II) and Pb(II) the adsorption of Pb(II) was favoured. HCIX-HFO was effectively regenerated by

NaCl with 99.9% of Cd(II) and 98.8% of Pb(II) recovered. On contacting HCIX-HFO with real AMD containing ten different metal ions, high percentage removals were found for Ni(II) (92.6%), Cu(II) (92.5%) and Pb(II) (46.8%). HCIX-HFO has been shown to adsorb cationic metal species in the presence of sulphate and HAIX-HFO has been shown to effectively adsorb Cr(IV) in the presence of sulphate.

TABLE OF CONTENTS

LIST OF FIGURES

LIST OF TABLES

LIST OF ABBREVIATIONS

ABC   Alkali-barium-calcium

AMD   Acid mine drainage

DWA   Department of water Affairs

DWS   Department of Water and Sanitation

EDS   Energy Dispersive Spectroscopy

ESR   Electron Spin Resonance

FT-IR   Fourier Transform Spectroscopy

HAIX-HFO   Hybrid anion exchange resin with hydrated ferric oxide nanoparticles

HCIX_HFO   Hybrid cation exchange resin with hydrated ferric oxide nanoparticles

HDS   High-density sludge

HFO   Hydrous ferric oxide

ICP-OES   Inductively coupled plasma-optical emission spectroscopy

NPs   Nanoparticles

PZC   Point of Zero Charge

SANS 241   South African National Standard: 241

SAVMIN   Savannah and Mintek process

SEM   Scanning electron microscopy

SRBs   Sulphate-reducing bioreactors

XRD   X-Ray diffractometry

XPS   X-Ray photoelectron spectroscopy

CHAPTER 1
INTRODUCTION

In this chapter, an overview of the problem of acid mine drainage, its adverse effects on nature as well as a brief justification of the study is given. The aims, objectives, problem statement of the study and outline of the dissertation are given in this chapter.

Pollution of the environment due to toxic chemicals is increasingly degrading the quality of the environment including the water sources globally. This is a global concern as water is the basic need of life and anything that impacts on water quality tends to endanger life as a whole. Currently a number of freshwater sources are polluted by acid mine drainage (AMD). AMD results when pyrite (FeS_2, iron (II) disulfide) and other iron sulphide minerals are exposed through underground excavations, open pits, leach pads, tailings and waste rock piles (Akcil and Koldas, 2006). The exposed sulphide minerals (especially pyrite (FeS_2)) react with water and oxygen which results in the oxidation of pyrite. This releases ferrous iron (Fe(II)) as well as producing sulphuric acid (Equation 1.1). The resulting high concentrations of sulphate ions and the low pH facilitates further solubilisation of toxic metal species.

$$2FeS_2\ (s) + 7O_2(g) + 2H_2O(l) \rightarrow 2Fe^{2+}(aq) + 4SO_4^{2-}(aq) + 4H^+\ (aq) \qquad (1.1)$$
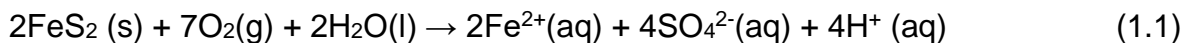
The ferrous iron then oxidises to form ferric iron (Fe(III)) (equation 1.2).

$$4Fe^{2+}(aq) + O_2(g) + 4H^+(aq) \rightarrow 4Fe^{3+}(aq) + 2H_2O(l) \qquad (1.2)$$
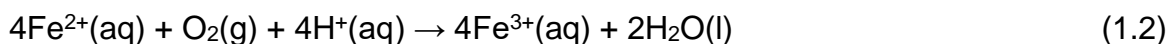
The ferric iron is responsible for the oxidation of additional pyrite (equation 1.3).

$$FeS_2(l) + 14Fe^{3+}(aq) + 8\ H_2O(l) \rightarrow 15Fe^{2+}(aq) + 2SO_4^{2-}(aq) + 16H^+ \qquad (1.3)$$
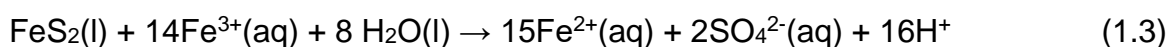
Additional metal sulphide ores are also oxidized resulting in the solubilisation of toxic metals in AMD. The resultant AMD harms aquatic organisms degrades the quality

of surface water and subsequently makes the ground water not only unfit for human consumption but also unfit for the ecosystem as a whole (Falayi and Ntuli, 2014; Gray, 1998).

South Africa is a well-known mineral resource rich country with several mining activities such as gold, platinum, manganese, chromium and vanadium. One of the most active South African mining areas is the Witwatersrand Basin of the Gauteng province, where gold mining commenced in the 1880s (Pooley, 2009; Mudd et al., 2012). However, mining activities in Witwatersrand Basin has decreased over the years leading to the closure of several mines in the area (Winde and Stoch, 2010). Most of closed mines have been left with open shafts that are being filled by rain or other water sources. Dissolution of mineral components into the water in these old mines is one of the causes of AMD. Overtime the water in these shafts overflows into the surrounding areas releasing AMD into the environment. The issue of AMD in the Witwatersrand Basin has reached a crisis point as huge volumes are overflowing to the environment and contaminating ground and surface waters and threatening to reach potable water sources like the Vaal River (DWA, 2013).

This problem needs an urgent solution to remedy and prevent further pollution of the environment, ecosystem and freshwater resources. For sustainability of the remediation strategies it is required that these approaches and technologies be both economical and efficient.

Currently, there are several remediation technologies to address the issue of AMD pollution of water resources, with the most widely used being lime (CaO) neutralization. The addition of lime increases the pH which causes precipitation of the metals as well as the formation of gypsum ($CaSO_4$) which is then removed as a sludge. The most effective lime neutralisation process uses a high density sludge (HDS) process, which produces a sludge that contains a mixture of heavy metals that needs to be disposed of and/ or recycled for alternative uses. Due to the potential toxicity of the sludge and its potential as a future source of pollution it would be beneficial to have treatment stages prior to the production of the HDS to remove

toxic metals and reduce the toxicity of the sludge due to the presence of heavy metals.

In most cases, AMD contains high concentrations of heavy metals including chromium (Cr), cadmium (Cd), and lead (Pb) (Akcil and Koldas, 2006). Certain heavy metals are toxic because they bioaccumulate and change the biological functions of vital organs including the liver, heart, kidney, and brain and other neuro or endocrinal systems in the human body (Duruibe et al., 2007, Hu, 2002, Jaishanker et al., 2014; Martin and Griswold, 2009, Mudgal et al., 2010). Due to the toxicity of these metals, conventional treatment methods are normally employed in their removal prior lime neutralisation to minimize levels of toxic metals in subsequent sludge that is produced.

Ion exchange processes provide a strategic technology that has been proposed for the treatment of AMD especially for the removal of metals because they have the requisite high strength and mechanical properties needed for large scale water purification and can be regenerated for many cycles of purification. Ion exchange resins make use of the Donnan membrane effect, in which the fixed charges within the ion exchange resin attract ions with an appropriate counter charge into the pores of the resin (SenGupta, 2017). However, ion exchange resins have limited selectivity and efficiency for specific ions that limits their adsorption capacity (Vaaramaa and Lehto, 2003). The limitation in selectivity results in the need for frequent regeneration of the ion exchange resins and higher operating costs. In addition, during the regeneration process, all the adsorbed metal ions are eluted as a mixture, thus reducing the potential economic value of the recovered metal ions.

Recent studies report that metal oxides, particularly iron oxides are promising adsorbents for the adsorption of heavy metals from water (Hua et al., 2012, Zou et al., 2016). Nanoparticles like hydrous ferric oxides (HFO) have increased adsorption capacities because of their comparatively large surface areas. The main drawback in using nanoparticles alone is their tendency to self-aggregate (Sarkar et al., 2012). Aggregation reduces the surface area available for adsorption, and that consequently results in the loss of the unique properties provided by the

nanoparticle sizes. Another disadvantage is that nanoparticles do not have the physical characteristics necessary for large scale processing. The nanoparticles tend to pack together too closely resulting in high backpressures and reduced throughput rates (Hu and Apblett, 2014).

To address the limitations of using iron oxide nanoparticles alone, hybrid ion exchange resins with encapsulated hydrous ferric oxide nanoparticles provides unique and combined properties that can address the shortcoming significantly. The ion exchange resins provide support for the iron oxides nanoparticles while the iron oxide nanoparticles provide the high adsorption capacities and selectivity phenomena for the targeted pollutant.

1.1   Problem statement

AMD contains a significant amount of toxic metals. The available and proposed processes to treat AMD in the Witwatersrand Basin tend to produce large quantities of sludge that contains toxic heavy metal oxides (DWA, 2013). Due to the presence of these toxic metal oxides, the sludge is subjected to strict disposal guidelines as the discarded sludge presents a potential future source of environmental pollution. Therefore, the removal (and possibly recovery) of toxic heavy metals, such as Cr, Cd and Pb prior to neutralization and sludge production can reduce the hazardous nature of the sludge.

Hydrous ferric oxide nanoparticles have been reported as having high adsorption capacities for metals in aqueous media (Hua et al., 2012; Zou et al., 2016). Limitations about using hydrous ferric oxide nanoparticles in the remediation strategies for toxic heavy metal ions include aggregation and the fact that they do not have the physical characteristics necessary for large scale processes.

Ion exchange resins have also been reported as being able to adsorb metal ions, but they suffer from reduced adsorption capacities when competing ions are present in high concentrations. This is due to the adsorption process not being selective with many metal ions being adsorbed simultaneously in different ratios.

Thus, encapsulating the hydrous ferric oxide nanoparticles within the ion exchange resin matrix provides a hybrid adsorbent that retains the adsorption characteristics of the ferric oxide nanoparticle and provides a support material that has the necessary characteristics for large scale treatment processes.

The proposed work is aimed at employing ion exchange resins embedded with hydrous ferric oxide nanoparticles to remove toxic heavy metals, mainly Cr(VI), Cd(II) and Pb(II) from AMD water.

1.2   Significance of the study

There are several AMD treatment technologies available for the remediation of Cr(VI), Pb(II) and Cd(II). These include lime neutralisation, HDS process and ion exchange (Simate and Ndlovu, 2014). These treatment technologies are faced with several disadvantages such as extensive land utilization, large quantities of secondary solid waste produced and high capital and operating costs (Name and Sheridan, 2014). Generally, the choice of AMD treatment strategy depends upon many factors including the type and concentrations of dissolved metal ions in the AMD solutions.

In conventional AMD remediation processes, lime and limestone are employed to increase the pH and precipitate metals as oxides as a sludge (Kuyucak, 2002). In the Witwatersrand mining basin, the HDS process has been proposed for neutralizing AMD (DWA, 2013). The main limitation associated with the HDS process is the production of sludge that consists of gypsum together with metal hydroxides. The produced sludge has no direct value; instead, it requires special disposal and treatment technologies which again adds to the treatment costs. In addition, the HDS process is generally expensive to manage. A further drawback is a high future potential of migration of hazardous metal ions from the sludge to the biosphere (Name and Sheridan, 2014). Additionally, the treated water does not typically meet the environmental and potable water specifications and further treatment methods are always required (DWA, 2013).

The adsorption of metals by hydrous ferric oxides (HFO) has been reviewed (Adegoke et al., 2014, Rout et al., 2012). Currently, the use of nanoparticulate HFO is gaining popularity in adsorption studies because of high adsorption capacities due to the high surface area to volume ratio. HFO have been studied for the remediation of Cr(VI), Cd(II) and Pb(II) (Cornell and Schwertmann, 2003; Suh et al., 2015,). Ion exchange resins embedded with HFO for the adsorption of heavy metals from aqueous solution have been reported (Demirbas et al., 2005; Kowalczyk et al., 2013). The hybrid ion exchange resins embedded with hydrous ferric oxide nanoparticles offer exceptional selectivity because the ferric oxide can adsorb a pollutant in the presence of other commonly co-occurring ions (Chanthapon et al., 2018, Pan et al., 2010). This dissertation reports on using hybrid ion exchange resins embedded with hydrous ferric oxide nanoparticles for the removal of Cr (VI), Cd (II) and Pb (II) in the presence of high sulphate concentration matrices and low pH conditions. This was done in order to imitate or mimic the conditions of AMD and to test the applicability of the ion exchange resins embedded with hydrous ferric oxide nanoparticles for the adsorption of metals in real AMD samples.

The ion exchange resins provide durability and extensive surfaces within their pores and hold the dispersed hydrous ferric oxides nanoparticles preventing agglomeration (Blaney et al., 2007). Ion exchange resins also provide favourable conditions for adsorption as a result of the Donnan membrane effect which increases the concentration of suitably charged ions within the resin bead resulting in greater adsorption capacities.

1.3   The aims and objectives of the study

This project aims are to evaluate the adsorption of Cr (IV), Cd (II) and Pb (II) ions from synthetic solution and acid mine drainage using hybrid anionic and cationic exchange resins embedded with hydrous ferric oxides nanoparticles.

The objectives of the study are detailed below:

(i)   To synthesise and characterize hybrid anion and cation exchange resins embedded with hydrous ferric oxide nanoparticles.

6

(ii)   To determine the effect of pH and sulphate concentration on the adsorption efficiency of the hybrid anionic and cationic resins embedded with hydrous ferric oxide nanoparticles for Cr(VI), Cd(II) and Pb(II) from AMD.

1.4   Dissertation outline

Chapter 1: This introductory chapter gives an overview of the project, the background of acid mine drainage, the focus of the study, research approach and objectives of the study.

Chapter 2: This chapter presents a concise review of the literature relating to acid mine drainage remediation technologies with a particular focus on the use of metal oxides and hybrid ion exchange resins for the adsorption of heavy metals from AMD.

Chapter 3: This chapter presents the experimental methods and procedures followed in the synthesis and batch adsorption studies.

Chapter 4: This chapter presents the results and discussions relating to the adsorption removal of Cr(VI), Cd(II) and Pb(II) from AMD onto the hybrid anionic and cationic exchange resins embedded with hydrous ferric oxide nanoparticles, as a function of pH, contact time, initial concentration, and sulphate as the competing ions.

Chapter 5: This chapter presents the conclusions made from the study of the adsorption of Cr(VI) , Pb(II) and Cd(II). It also includes recommendations for further work.

1.5   References

Adegoke, H.I., AmooAdekola, F., Fatoki, O.S. and Ximba, B.J., 2014. Adsorption of Cr (VI) on synthetic hematite (α-Fe 2 O 3) nanoparticles of different morphologies. Korean Journal of Chemical Engineering, 31(1), pp.142-154.

Akcil, A. and Koldas, S., 2006. Acid Mine Drainage (AMD): causes, treatment and case studies. Journal of cleaner production, 14(12-13), pp.1139-1145.

Blaney, L.M., Cinar, S. and SenGupta, A.K., 2007. Hybrid anion exchanger for trace phosphate removal from water and wastewater. Water research, 41(7), pp.1603-1613.

Chanthapon, N., Sarkar, S., Kidkhunthod, P. and Padungthon, S., 2018. Lead removal by a reusable gel cation exchange resin containing nano-scale zero valent iron. Chemical Engineering Journal, 331, pp.545-555.

Cornell, R.M. and Schwertmann, U., 2003. The iron oxides: structure, properties, reactions, occurrences and uses. John Wiley & Sons.

Demirbas, A., Pehlivan, E., Gode, F., Altun, T. and Arslan, G., 2005. Adsorption of Cu (II), Zn (II), Ni (II), Pb (II), and Cd (II) from aqueous solution on Amberlite IR-120 synthetic resin. Journal of Colloid and Interface Science, 282(1), pp.20-25.

Department of Water Affairs (DWA), 2013: Feasibility Study for a Long-term Solution to address the Acid Mine Drainage associated with the East, Central and West Rand underground mining basins. Study Report No. 5.4: Treatment Technology Options –DWA Report No.: P RSA 000/00/16512/4

Duruibe, J.O., Ogwuegbu, M.O.C. and Egwurugwu, J.N., 2007. Heavy metal pollution and human biotoxic effects. International Journal of physical sciences, 2(5), pp.112-118.

Falayi, T. and Ntuli, F., 2014. Removal of heavy metals and neutralisation of acid mine drainage with un-activated attapulgite. Journal of industrial and Engineering Chemistry, 20(4), pp.1285-1292.

Gray, N.F., 1998. Acid mine drainage composition and the implications for its impact on lotic systems. Water Research, 32(7), pp. 2122-2134.

Hu, A. and Apblett, A. eds., 2014. Nanotechnology for water treatment and purification. Switzerland: Springer International Publishing.

Hu, H., 2002. Human health and heavy metals. Life Support: The Environment and Human Health; MIT Press: Cambridge, MA, USA, p.65.

Hua, M., Zhang, S., Pan, B., Zhang, W., Lv, L., Zhang, Q., 2012. Heavy metal removal from water/wastewater by nanosized metal oxides: A review. *Journal of Hazardous Materials*, *211-212, pp. 317-331*

Jaishankar, M., Tseten, T., Anbalagan, N., Mathew, B.B. and Beeregowda, K.N., 2014. Toxicity, mechanism and health effects of some heavy metals. Interdisciplinary toxicology, 7(2), pp.60-72.

Kowalczyk M., Hubicki Z., Kołodyńska D., 2013. Modern hybrid sorbents – New ways of heavy metal removal from waters. Chemical Engineering and Processing: Process Intensification. 70, pp. 55-56.

Kuyucak, N., 2002. Acid mine drainage prevention and control options. CIM bulletin, 95, pp.96-102.

Martin, S. and Griswold, W., 2009. Human health effects of heavy metals. Environmental Science and Technology briefs for citizens, 15, pp.1-6.

Mudd, G., Giurco, D., Mohr, S., Mason, L., 2012 . Gold resources and production: Australia in a global context. Prepared for CSIRO Minerals Down Under Flagship, by the Department of Civil Engineering (Monash University) and the Institute for

Sustainable Futures (University of Technology, Sydney), October 2012. ISBN978-1-922173-47-8.

Mudgal, V., Madaan, N., Mudgal, A., Singh, R.B. and Mishra, S., 2010. Effect of toxic metals on human health. The Open Nutraceuticals Journal, 3(1), pp.94-99.

Name, T. and Sheridan, C., 2014. Remediation of acid mine drainage using metallurgical slags. Minerals Engineering, 64, pp.15-22.

Pan, B., Qiu, H., Pan, B., Nie, G., Xiao, L., Lv, L., Zhang, W., Zhang, Q. and Zheng, S., 2010. Highly efficient removal of heavy metals by polymer-supported nanosized hydrated Fe (III) oxides: behaviour and XPS study. Water Research, 44(3), pp.815-824.

Pooley, S., 2009. Jan van Riebeeck as pioneering explorer and conservator of natural resources at the Cape of Good Hope (1652-62). Environment and History, 15(1), pp.3-33.

Rout, K., Mohapatra, M. and Anand, S., 2012. 2-Line ferrihydrite: synthesis, characterization and its adsorption behaviour for removal of Pb (II), Cd (II), Cu (II) and Zn (II) from aqueous solutions. Dalton transactions, 41(11), pp.3302-3312.

Sarkar, S., Guibal, E., Quignard, F. and SenGupta, A.K., 2012. Polymer-supported metals and metal oxide nanoparticles: synthesis, characterization, and applications. Journal of Nanoparticle Research, 14(2), p.715.

SenGupta, A.K., 2017. Ion Exchange in Environmental Processes: Fundamentals, Applications and Sustainable Technology. John Wiley & Sons.

Simate, G.S. and Ndlovu, S., 2014. Acid mine drainage: Challenges and opportunities. Journal of Environmental Chemical Engineering, 2(3), pp.1785-1803.

Suh, Y.J., Chae, J.W., Jang, H.D. and Cho, K., 2015. Role of chemical hardness in the adsorption of hexavalent chromium species onto metal oxide nanoparticles. Chemical Engineering Journal, 273, pp.401-405.

Vaaramaa, K. and Lehto, J., 2003. Removal of metals and anions from drinking water by ion exchange. Desalination, 155(2), pp.157-170

Winde, F. and Stoch, E.J., 2010. Threats and opportunities for post-closure development in dolomitic gold mining areas of the West Rand and Far West Rand (South Africa)–a hydraulic view Part 1: Mining legacy and future threats. Water SA, 36(1).

Zou, Y., Wang X., Khan A., Wang P., Liu Y., Alsaedi A., Hayat T., Wang X., 2016. Environmental Remediation and Application of Nanoscale Zero-valent Iron and its composites for the removal of Heavy Metal Ions: A Review. Environmental Science and Technology, 50(14), pp. 7290-7304.

CHAPTER 2
LITERATURE REVIEW

This chapter presents a survey of the literature related to AMD treatment and heavy metal remediation technologies. Advantages and disadvantages of these approaches are discussed critically. Moreover, the knowledge gaps in the treatment technologies for AMD are highlighted in this chapter. A review of the work done using hybrid ion exchange resins with encapsulated nanoparticulate ferric oxide for the adsorption of metals from water is given.

The toxicity of heavy metals in AMD poses a threat to the environment (Gray, 1998). The largest volume of waste produced in the world is from AMD (Lecornu, 1996). There are several treatment processes for AMD such as lime neutralization, high-density sludge (HDS), Sulphate-reducing bioreactors (SRBs), Alkali-barium-calcium (ABC) and the SAVMIN (Savannah and Mintek process) (Aubé *et al.*, 2013). However, these treatment processes have shortcomings due to the production of large volumes of sludge that contains toxic metals. In most cases, there is a need to involve a variety of treatment technologies in series or in parallel to treat the sludge produced and to recover precious metals and chemicals.

Several technologies have been reported for the remediation of heavy metals, including Cr(VI), Cd(II) and Pb(II). These include membrane technology, bioremediation, phytoremediation and adsorption by ion exchange resins and metal oxides nanoparticles.

Each of these methods have their own strengths and limitations. Limitations include poor efficiency of metal removal, large quantities of reagent required, high energy requirements and the generation of large quantities of potentially toxic wastes which are difficult to dispose of.

The removal of Cr(VI), Cd(II) and Pb(II) by adsorption with hybrid ion exchange resins embedded with hydrous ferric oxide (HFO) nanoparticles has been reported. (Chanthapona et al., 2018; Hua et al., 2017). The hybrid adsorbents are attractive as they provide selective adsorption, regeneration and capacity for large scale treatment (Padungthon et al 2015).

2.1 AMD in the Witwatersrand Basin

South Africa's mining started in the 1880s. The Witwatersrand Basin, which consists of the Eastern, Central and Western Basins, has been the largest gold mining producer in South Africa. After the 1990s, there has been a decline in the scale of mining in the Witwatersrand Basin and that has led to closure of several operating mines. When the mines were operational, they pumped water to the surface to dewater the mines. After the closure of the mines, the underground mine shafts filled water which then reacts with metal sulphide minerals such as pyrite. This reaction results in decreased pH and high acidic environments which promotes the dissolution of metal ions (Akcil and Koldas, 2006).

Currently, AMD in the Witwatersrand region has reached a critical point and is threatening to reach the Vaal River which is the main source of raw water for potable water production for the surrounding areas (Coetzee et al., 2010). AMD is characterised by low pH, high concentration of metals and a high sulphate concentration.

The Department of Water and Sanitation (DWS), or as it used to be formerly known, Department of Water Affairs (DWA), has reported the average concentrations of heavy metals for the Witwatersrand Basin (DWA, 2013). Table 2.1 gives the average pH, sulphate, Cr, Pb and Cd concentrations in the Central Basin as well as the SANS 241 limits for these heavy metals and sulphate concentrations for drinking water.

13

Table 2.1: Characteristics of AMD in the Witwatersrand Basin and associated SANS 241 limits.

Determinant	Central Basin (95th Percentile)	Permissible Concentration (SANS, 2015)	
	(DWA, 2013)	Risk	Standard Limits
pH	2.4	Operational	≥ 5 to ≤ 9.7
SO_4	3062 mg/L	Acute Health	≤ 500 mg/L
		Aesthetic	≤ 250 mg/L
Cr	148 µg/L	Chronic Health	≤ 50 µg/L
Cd	15 µg/L	Chronic Health	≤ 3 µg/L
Pb	276 µg/L	Chronic Health	≤ 10 µg/L

2.2   Health impact of selected heavy metals

The toxic effect of a metal depends on many factors. These include the oxidation state and its concentration. This section will focus on the impact of Cd, Pb and Cr. These heavy metals are toxic because they bioaccumulate and change the biological functions of vital organs (Jaishanker et al., 2014; Mudgal et al., 2010). Bioaccumulation causes irreversible damage to vital organs including the heart, brain, liver and kidneys (Duruibe et al., 2007; Martin and Griswold, 2009).

Cadmium is a highly toxic metal that is carcinogenic and teratogenic to humans when ingested or inhaled (Jaishankar *et al.*, 2014). Cadmium can also cause

reproduction problems and renal dysfunction. It typically occurs in the +2 oxidation state (Cd(II)).

Lead, which is also predominately found in the +2 oxidation state (Pb(II)), is known to cause brain damage, anaemia as well as liver and kidney damage. Pb poisoning also causes cardio intoxication, leading to diseases such as high blood pressure (Flora et al., 2012).

Chromium is found primarily in two oxidation states, namely the trivalent state as Cr(III), which is cationic and the hexavalent state as Cr(VI). Cr(VI) exists as chromate (CrO_4^{2-}) and dichromate ($Cr_2O_7^{2-}$). Cr(III) is the essential oxidation state of Cr that is used for the metabolism of insulin in humans. However, Cr(VI) as either the chromate or dichromate is carcinogenic and also causes gastrointestinal disorders and skin allergies (Zhitkovich, 2011).

2.3   AMD remediation technologies

The technologies and approaches for the remediation of AMD have been reviewed (Chowdhury *et al.*, 2015; Kefeni *et al.*, 2017; Naidu *et.al.*, 2019; Rodríguez-Galán *et al.,* 2019). These technologies focus on the simultaneous increase of pH and removal of metal ions. These methods include membrane technology (Ambiado et al., 2016), bioremediation (Bwapwa et al., 2017), phytoremediation (Sarma, 2011), and adsorption using ion exchange resins (Feng et al., 2000) and metal oxides nanoparticles as well as other adsorbent materials (Rios et al., 2008). Each of these methods have their own strengths and limitations. Limitations include poor efficiency, large reagent requirements, energy intensive and the production of toxic waste with specific disposal requirements.

The major treatment processes for AMD generated in the Witwatersrand Basin in South Africa are given in Table 2.2.

Table 2.2: Conventional AMD treatment process.

Treatment	Disadvantages	Advantages	References
HDS	• Produces large volume of sludge	• Nontoxic chemicals. • Operational for years.	• Aubé et al., 2003
Sulphate-reducing bioreactors (SRBs)	• Requirement of carbon source. • Large primary sludge. • Time consuming	• Produces water that complies with wastewater standards.	• Masindi et al., 2017
Alkali-barium-calcium (ABC)	• Produces low levels of sulphate economically. • Works for large capacity.	• High environmental risks	• Mulopo and Motaung, 2014
SAVMIN	• High quantity of lime leading to large amount of sludge. • Requires narrow pH band.	• Produces water that complies with wastewater standards	• Smit and Pretorius, 2000

From Table 2.2 it can be observed that the are several disadvantages associated with the existing treatment technologies that are being applied in South Africa.

2.4   Remediation of metals from Acid Mine Drainage

Different conventional techniques have been employed for the remediation of metals. The conventional methods with their advantages, and disadvantages are discussed below.

2.4.1   Chemical precipitation

Chemical precipitation is a widely used method for the removal of heavy metals. In chemical precipitation a precipitating agent (lime or iron salts) is added to the water to convert the dissolved metal ions into an insoluble solid phase. It is a favourable treatment option for treating large volumes of water with low concentrations of heavy metals. The metals are normally precipitated as metal hydroxides. (Aube et al., 2003).

The precipitation of 150 mg/L Cd(II) in the presence of Zn(II) showed an incomplete removal for both metals at pH 11 (Aube *et al.*, 2003). In these instances, the effluent produced will not meet the effluent limits for discharge and additional treatment would be required. Also, the precipitation of the metal hydroxides step takes longer leading to aggregation of the metal hydroxides (Aziz et al., 2008).

Additional shortcomings of chemical precipitation are: 1) The need for large amounts of chemicals; 2) the generation of large amounts of sludge with toxic metal hydroxides. It is also expensive to treat the sludge generated through this approach. For chemical precipitation to be useful, a combination of other techniques is required.

2.4.2   Membrane separation processes

Membrane separation processes encompass a wide variety of processes, each with their own advantages and disadvantages. Recent review by Abdullah *et al.* (2019) describes the membrane processes to have relevant applications and performance characteristics.

Reverse osmosis membranes are the most frequently used membranes for AMD remediation as they are capable of very good heavy metal rejection rates. However, they have low water permeability and require high operating pressures which result in high operating costs. Recent work has focussed on integrated membrane systems (Amaral *et al.*, 2018), membrane distillation (Foureaux *et al.,*2010; Reis *et al.,* 2018) and electrodialysis using ion exchange membranes (Buzzi *et al.,* 2013). Amaral et al. (2018) report on the pilot scale operation of an integrated Ultra-filtration-Nano-filtration-Reverse Osmosis membrane system for the recovery of acid and water as well as the concentration of metals. From the perspective of metal recovery, the drawback of this process is that the concentrated metals are still present as a mixture. Foureaux *et al.* (2020) reviewed direct contact membrane distillation for metal removal from acidic wastewater.

Direct contact membrane distillation is the oldest and most widely used membrane distillation configuration. In this process a vapor pressure difference between the two surfaces of a hydrophobic membrane facilitates the transport of volatile molecules through the pores of the membrane. In theory, membrane distillation is capable of 100% rejection of non-volatile and inorganic components. There are numerous advantages, these include being able to operate at lower temperatures than conventional distillation processes, lower operating pressures compared to conventional membrane processes, and a decreased potential for fouling as a result of the minimal interaction between the solution and the membrane surface. These advantages are further elaborated by Reis (2018) when compared to nanofiltration membrane processes.

Electrodialysis is an electrochemical separation method that makes use of ion-exchange membranes to separate cationic and anionic species under the influence of a potential difference applied to a cathode and an anode. Buzzi (2013) reported the separation of water and metals from coal acid mine drainage. While a contaminate removal of 97% was achieved, the authors reported scaling on the surface of the cation exchange membrane as a result of iron precipitation.

2.4.3   Adsorption Technologies

Various pollutants are removed from the aqueous environment by a wide variety of natural and engineered adsorbents. Natural adsorbents for heavy metals include clay minerals (Uddin, 2017), waste agricultural products (Demirbas, 2005) and a wide variety of other low-cost materials (Joseph *et al.,* 2019). While the prevalence and low cost of these adsorbents is an advantage, especially in the developing world, the major drawbacks of these materials are the low selectivity and capacity as well as variability in performance due to variability in the materials themselves. Because of the disadvantages, the use of engineered adsorbents with higher selectivity, capacity and minimal variability has become more prevalent. These engineered adsorbents include ion-exchange resins and nanomaterials.

2.4.3.1 Ion exchange resins

Ion exchange resins consist of macroporous or gel (microporous) type polymeric matrices with fixed ion-exchange sites. The ion-exchange sites are either cationic or anionic. The removal of charged pollutants in water occurs through the exchange of the pollutant with the counter ion on the fixed ion-exchange site within the resin. Ion exchange resins are classified as either strong or weak exchangers depending on the nature of the functional groups. Strong acid cation exchangers typically have fixed sulfonate ($-SO_3^-$) groups, while weak acid cation exchangers typically have carboxylic ($-COO^-$) groups. Strong base anion exchangers most commonly have quaternary ammonium ($-^+N(CH_3)_3$) groups and weak base anion exchanger commonly have tertiary ammonium, ($-^+N(CH_3)_2$) groups. There are also special types of polymeric ion exchange resins that contain fixed chelating functional groups.

The selective removal of heavy metals, including Cr(VI), Cd(II) and Pb(II) by ion-exchange has been included in a review of general removal technologies (Dąbrowski et al., 2004).

2.4.3.1.1 Anion exchange resins for Cr(VI) removal

Cr(VI) exits as an oxy anion. The predominate Cr(VI) species is dependent on the pH (Figure 2.1). Below pH 5, protonation of chromate (CrO_4^{2-}) occurs, with only hydrogen chromate ($HCrO_4^-$) and dichromate ($Cr_2O_7^{2-}$) existing in equilibrium (Szabó *et al.*, 2018). As all of the chromate species are negatively charged, adsorption by anionic exchange resins is possible.
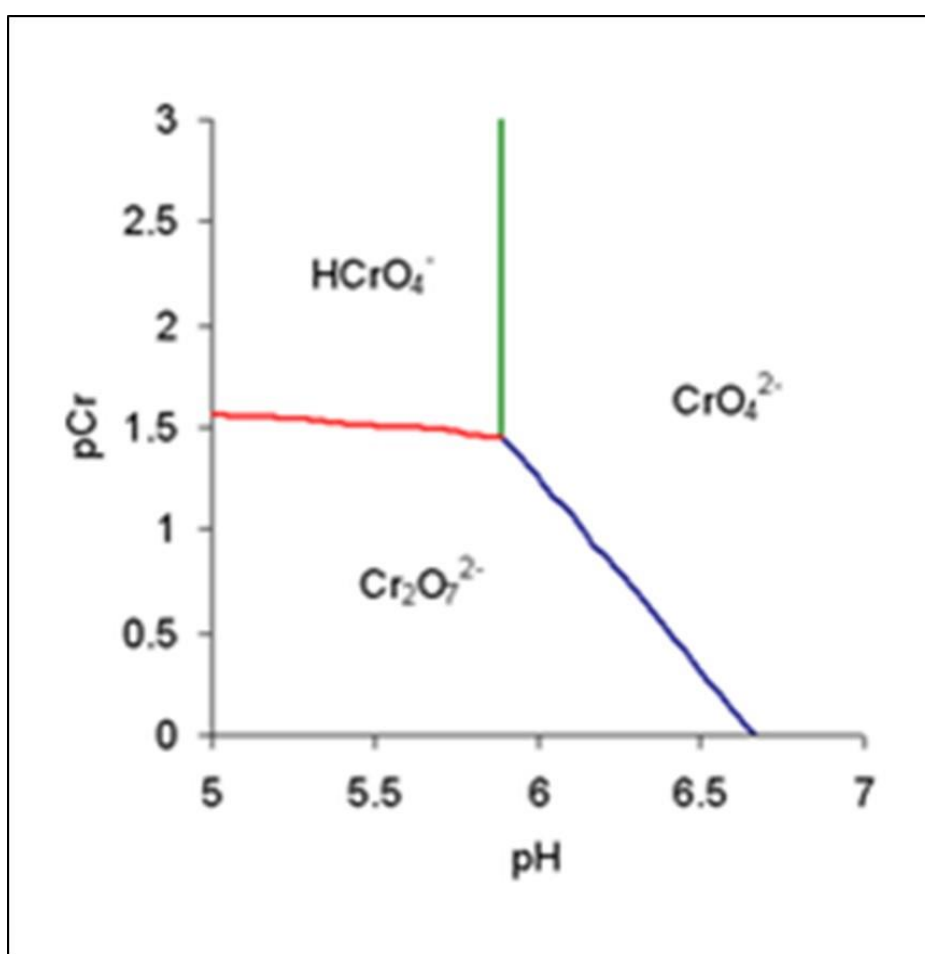
Figure 2.1: Cr(VI) speciation with pH (Tandon *et al.*, 1984).

Cr(VI) adsorption by anion exchange resins showed higher exchange capacities at acidic pH's (Sengupta and Clifford, 1986a) than at alkaline pH (Sengupta *et al.*, 1986). The adsorption of Cr(VI) when present together with high concentrations of competing sulphate and chloride (2000 mg/L) ions was studied using a variety of

polystyrene and polyacrylic anion exchange resin (Sengupta and Clifford, 1986b). A significant difference in the performance of the two resin matrix types was observed, with the polystyrene resins having a significantly higher selectivity for Cr(VI) than the polyacrylic resins. This difference was attributed to the greater hydrophobicity of the polystyrene backbone as the ion-exchange capacities and pk values were very similar.

Jachula and Hubicki (2013) also compared the effect of resin matrix as well as porosity and nature of competing ions on Cr(VI) adsorption by 4 different strong base anion exchange resins. In the absence of competing ions, the adsorption capacity for Cr(VI) did not differ significantly between the polyacrylic and polystyrene resins tested. Cr(VI) adsorption capacities were determined in the pH range 2 -7. Maximum adsorption occurred between pH 3 to 6, with very little variation in this range. Porosity (gel vs macroporous) also did not make a difference to the adsorption capacities reported. A difference was observed when NaCl, NaNO$_3$ and Na$_2$SO$_4$ were used as competitor ions. The largest decrease in capacity was observed for the polyacrylate anion exchange resins. The impact of the competing anions followed the trend Cl$^-$ > SO$_4^{2-}$ > NO$_3^-$ in decreasing the capacity of all resins. All of the resins studied followed pseudo-second order kinetics and the isotherm adsorption data was best described by the Langmuir isotherm.

Cr(VI) adsorption by strong and weakly basic anion exchange resins have been reported (Pehlivan and Cetin, 2009). The ion exchange resins tested were both macroporous with a polystyrene backbone, the only difference being the fixed functional groups (quaternary and tertiary amine groups). For both resins maximum adsorption was observed in the pH range 3 to 5. Above pH 5, the adsorption capacity decreased for both resins, but more rapidly for the weak base anion exchange resin. For both resins, equilibrium was achieved within 60 minutes and adsorption of Cr(VI) was a good fit to the Freundlich isotherm.

The impact of the resin matrix on Cr(VI) adsorption was also reported by Shi (2009). The effect of pH contact time and adsorbent dosage on the adsorption of Cr(VI) by three macroporous, weakly basic anion exchange resins was assessed. Two of the

resins had a polystyrene matrix and the third a polyacrylate matrix. All three resins had an equivalent equilibration time, and the adsorption isotherm data was a good fit to the Langmuir model. For the two polystyrene based exchange resins, the highest adsorption capacity occurred at a pH of 5, while for the polyacrylate based resin, highest adsorption capacity was found at pH 3. Above pH 5 adsorption capacity decreased rapidly for all three resins. The polystyrene resins had an adsorption capacity of 152.52 mg/L and 156.25 mg/L when contacted with a 100 mg/L Cr(VI) solution. The adsorption capacity of the polyacrylate resin was lower (120.48 mg/L) under the same conditions.

Edebali and Pehlivan (2010) compared the Cr(VI) adsorption of a macroporous, weak base anion exchanger to that of a gel type (microporous), strong base anion exchanger. Both anion exchangers followed pseudo-second order kinetics. The Langmuir isotherm model was best able to describe the adsorption of Cr(VI). The macroporous, weak base exchanger had the highest adsorption capacity at a pH of 3, while for the gel type strong base maximum adsorption was observed at pH 4. At pHs higher than 3 and 4 respectively, the adsorption capacity decreased significantly. The maximum Cr(VI) adsorption capacities determined from the Langmuir equation for the macroporous, weak base resin and the gel type strong base resin were 0.46 mmol/g and 0.54 mmol/g respectively.

Two recent studies (Wójcik and Hubicki., 2016; Xiao *et al.,* 2016) have demonstrated that Cr(VI) is reduced to Cr(III) during adsorption by macroporous, acrylic weak base and gel type, polystyrene strong base exchange resins. In both studies, it was reported that reduction of Cr(VI) to Cr(III) occurred at acidic pH and that the extent of reduction as monitored by Cr(III) concentration in the contacting solution decreased as the pH increased. Spectroscopic analysis (FT-IR and XPS) of pristine and exhausted ion exchange resins showed changes to the bands associated with the fixed ammonium functional groups of the resins. It was concluded that the functional groups of the anion exchange resin had been oxidized. This was supported by decreased adsorption capacities after cyclic adsorption-regeneration cycles. Xiao (2016) also reported that the extent of Cr(VI) reduction

and oxidation of the ion-exchange resin was dependent on pH, contact time and initial concentration of Cr(VI).

2.4.3.1.2 Cation exchange resins for Cd(II) and Pb(II) removal

The sorption of Cd(II) by non-commercial polymeric cation exchange resins was included in a comprehensive review (Purkayastha *et al.,* 2014). The sorption of Pb(II) and Cd(II) by a gel type strong acid cation exchange resin was reported by Demirbas *et al* (2005). Adsorption for both Cd(II) and Pb(II) was pH dependent and increased as pH increased from 2 to 9. The equilibrium time was found to be 90 minutes for Pb(II) and 75 minutes for Cd(II). The adsorption of both metals was best described by the Langmuir isotherm model. The adsorption capacity for Cd(II) (201.1 mmol/g) was significantly higher than that of Pb(II) (19.6 mmol/g). Wang (2009) studied the adsorption behaviour of Cd(II) on a strong acid cation exchange resin with a sulfonated functional group. Adsorption was dependent on pH, with maximum adsorption occurring at pH 4-5 with an adsorption capacity of 355 mg/g. The adsorption process was well described by the Freundlich isotherm model. Temperature studies showed that the adsorption process was exothermic as adsorption decreased with increasing temperature.

Pehlivan and Altun (2006) reported the adsorption of Cd(II) and Pb(II) with co-competing Cu(II), Zn(II), Ni(II) by a gel type strong acid cation exchange resin. The adsorption process was pH dependent, with maximum adsorption for all metals occurring at pH 8 to 9. The adsorption process followed the Langmuir isotherm model. Selectivity was observed to follow the series: Pb >Cd >Cu > Zn > Ni. Similarly, Bedoui (2008) reported the adsorption of Cd(II). The equilibration time was 120 minutes and the adsorption was best described by the Langmuir isotherm model.

Rao (2010) reported the adsorption of Cd(II) by a cation exchange resin with amino phosphonic functional groups. The adsorption process was described by the pseudo-second order kinetic model and the Langmuir isotherm model. The effect of ionic strength of the contacting solution was investigated by the addition of

increasing amounts of NaCl. As ionic strength increased, Cd(II) adsorption decreased with the adsorption capacity decreasing from 6.32 mg/g to 1.85 mg/g. This was attributed to competition by Na^+.

Lalmi (2018) reported the adsorption of Pb(II) by continuous column mode studies using a gel type, polystyrene based strong acid cation exchange resin with sulphonic acid functional groups with Ca^{2+} as the counter ion rather than the commercially available Na^+ form. The adsorption capacity for Pb(II) was dependent on pH (optimum adsorption at pH 2.4 – 4.8) and flow rate which impacts contact time. The study also reported the regeneration of the exhausted resin with $Ca(NO_3)_2$ followed by the precipitation of $Pb(OH)_2$ from the brine solution and recovery of $Ca(NO_3)_2$.

Vergili (2017) reported the adsorption of Pb(II) by a weak acid cation exchange resin in column mode studies. Preliminary studies showed that the equilibration time was 360 minutes and that adsorption followed pseudo-second order kinetics.

2.4.3.2 Metal oxides as adsorbents for Cr(VI), Cd(II) and Pb(II)

Recent reviews (Hua *et al.*, 2012; Kumari *et al.,* 2019; Lu and Astruc, 2018; Sarma *et al.*, 2019; Wadhawan *et al.,* 2020) have included the adsorption of heavy metals by metal oxides. Hu et al. (2008) discussed the use of hierarchically structured metal oxides as adsorbents for metal ions. Specific metal oxides that have reported as adsorbents for heavy metals include manganese oxides (Kang *et al.*, 2011; Puppa *et al.*, 2013), copper oxides (Taman *et al.,* 2015), zinc oxide and mixed metal oxides (Sharma *et al.*, 2019). For the purposes of this review, the focus will be on the use of iron oxide as an adsorbent for Cr(VI), Cd(II) and Pb(II).

2.4.3.2.1 Iron oxides as adsorbents for Cr(VI), Cd(II) and Pb(II)

Iron oxides and oxy(hydroxides) have exceptional adsorption properties which make them favourable for the remediation of metals (Sarkar et al., 2007). Nanosized iron oxides have higher adsorption capacities than bulk oxides as a result of the high surface area to volume ratio (Cornell and Schwertmann, 2003). Nanoparticulate iron

oxides have been widely studied for the adsorption of heavy metal ions because of their low cost, environmentally friendly nature and excellent adsorption properties. Some of these Fe hydro(oxides) are goethite (α-FeOOH), lepidocrocite (γ-FeOOH), akaganite (β-FeOOH), feroxyte (δ'-FeOOH), bernalite $Fe(OH)_3$ and hydrous ferric oxide ($Fe_5HO_8 \cdot 4H_2O$) (Cornell and Schwertmann, 2003). Common naturally occurring forms of iron oxide are hematite (α-Fe_2O_3), magnetite (Fe_3O_4), goethite (α-FeOOH) and hydrous ferric oxide ($Fe_5HO_8 \cdot 4H_2O$).

Iron oxides and oxy(hydroxides) exhibit high selectivity because the adsorbent phase can be tailored due to the amphoteric nature of the surface of the material. The amphoteric nature of iron oxides is brought about by the point of zero charge (PZC). The PZC occurs at the pH at which the net surface charge of a particle is zero. In iron oxides and oxy(hydroxides) the PZC occurs due to the oxide OH groups being prone to protonation or deprotonation depending on the pH (Murray, 1975). At pH values lower than the PZC the iron oxide surface is positively charged and negatively charged at pH values higher than PZC. At a pH below PZC anionic metals will be adsorbed e.g. Cr(VI), and at a pH higher than the PZC cationic heavy metals like Cd(II) and Pb(II) will be adsorbed. The reported PZC value for goethite is 8.32; synthetic hematite, 7.82 and for Fe(III) hydroxides and hydrous oxides 7.99 (Kosmulski *et al.*, 2003).

The adsorption of Cr(VI) by different forms of ferric oxide has been extensively reviewed (Bhateria & Singh, 2019; Dubey *et al.*, 2017; Hua *et al.,* 2012; Jawed *et al.,* 2020; Kumari *et al.,* 2019; Lu & Astruc, 2018; Singh *et al.,* 2018).

The adsorption of Cr(VI) by magnetite (Fe_3O_4) has been reported (Chowdhury and Yanful, 2010; Jiang *et al.*, 2013). Jiang (2013) reported that maximum adsorption occurred at a pH of 4 and that adsorption was best described by a blended Langmuir-Freundlich isotherm model. The calculated maximum capacity was 1.62 mg/g. Chowdhury and Yanful (2010) reported the adsorption of Cr(VI) with an initial concentration of 1mg/L at a pH of 2. The maximum capacity was 2.4 mg/g. The adsorption process was described by the Freundlich isotherm model.

Hydrous ferric oxide (HFO), sometimes referred to as amorphous ferric oxide or ferrihydrite are found as nano-crystals of a reddish-brown colour. HFOs exist as nanocrystals and are synthesized through iron hydrolysis under neutral to alkaline conditions (Michel et al., 2007). HFO exists in two different forms (2- and 6-line) (Drits et al., 1993) and can be differentiated by XRD analysis (Cornell and Schwertmann, 2003).

The PZC of HFO is 8.7 (Antelo et al., 2015) and is reportedly a suitable adsorbent for many metals including Cd and Pb (Antelo et al., 2015, Pinney et al., 2009, Xu et al., 2011). The adsorption selectivity of HFO follows the order: Pb > Cu > Cd > Zn> Ni > Ca (Cornell and Schwertmann, 2003). At pH below the PZC, the surface of HFO is positively charged and will adsorb anionic ligands; thus, Cr(VI) will be adsorbed at a pH lower than that which is equivalent to the PZC. Therefore, the adsorption of Cr(VI) is favourable in acid conditions (Pieczara and Rzepa, 2016). Zelmanov and Semiat (2011) reported that Cr(VI) adsorption by HFO was at a maximum at a pH of 4. The Langmuir isotherm model was only able to describe adsorption at very low Cr(VI) concentrations. For higher Cr(VI) concentrations, adsorption was described by the Freundlich model. Hilbrandt (2019) reported the effect of competing ions on Cr(VI) adsorption by granular ferric hydroxide. Carbonate (HCO_3^-) and phosphate (PO_4^{3-}) had the greatest effect on Cr(VI) adsorption with Cr(VI) adsorption decreasing as concentrations of HCO_3^- and PO_4^{3-} increased. Increasing sulphate (SO_4^{2-}) concentrations resulted in a much smaller decrease in Cr(VI) adsorption.

Kumari (2015) reported the adsorption of Pb(II) by mesoporous magnetite. The highest adsorption capacity (13.40 mg/g) was found at a pH of 5. Adsorption followed pseudo-second order kinetics and the Koble-Corrigan isotherm model. Li (2018) reported the adsorption of Pb(II) by synthetic Fe_2O_3. The Langmuir isotherm model described adsorption well and gave a maximum capacity of 97.8 mg/g. Tamez (2016) reported that the adsorption of Pb(II) by iron oxide nanoparticles (Fe_2O_3) was favoured at pH 4 and above and that the presence of Na^+, K^+, Mg^{2+} and Ca^{2+} had no impact on Pb(II) adsorption.

The adsorption of Cd(II) by nano sized zerovalent iron particles was described by the pseudo-second order kinetic model and the Langmuir and Temkin isotherm models (Boparari *et al.,* 2011). The adsorption capacity when contacted with a 450 mg/L Cd(II) solution was 769.2 mg/g. Streat (2008) reported the adsorption of Cd(II) by hydrous ferric oxide. Very little adsorption occurred below pH 6 and maximum adsorption was reported to occur at pH 9. Liu (2018) reported the co-adsorption of Cd(II) with phosphate and sulphate by ferrihydrate. It was found that in the absence of oxyanions very little Cd(II) adsorption occurred (0.04 mmol/g) while sulphate increased the adsorption capacity to 0.45 mmol/g. ATR-FTIR was used to describe the adsorption as being via an electrostatic interaction and the formation of cation-bridged ternary complexes. Swedlund (2003) also reported increased Cd(II) adsorption when sulphate was present. The diffuse layer model was found not to be able to predict adsorption when adsorption constant obtained from single component systems were used. More applicable adsorption constant from binary systems were proposed.

2.4.3.3 Hybrid ion exchange resins with encapsulated hydrous ferric oxide nanoparticles as adsorbents

The removal of Cr(VI), Cd(II) and Pb(II) with hybrid ion exchange resins embedded with HFO nanoparticles has been reported. (Chanthapona *et al.*, 2018; Hua *et al.*, 2017; Kowalczyk *et al.,* 2013). The hybrid adsorbents are attractive as they provide selective adsorption, regeneration is possible, and they are suitable for treatment at a large scale (Padungthon et al 2015). The adsorption of metals from water by polymer functionalised nanocomposites, including hybrid ion-exchange resins has been reviewed (Lofrano *et al.*, 2016).

A hybrid ion exchange resin contains two components: a functionalized polymeric ion exchanger host and HFO nanoparticles embedded in the host polymer phase (Padungthon, 2015). The HFO nanoparticles can be embedded in anion exchanger containing quaternary ammonium functional (R_4N^+) groups to form a hybrid referred to as hybrid anion exchange resin embedded with hydrous ferric oxides (HAIX-HFO). When the hydrous ferric oxides are dispersed within a cation exchange resin

containing sulfonate (SO_3^-) functional groups they are referred to as hybrid cationic exchange resins embedded with hydrous ferric oxides (HCIX-HFO).

This class of hybrid nanocomposite provides an interaction that cannot be attained by either nanoparticles or polymeric exchangers alone. The hydrous ferric oxides provide high selectivity and high adsorption capacities. The ion exchange resins are suitable for fixed bed adsorption process. In addition, the fixed ion-exchange functional groups of the resin may increase adsorption capacities due to the Donnan membrane effect (Cumbal and Sengupta; 2005). The hybrid material is environmentally safe, suitable for fixed bed adsorption processes due to its high mechanical strength, while the high surface and the Donnan membrane effect provide high adsorption capacities; and selectivity is enhanced by the amphoteric nature of the ferric oxide surface and the pH of the contacting solution.

The synthesis of HAIX-HFO and HCIX-HFO via an inter-matrix synthesis method where the ferric oxide is reduced inside the matrix of the polymer has been reported (SenGupta, 2017). The use of commercially available anion exchange resins with HFO nanoparticles (Arsen X^{np} and Lewatit FO36) for the adsorption of Cr(VI) has been reported (Kołodyńska *et al.,* 2015; Kowalczyk *et al.,* 2013; Rafati *et al.*, 2010). Rafati (2010) found that the adsorption of Cr(VI) by Lewatit FO36 in single component solutions was described by first-order reversible kinetics and the Langmuir isotherm model. The maximum adsorption capacity was reported to be 0.29 mmol/g. The optimum pH for adsorption was reported to be 6.

Kołodyńska *et al* (2015) and Kowalczyk *et al* (2013) reported the effect of competitor ions (Cl^-, NO_3^-, SO_4^{2-}) and ethyllenediaminedisuccinic acid on the adsorption of Cr(VI), Cd(II) and Pb(II) from multi metal ion component solutions at pH 4.5. Kowalczyk (2013) found that the presence of ethyllenediaminedisuccinic acid only increased the adsorption capacities of Cu(II) and Zn(II). The adsorption capacities of Cr(VI), Cd(II) and Pb(II) remained unchanged. Anionic competitor ions (Cl^-, NO_3^-, SO_4^{2-}) resulted in a decrease in adsorption capacities for all metal ions studied. Kołodyńska et al (2015) carried out a similar study where the adsorption performance of Arsen X^{np} was compared to that of Lewatit FO36 for Cr(VI), Cd(II)

and Pb(II) adsorption. The adsorption capacities obtained using Arsen X^{np} were found to be higher than those obtained using Lewatit FO36. This was attributed to differences in the encapsulated ferric oxide particles. Characterization by Electron Spin Resonance (ESR) showed the Lewatit FO36 had supraparamagnetic properties, while Arsen X^{np} had none.

Hua (2017) reported the simultaneous adsorption of As(V) and Cr(VI) by a HFO impregnated macroporous anion exchange resin. For both As(V) and Cr(VI) the adsorption followed pseudo-first order kinetics. By comparing the adsorption capacities of both the parent and the hybrid anion exchange resins, it was concluded that As(V) was preferentially adsorbed by the hydrated ferric oxide nanoparticles and the Cr(VI) by the fixed quaternary ammonium exchange sites of the parent resin.

The adsorption of Cd(II) and Pb(II) by hybrid anion exchangers (Lewatit FO36) has been reported (Kołodyńska *et al.,* 2015; Kowalczyk *et al.,* 2013). For both metal ions adsorption followed pseudo-second order kinetics. The time required to reach equilibrium differed significantly with Pb(II) taking 15 minutes to reach equilibrium and Cd(II) 40 minutes. The capacity for Pb(II) was much higher (12.11 mol.l^{-1}/g) than for Cd(II) (1.50 mol.l^{-1}/g). No mechanism was proposed for the adsorption of positively charged cations by an anionic exchange resin. It is surprising that there was any adsorption as the positively charged fixed ion exchange sites of the resin matrix can be expected to hinder diffusion of positive metals ions into the pores of the resin (Donnan membrane effect).

The adsorption of metal ions by hybrid cationic exchange resins have been reported (Chanthapon *et al.,* 2018; Pan *et al.,* 2010). A hybrid cation gel-type resin was used for the adsorption of Pb(II) (Chanthapon *et al.,* 2018). Adsorption was pH dependent with maximum adsorption occurring at pH 7. The adsorption process followed the Freundlich isotherm with a maximum adsorption capacity of 22.5 mg/g. Pan (2010) reported the adsorption of Cd(II) and Pb(II) using a hybrid cationic resin. Significant adsorption only occurred at pHs greater than 4 with the hybrid resin having a greater affinity for Pb(II) than Cd(II). The adsorption of both metals followed pseudo-second

order kinetics. Regeneration of the exhausted hybrid resin was achieved with a HCl/NaCl solution at a pH of 3.

2.5   References

Abdullah, N., Yusof, N., Lau, W.J., Jaarfar, J., Ismail, A.F., 2019, Recent trends of heavy metal removal from water/wastewater by membrane technologies., Journal of Industrial and Engineering Chemistry, 76, pp. 17-38.

Akcil, A. and Koldas, S., 2006. Acid Mine Drainage (AMD): causes, treatment and case studies. Journal of Cleaner Production, 14(12-13), pp.1139-1145.

Amaral, M.C.S., Grossi, L.B., Ramos, R.L., Ricci, B.C., Andrade, L.H., 2018, Integrated UF-NF-RO route for gold mining effluent treatment: From bench-scale to pilot-scale., Desalination, 440, pp. 111-121.

Ambiado, K., Bustos, C., Schwarz, A. and Bórquez, R., 2016. Membrane technology applied to acid mine drainage from copper mining. Water Science and Technology, 75(3), pp.705-715.

Antelo, J., Arce, F. and Fiol, S., 2015. Arsenate and phosphate adsorption on ferrihydrite nanoparticles. Synergetic interaction with calcium ions. Chemical Geology, 410, pp.53-62.

Aubé, B., Zinck, J. and Eng, M., 2013, Lime treatment of acid mine drainage in Canada. In Brazil-Canada Seminar on Mine Rehabilitation (pp. 23-39). Florianópolis: Desktop Publishing.

Aziz, H.A., Adlan, M.N. and Ariffin, K.S., 2008. Heavy metals (Cd, Pb, Zn, Ni, Cu and Cr (III)) removal from water in Malaysia: post treatment by high quality limestone. Bioresource technology, 99(6), pp.1578-1583.

Bedoui, K., Bekri-Abbes, I., Srasra, E., 2008, Removal of cadmium(II) from aqueous solution using pure smectite and Lewatite S100: the effect of time and metal concentration. Desalination, 223, pp. 269-273.

Bhateria, R. and Singh, R., 2019, A review on nanotechnological application of magnetic iron oxides for heavy metal removal, Journal of Water Process Engineering, 31, pp.100845.

Boparari, H.K., Joseph, M., O'Carrol, D.M., 2011, Kinetics and thermodynamics of cadmium ion removal by adsorption onto nano zerovalent iron particles, Journal of Hazardous Materials, 186, pp. 458-465.

Buzzi, D.C., Viegas, L.S., Roderigues, M.A.S., Bernades, A.M., Tenório, J.A.S., 2013, Water recovery from acid mine drainage by electrodialysis., Minerals Engineering, 40, pp. 82-89.

Bwapwa, J.K., Jaiyeola, A.T. and Chetty, R., 2017. Bioremediation of acid mine drainage using algae strains: A review. South African Journal of Chemical Engineering, 24, pp.62-70.

Chanthapon, N., Sarkar, S., Kidkhunthod, P. and Padungthon, S., 2018. Lead removal by a reusable gel cation exchange resin containing nano-scale zero valent iron. *Chemical Engineering Journal*, *331*, pp.545-555.

Chowdhury, S.R., Sarkar, D., Datta, R., 2015, Remediation of Acid Mine Drainage-Impacted Water., Current Pollution Report, 1, pp. 131-141., DOI 10:1007/540726-015-0011-3.

Chowdury, S.R. and Yanful, E.K., 2010, Arsenic and chromium removal by mixed magnetite-maghemite nanoparticles and the effect of phosphate on removal, Journal of Environmental Management, 91, pp. 2238-2247.

Coetzee, H., Hobbs, P.J., Burgess, J.E., Thomas, A., Keet, M., Yibas, B., VanTonder, D., Netili, F., Rust, V., Wade, P. and Maree, J., 2010. Mine water

management in the Witwatersrand Gold Fields with special emphasis on acid mine drainage. Report to the inter-ministerial committee on acid mine drainage, pp.1-128.

Cornell, R.M. and Schwertmann, U., 2003. The iron oxides: structure, properties, reactions, occurrences and uses. John Wiley & Sons.

Cumbal, L. and SenGupta, A.K., 2005. Arsenic removal using polymer-supported hydrated iron (III) oxide nanoparticles: role of Donnan membrane effect. Environmental science & technology, 39(17), pp.6508-6515.

Dąbrowski, A., Hubicki, Z., Podkościelny, P., Robens, E., 2004, Selective removal of the heavy metal ions from waters and industrial wastewaters by ion-exchange method, Chemosphere, 56, pp. 91-106.

Demirbas, A., Pehlivan, E., Gode, F., Altun, T. and Arslan, G., 2005. Adsorption of Cu (II), Zn (II), Ni (II), Pb (II), and Cd (II) from aqueous solution on Amberlite IR-120 synthetic resin. Journal of Colloid and Interface Science, 282(1), pp.20-25.

Department of Water Affairs (DWA), 2013: Feasibility Study for a Long-term Solution to address the Acid Mine Drainage associated with the East, Central and West Rand underground mining basins. Study Report No. 5.4: Treatment Technology Options – DWA Report No.: P RSA 000/00/16512/4

Drits, V.A., Sakharov, B.A., Salyn, A.L. and Manceau, A., 1993. Structural model for ferrihydrite. Clay Minerals, 28(2), pp.185-207.

Dubey, S., Banerjee, S., Upadhyay, S.N., Sharma, Y.C., 2017, Application of common nano-materials for removal of selected metallic species from water and wastewaters: A critical review, Journal of Molecular Liquids, 240, pp. 656-777.

Duruibe, J.O., Ogwuegbu, M.O.C. and Egwurugwu, J.N., 2007. Heavy metal pollution and human biotoxic effects. International Journal of physical sciences, 2(5), pp.112-118.

Edebali, S. and Pehlivan, E., 2010. Evaluation of Amberlite IRA96 and Dowex 1× 8 ion-exchange resins for the removal of Cr (VI) from aqueous solution. Chemical Engineering Journal, 161(1-2), pp.161-166.

Feng, D., Aldrich, C. and Tan, H., 2000. Treatment of acid mine water by use of heavy metal precipitation and ion exchange. Minerals Engineering, 13(6), pp.623-642.

Flora, G., Gupta, D. and Tiwari, A., 2012. Toxicity of lead: a review with recent updates. Interdisciplinary toxicology, 5(2), pp.47-58.

Foureax, A.F.S., Moreira, V.R., Lebron, Y.A.R., Santo, L.V.S., Amaral, M.C.S., 2020, Direct contact membrane distillation as an alternative to the conventional methods for value-added compounds recovery from acidic effluents: A review., Separation and Purification Technology, 236, pp. 116251. https://doi.org/10.1016/j.seppur.2019.116251.

Giugni, M., Meric, S., 2016, Polymer functionalized nanocomposites for metals removal from water and wastewater: An overview, Water Research, 92, pp. 22-37.

Gray, N.F., 1998. Acid mine drainage composition and the implications for its impact on lotic systems. Water Research, 32(7), pp.2122-2134.

Hilbrandt, I., Ruhl, A.S., Zietzschmann, F., Molkenthin, M., Jekel, M., 2019, Competition in chromate adsorption onto microsized granular ferric hydroxide, Chemosphere, 216, pp. 749-757.

Hu, J-S., Zhong, L-S., Song, W-G., Wan, L-J., 2008, Synthesis of Hierarchically Structured Metal Oxides and Their Application in Heavy Metal Ion Removal, Advanced Materials, 20. Pp. 2977-2982.

Hua, M., Zhang, S., Pan, B., Zhang, W., Zhang, Q., 2012, Heavy metal removal from water/wastewater by nanosized metal oxides: A review, Journal of Hazardous Materials, 211-212, pp. 317-331.

Hua, M., Yang, B., Shan, C., Zhang, W., He, S., Lv, L. and Pan, B., 2017. Simultaneous removal of As (V) and Cr (VI) from water by macroporous anion exchanger supported nanoscale hydrous ferric oxide composite. Chemosphere, 171, pp.126-133.

Jachula, J. and Hubicki, Z., 2013, Removal of Cr(VI) and As(V) ions from aqueous solutions by polyacrylate and polystyrene anion exchange resins., Applied Water Science, 3, pp. 653-664.

Jawed, A., Saxena, V., Pandey L.M., 2020, Engineered nanomaterials and their surface functionalization for the removal of heavy metals: A review, Journal of Water Process Engineering, 33, pp. 101009.

Jaishankar, M., Tseten, T., Anbalagan, N., Mathew, B.B. and Beeregowda, K.N., 2014. Toxicity, mechanism and health effects of some heavy metals. Interdisciplinary toxicology, 7(2), pp.60-72.

Jiang, W., Pelaez, M., Dionysiou, D.D., Entezari, M.H., Tsoutsou, D., O'Shea, K., 2013, Chromium(VI) removal by maghemite nanoparticles. Chemical Engineering Journal, 222, 527-533.

Joseph, L., Jun, B-M., Flora, J.R.V., Park, C.M., Yoon, Y., 2019, Removal of heavy metals from water sources in the developing worl using low-cost materials: A review. Chemosphere, 229, pp142-159.

Kang, K.C., Ju, J.H., Kim, S.S., Baik, M.H., Rhee, S.W., 2011, Sorption of aqueous Pb^{2+} ion on synthetic manganese oxides-intercalated with exchangeable cations, Journal of Industrial and Engineering Chemistry, 17, pp 565-569.

Kefeni, K.K., Msagati, T.A.M., Mamba, B.B. 2017, Acid Mine Drainage: Prevention, treatment options and resource recovery: A review., Journal of Cleaner Production, 151, pp. 475-493.

Kołodyńska, D., Kowalczyk, M., Hubicki, Z., Shvets, V., Golub, V., 2015, Effect of accompanying ions and ethylenediaminedisuccinic acid on heavy metals sorption using hybrid materials Lewatit FO36 and Purolite Arsen X. Chemical Engineering Journal, 276, pp. 376-387.

Kosmulski, M., Maczka, E., Jartyeh, E., Rosenholm, J.B., 2003, Synthesis and characterization of goethite and goethite-hematite composite: Experimental study and literature review, Advances in Colloid and Interface Science, 103, pp. 57-76.

Kowalczyk, M., Hubiccki, Z., Kołodyńska, D., 2013, Modern hybrid sorbents-New way of heavy metal removal from waters, Chemical Engineering and Processing: Process Intensification, 70, pp. 55-65.

Kumari, P., Alam, M., Siddiqi, W.A., 2019, Usage of nanoparticles as adsorbents for waste water treatment: An emerging trend, Sustainable Materials and Technologies, 22, e00128.

Lalmi, A., Bouhidel, K-E., Sahraoui, B., Anfif, C.E.H., 2018, Removal of lead from polluted water using ion-exchange resin with $Ca(NO_3)_2$ for elution., Hydromettallurgy, 178, pp. 287-293.

Lecornu, J., 1996. Dam safety in 1996, from engineer's duty to risk management. ICOLD web.

Li, X., Lan, S., Zhu, Z., Zhang, C., Zang, G., Liu, Y., Cao, W., Song, B., Yang, H., Wang, S., Wu, S., 2018, The bioenergetics mechanisms and applications of sulphate-reducing bacteria in remediation of pollutants in drainage: A review., Ecotoxicology and Environmental Safety, 158, pp. 162-170.

Liu, J., Zhu, R., Liang, X., Ma, L., Lin, X., Zhu, J., He H., Parker S.C., Molinari, M., 2018, Synergistic adsoprtion of Cd(II) with sulphate/phosphate on ferrihydrite: An in situ ATR-FTIR/2D-COS study. Chemical Geology, 477, pp. 12-21.

Lofrano, G., Carotenuto, M., Libralato, G., Domingo, R.F., Markus, A., Dini, L., Gautam, R.K., Baldantoni, D., Ross, M., Sharma, S.K., Chattopadhyaya, M.C.,

Lu, F. and Astruc, D., 2018, Nanomaterials for removal of toxic elements from water, Coordination Chemistry Reviews, 356, pp. 147-164.

Martin, S. and Griswold, W., 2009. Human health effects of heavy metals. Environmental Science and Technology briefs for citizens, 15, pp.1-6.

Masindi, V., Osman, M.S. and Abu-Mahfouz, A.M., 2017. Integrated treatment of acid mine drainage using BOF slag, lime/soda ash and reverse osmosis (RO): Implication for the production of drinking water. Desalination, 424, pp.45-52

Michel, F.M., Ehm, L., Antao, S.M., Lee, P.L., Chupas, P.J., Liu, G., Strongin, D.R., Schoonen, M.A., Phillips, B.L. and Parise, J.B., 2007. The structure of ferrihydrite, a nanocrystalline material. Science, 316(5832), pp.1726-1729.

Mudgal, V., Madaan, N., Mudgal, A., Singh, R.B. and Mishra, S., 2010. Effect of toxic metals on human health. The Open Nutraceuticals Journal, 3(1).

Mulopo, J. and Motaung, S., 2014. Carbothermal reduction of barium sulphate-rich sludge from acid mine drainage treatment. Mine Water and the Environment, 33(1), pp.48-53

Murray, J.W., 1975. The interaction of metal ions at the manganese dioxide-solution interface. Geochimica et Cosmochimica Acta, 39(4), pp.505-519.

Naidu, G., Ryu, S., Thiruvenkatachari, R., Choi, Y., Jeong, S., Vigneswaran, S., 2019, A critical review on remediation, reuse and resource recovery from acid mine drainage., Environmental Pollution, 247, pp. 1110-1124.

Padungthon, S., German, M., Wiriyathamcharoen, S. and SenGupta, A.K., 2015. Polymeric anion exchanger supported hydrated Zr (IV) oxide nanoparticles: a

reusable hybrid sorbent for selective trace arsenic removal. Reactive and Functional Polymers, 93, pp.84-94.

Pan, B., Qiu, H., Pan, B., Nie, G., Xiao, L., Lv, L., Zhang, W., Zhang, Q. and Zheng, S., 2010. Highly efficient removal of heavy metals by polymer-supported nanosized hydrated Fe (III) oxides: behavior and XPS study. Water Research, 44(3), pp.815-824.

Pehlivan, E. and Altun, T., 2006. The study of various parameters affecting the ion exchange of Cu2+, Zn2+, Ni2+, Cd2+, and Pb2+ from aqueous solution on Dowex 50W synthetic resin. Journal of hazardous materials, 134(1-3), pp.149-156.

Pehlivan, E. and Cetin, S., 2009. Sorption of Cr (VI) ions on two Lewatit-anion exchange resins and their quantitative determination using UV–visible spectrophotometer. Journal of Hazardous Materials, 163(1), pp.448-453.

Pieczara, G. and Rzepa, G., 2016. THE EFFECT OF Si CONTENT ON FERRIHYDRITE SORPTION CAPACITY FOR Pb (II), Cu (II), Cr (VI), AND P (V). Environmental Engineering & Management Journal (EEMJ), 15(9).

Pinney, N., Kubicki, J.D., Middlemiss, D.S., Grey, C.P. and Morgan, D., 2009. Density functional theory study of ferrihydrite and related Fe-oxyhydroxides. Chemistry of Materials, 21(24), pp.5727-5742.

Puppa, L.D., Komárek, M., Bordas, F., Bollinger, J-C., Joussein, E., 2013, Adsorption of copper, cadmium, lead and zinc onto synthetic manganese oxide, Journal of Colloid and Interface Science, 399, pp. 99-106.

Purkayastha, D., Mishra, U. and Biswas, S., 2014. A comprehensive review on Cd (II) removal from aqueous solution. Journal of water process engineering, 2, pp.105-128.

Rafati, L., Mahvi, A.H., Asgari, A.R., Hosseini, S.S., 2010, Removal of Chromium(VI) from aqueous solutions using Lewatit FO36 nano ion exchange resin, International Journal of Environmental Science and Technology, 7(1), pp. 147-156.

Rao, K.S., Chaudhury, G.R., Mishra, B.K., 2010, Kinetics and equilibrium studies for the removal of cadmium ions from aqueous solutions using Duolite ES 467 resin, Internationational Journal of Mineral Processing, 97, pp. 68-73.

Reis, B.G., Araújo, A.L.B., Amaral, M.C.S., Ferraz, H.C., 2018, Comparison of Nanofiltration and Direct Contact Membrane Distillation as an alternative for gold mining effluent reclamation., Chemical Engineering and Processing: Process Intensification., 133, 24-33.

Rios, C.A., Williams, C.D. and Roberts, C.L., 2008. Removal of heavy metals from acid mine drainage (AMD) using coal fly ash, natural clinker and synthetic zeolites. Journal of hazardous materials, 156(1-3), pp.23-35.

Rodríguez-Galán, M., Baeno-Moreno, F.M., Vázquez, S., Arroyo-Torralvo, F., Vilches, L.F., Zhang, Z., 2019, Remediation of acid mine drainage., Environmental Chemistry Letter, 17, pp. 1529-1538.

SANS 241-1:2015. South African National Standard. Drinking water. Part 1: Microbiological, physical, aesthetic and chemical determinants. ISBN 978-0-626-29841-8.

Sarkar, S., Blaney, L.M., Gupta, A., Ghosh, D. and SenGupta, A.K., 2007. Use of ArsenXnp, a hybrid anion exchanger, for arsenic removal in remote villages in the Indian subcontinent. Reactive and Functional Polymers, 67(12), pp.1599-1611.

Sarma, H., 2011, Metal hyperaccumulation in plants: A review focusing on phytoremediation technology., Journal of Environmental Science and Technology. 4(3) pp.118-138.

Sarma, G.K., Gupta, S.S., Bhattacharyya, K.G., 2019, Nanomaterials as versatile adsorbents for heavy metal ions in water: a review, Environmental Science and Pollution Research, 26, pp. 6245-6278.

Sengupta, A.K. and Clifford, D., 1986a. Chromate ion exchange mechanism for cooling water. Industrial & engineering chemistry fundamentals, 25(2), pp.249-258.

Sengupta, A.K. and Clifford, D., 1986b. Some Unique Characteristics of Chromate ion exchange., Reactive Polymers, 4, pp. 113-130

Sengupta, A.K., Clifford, D., Subramonian, S., 1986, Chromate ion-exchange process at alkaline pH., Water Research, 20(9), pp. 1177-1184.

SenGupta, A.K., 2017. Ion Exchange in Environmental Processes: Fundamentals, Applications and Sustainable Technology. John Wiley & Sons.

Sharma, M., Singh, J., Hazra, S., Basu, S., 2019, Adsorption of heavy metal ions by mesoporous ZnO and TiO_2@ZnO monoliths: Adsorption and kinetic studies. Microchemical Journal, 145, pp. 105-112.

Shi, T., Wang, Z., Liu, Y., Jia, S., Changming, D., 2009, Removal of hexavalent chromium from aqueous solutions by D301, D314, D354 anion exchange resins, Journal of Hazardous Materials, 161, pp. 900-906.

Singh, N.B., Nagpal, G., Agrawal, S., Rachna, 2018, Water purification by using Adsorbents: A review, Environmental Technology & Innovation, 11, pp. 187-240

Smit, J.P. and Pretorius, L.E., 2000. The treatment of polluted mine water. Journal of African Earth Sciences, 31(1), pp.72-72.

Streat, M., Hellgardt, K., Newton, N.L.R., 2008, Hydrous ferric oxide as an adsorbent in Water treatment Part 3: Batch and mini-column adsorption of arsenic, phosphorous, fluorine and cadmium ions, Process Safety and Environmental Protection, 86, pp. 21-30.

Swedlund, P.J., Webster, J.G., Miskelly, G.M., 2003, The effect of SO_4 on the ferrihydrite adsorption of Co, Pb and Cd: ternary complexes and site heterogeneity, Applied Geochemistry, 18, pp. 1671-1689.

Szabó, M., Kalmar, J., Ditrói, T., Bellér, G., Lente, G., Simic, N., Fabián, I., 2018, Equilibria and kinetics of Chromium (VI) speciation in aqueous solution – A comprehensive study from pH 2 to 11. Inorganica Chimica Acta, 472, pp. 295-301.

Taman, R., Ossman, M.E., Mansour, M.S., Farag, H.A., 2015, Metal Oxide Nano-particles as an Adsorbent for removal of Heavy Metals, Journal of Advanced Chemical Engineering, 5, 3. DOI: 10.4172/2090-4568.1000125.

Tamez, C., Hernandez, R., Parson, J.G., 2016, Removal of Cu(II) and Pb(II) from aqueous solution using engineered iron oxide nanoparticles, Microchemical Journal, 125, pp. 97-104.

Tandon, R.K., Crisp, P.T., Ellis, J. and Baker, R.S., 1984. Effect of pH on chromium (VI) species in solution. Talanta, 31(3), pp.227-228.

Uddin, M.K., 2017. A review on the adsorption of heavy metals by clay minerals, with special focus on the past decade. Chemical Engineering Journal, 308, pp.438-462.

Vergili, I., Gönder, Z.B., Kaya, Y., Gürdag, G., Cavus, S., 2017, Sorption of Pb(II) from battery industry wastewater using a weak acid cation exchange resin. Process Safety and Environmental Protection, 107, pp. 498-507.

Wadhawan, S., Jain, A., Nayyar, J., Mehta, S.K., 2020, Role of nanomaterials as adsorbents in heavy metal ion removal from wastewater: A review, Journal of Water Process Engineering, 33, pp. 101038.

Wang, F., Wang, L.J., Li, J.S., Sun, X.Y. and Han, W.Q., 2009. Adsorption behavior and mechanism of cadmium on strong-acid cation exchange resin. Transactions of Nonferrous Metals Society of China, 19(3), pp.740-744.

Wójcik, G. and Hubicki, Z., 2016, Sorption and reduction of chromate(VI) ions on Purolite A830, Separation Science and Technology, 51 (15 and 16), pp. 2539-2546.

Xiao, K., Xu, F., Jiang, L., Duan, N., Zheng, S., 2016, Resin oxidation phenomenon and its influence factor during chromium(VI) removal from wastewater using gel-type anion exchangers, Chemical Engineering Journal, 283, pp. 1349-1356.

Xu, W., Hausner, D.B., Harrington, R., Lee, P.L., Strongin, D.R. and Parise, J.B., 2011. Structural water in ferrihydrite and constraints this provides on possible structure models. American Mineralogist, 96(4), pp.513-520.

Zhitkovich, A., 2011. Chromium in drinking water: sources, metabolism, and cancer risks. Chemical research in toxicology, 24(10), pp.1617-1629

Zelmanov, G and Semiat, R., 2011, Iron (Fe^{+3}) oxide/hydroxide nanoparticles based agglomerates suspension as adsorbent for chromium (Cr^{+6}) removal from water and recovery, Separation and Purification Technology, 80, pp. 330-337

.

.

CHAPTER 3
METHODOLOGY

This chapter details the preparation, characterization and application of hybrid ion exchange resins with encapsulated ferric oxide nanoparticles for the adsorption of Cr(VI), Cu(II) and Pb(II). The step-by-step procedures, experimental conditions and instrumentation used are narrated in this chapter.

3.1   Chemicals and Methodology

3.1.1   Chemicals

The following chemicals were used for the synthesis of hybrid ion exchange resins embedded with hydrous ferric oxides. Analytical grade $FeCl_3.6H_2O$, NaOH and NaCl (Sigma Aldrich, Johannesburg, South Africa). The two host resins used were Amberlite IRA 400 Cl form (Sigma Aldrich , Johannesburg, South Africa) and IMAC HP 1110 (Lenntech, Netherlands, Europe). The properties of the Amberlite IRA Cl form and IMAC HP 1110 are given in Table 3.1.

Adsorption studies were carried out with $K_2Cr_2O_7$ (0.0166 M) (Sigma Aldrich). Cr(VI) stock solutions were prepared by dispensing an appropriate volume of $K_2Cr_2O_7$ and making up to volume with deionized water. $CdSO_4.H_2O$ and $PbSO_4$ were both purchased from Sigma Aldrich (analytical grade). Stock solution of Cd(II) and Pb(II) were prepared from the salts and deionized water. Sulphate stock solutions were prepared from analytical grade Na_2SO_4 purchased from Rochelle chemicals.

Hydrochloric acid (32%), nitric acid (65%) and multi elemental standards were purchased from Sigma Aldrich.

Table 3.1: Properties of IRA 400 and HP1110 resins.

Resin	IRA 400	HPP110
Matrix	Styrene/ divinylbenzene (gel)	Styrene/ divinylbenzene (gel)
Matrix active group	Quaternary ammonium	Sulphonates
Capacity	1.4 eq/ L	2.2 eq/ L
Ionic form	Cl	Na

3.1.2   Equipment

All pH measurements were performed using a pH meter (XS instruments PC 80 pH/ Mv/ cond/ Tem meter, XS instruments, South Africa). Batch adsorption studies were conducted using a shaking incubator from Scientific, supplied and serviced by Monitoring and Control Laboratories (MCL) South Africa.

3.2   Analytical methods and characterization techniques

3.2.1   Scanning electron microscopy coupled with energy dispersive spectroscopy

Scanning Electron Microscopy (SEM-EDS) (FESEM, JOEL JSM-7800F version) coupled an EDS detector (Thermo Scientific Ultra dry) was used to characterize the distribution of nanoparticles throughout the interior of the hybrid ion exchange resins. The resins were sliced in half and the surface was scanned at a magnification of 14000 and 9500.

3.2.2   Raman spectroscopy

Raman spectroscopy (Witec, Alpha 300, TS 150 Raman spectrometer), with 100 X magnification and a laser power source of 532 mW and 784.898 mW as an excitation source was used to identify the form of the iron oxide in the hybrid ion-exchange resins.

3.2.3   Qualitative and quantitave determination of metals

Qualitative and quantitative determination of metals in aqueous samples were carried out using inductively coupled plasma optical emission spectrometer (ICP-OES)(Agilent Technologies 700 series). Quantification was carried out by external calibration; all measurements were done in triplicate with appropriate blanks.

3.3   Synthesis of the hybrid ion exchange resins embedded with hydrous ferric oxide nanoparticles

The synthesis of the cationic and anionic hybrid ion exchange resins embedded with HFO was based on the method described by Pan et al., 2009.All synthetic steps were carried out using a thermostatic shaker that was kept at a shaking speed of 180 revolutions per minute (rpm) and temperature of 25-26°C.

3.3.1   Synthesis of hybrid anionic exchange resins with embedded hydrous ferric oxide nanoparticles

Amberlite IRA 400 Cl form (100 g) was washed with 500 mL deionized (DI) water by shaking for two hours in order to remove fine particles and to remove any residual organic material.

The ferric chloride anionic complex was prepared by weighing 135,42 g of the ferric chloride hexahydrate ($FeCl_3.6H_2O$) and dissolving in 500 mL 1M HCl to form an anionic chloride complex ($FeCl_4^-$) that can be exchanged with the Cl^- on the quaternary ammonium ion exchange sites of the Amberlite IRA 400 Cl form.

The $FeCl_4^-$. solution was then added to the rinsed resin Amberlite IRA 400 Cl form, and the mixture was then shaken in a thermostatic shaker for 24 hours.

The $FeCl_4^-$ solution was decanted, and 300 mL of 1 M NaOH was added and shaken while monitoring the pH. When the pH was 12 the solution was decanted.

The resin was placed in an oven at 40°C for 24 hours.

After being cooled to room temperature, the resin then rinsed with aliquots of 1 M NaCl (300 mL) and shaken until the pH was 7.

The resin was then air dried before further use (Figure 3.1).
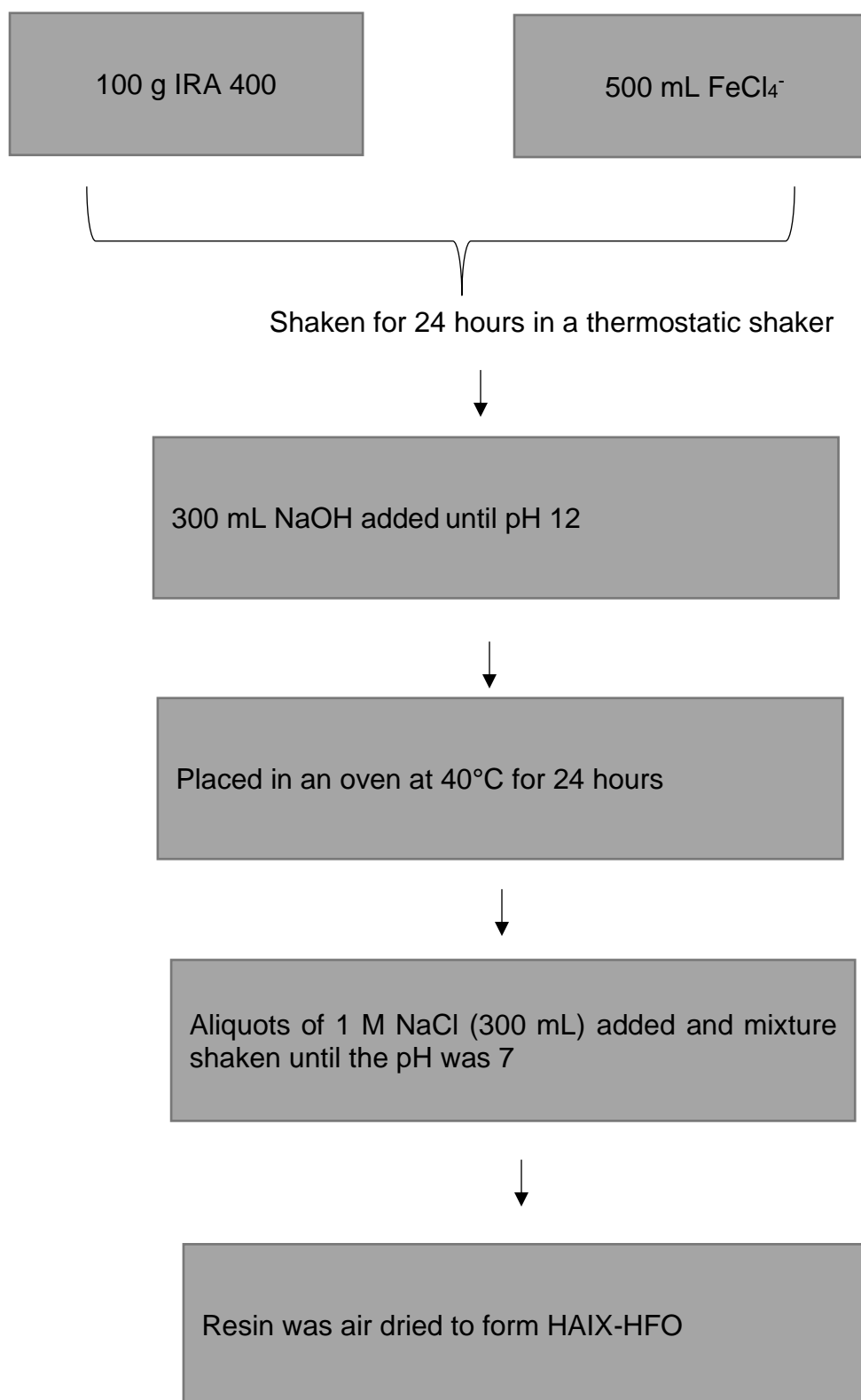
Figure 3.1: Synthesis of hybrid anion exchange resins embedded with hydrous ferric oxide nanoparticles.

3.3.2 Synthesis of hybrid cationic exchange resins with embedded hydrous ferric oxide nanoparticles

IMAC HP 1110 (100 g) was washed with 500 mL deionized (DI) water by shaking for two hours in a thermostatic shaker temperature set at 26 – 26 °C. 135,42 g of $FeCl_3.6H_2O$ was dissolved in 500 mL deionized water. Deionized water was used as solvent as Fe(III) can be exchanged with the Na^+ counter of the cation exchange resin. The $FeCl_3$ solution was then added to the rinsed IMAC HP 1110 resin in a 500 mL conical flask and shaken in a thermostatic shaker for 24 hours.

After the $FeCl_3$ solution was decanted, 300 mL of 1 M NaOH was added and the mixture shaken while monitoring the pH. When the pH was 12 the solution was decanted.

The resin was placed in an oven at 40°C for 24 hours.

After cooling to room temperature the resin was rinsed with 300 mL aliquots of 1M NaCl while shaking until the pH was 7. The supernatant was decanted, and the resin was then air dried before further use (figure3.2).

```
┌─────────────────────┐          ┌─────────────────────┐
│                     │          │                     │
│   100 g HP1110      │          │   500 mL FeCl₃⁺     │
│                     │          │                     │
└─────────────────────┘          └─────────────────────┘
```

100 g HP1110

500 mL $FeCl_3^+$

Shaken for 24 hours in a thermostatic shaker

300 mL NaOH added until pH 12

Placed in an oven at 40°C for 24 hours

Aliquots of 1 M NaCl (300 mL) added and mixture shaken until the pH was 7

Resin was air dried to form HCIX-HFO
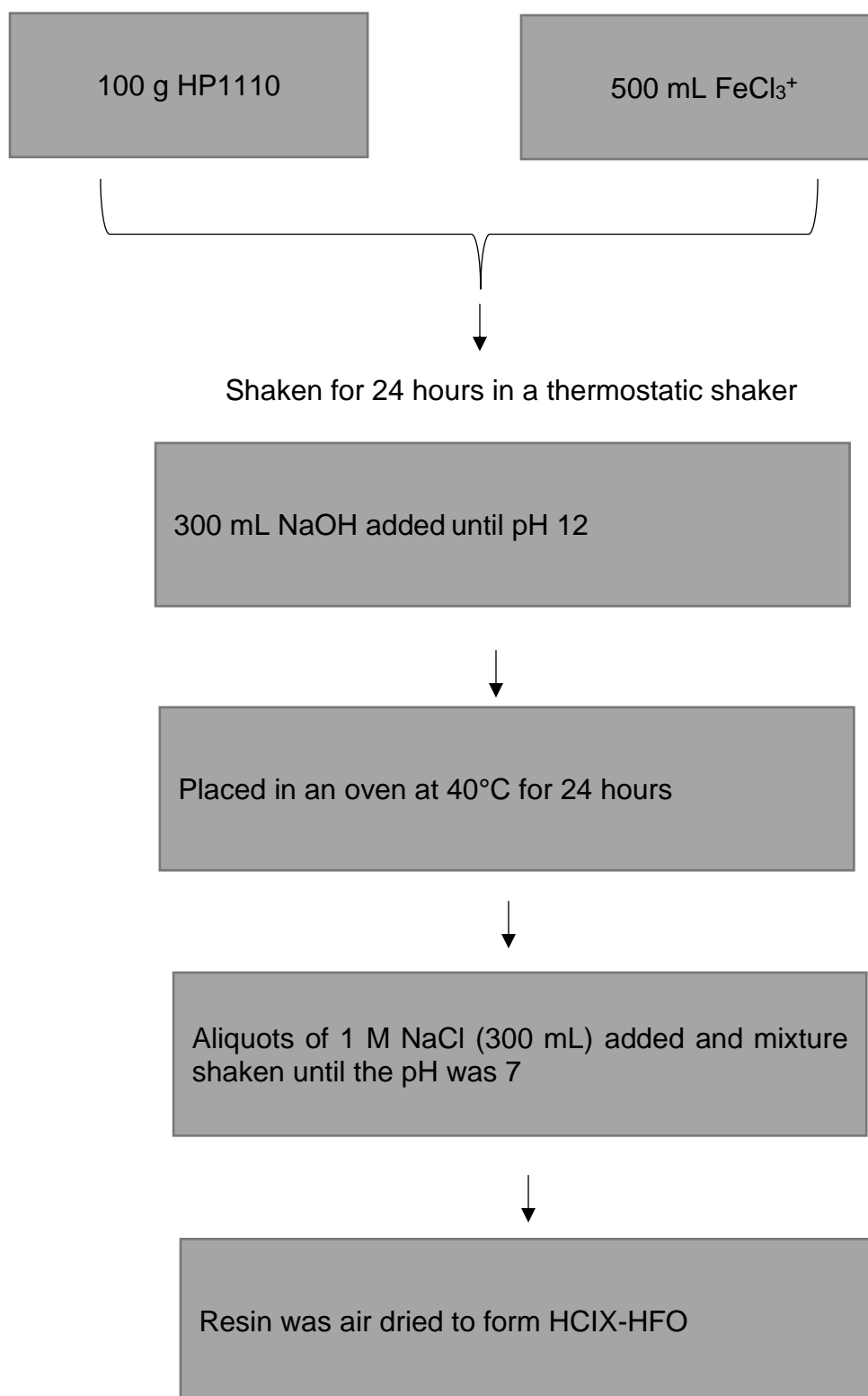
Figure 3.2: Synthesis of hybrid cation exchange resins embedded with hydrous ferric oxide nanoparticles.

3.4   Batch adsorption studies

The adsorption capacity, *q,* (mg.g^{-1}) was calculated using the formula expressed in equation 3.1.

$$q = \frac{V(C_{0-}\ C_t)}{m}$$
(3.1)

Where,

- C_0 is the initial metal concentration (mg/L),

- C_t is the remaining metal concentration (mg /L) at time t (min))

- V is the volume of metal solution (L),

- m is the mass of adsorbent (g).

3.4.1   Adsorption studies for Cr(VI)

3.4.1.1 Effect of pH on adsorption of Cr(VI) by HAIX-HFO

A Cr(VI) solution (1 mg/L) was prepared from the $K_2Cr_2O_7$ solution. The pH 25 mL aliquots of the Cr(VI) solution was adjusted with NaOH and HCl to pH 2, 3, 4 and 5. HAIX-HFO (0.05 g) was added to aliquot and placed on a thermostatic shaker (t200 rpm, temperature of 25-26°C) for 24 hours. The Cr(VI) concentration of the contacting solution after 24 hours of contact time was determined by ICP-OES. The Cr(VI) adsorption capacity at each pH was calculated using equation 3.1.

3.4.1.2 Effect of sulphate concentration on Cr(VI) adsorption

The effect of sulphate concentration of the adsorption of Cr(VI) was investigated by preparing solutions containing 1 mg/L Cr(VI) and sulphate concentrations of 0, 30, 300, 1000 and 3000 mg/L. The Cr(VI)/sulphate solutions were added to 0.005 g portions of HAIX-HFO resin and shaken for 24 hours (200 rpm, 25-26°C). The concentration of Cr(VI) remaining in solution was determined by ICP-OES.

3.4.1.3 Effect of contact time on Cr(VI) adsorption in the absence of sulphate.

To investigate the effect of contact time on Cr(VI) adsorption, 25 mL aliquots of Cr(VI) solution with an initial concentration of 1 mg/L Cr(VI) was added to nine 0.005 g portions of HAIX-HFO in 100 mL volumetric flasks. The pH of the Cr(VI) solution was adjusted to pH 4 with NaOH and HCl prior to addition to the HAIX-HFO. The mixtures were placed on a thermostatic shaker (200 rpm, 25-26°C) and the contact time was varied from 5,10,15, 30, 45, 60,180, 240 and 360 minutes. At each time interval, the solution was decanted and the concentration of Cr(VI) determined.

3.4.1.4 Effect of contact time on Cr(VI) adsorption in the presence of sulphate

The effect of contact time and co-competing sulphate on Cr(VI) adsorption was investigated by preparing a standard solution with 1 mg/L of Cr(VI) and 3000 mg/L sulphate. 25 mL aliquots of the Cr(VI)/sulphate solution were added to 0.005 g of HAIX-HFO and shaken (200 rpm,25-26°C). The amount of Cr(VI) remaining in solution was determined at 5,10,15, 30, 45, 60, 180, 240 and 360 minutes.

3.4.1.5 Effect of HAIX-HFO dosage on Cr(VI) adsorption in the absence of sulphate.

To investigate the effect of HAIX-HFO dosage, 25 mL of Cr(VI) solution with an initial concentration of 1 mg/L and a pH of 4 was added to 0.001 g, 0.003 g, 0.004 g, 0.005 g, 0.006 g, 0.007 g, 0.008 g, 0.009 g and 0.01g of HAIX-HFO. After shaking for 360 minutes (200 rpm, 25-26°C) the concentration of Cr(VI) remaining in solution was determined by ICP-OES.

3.4.1.6 Effect of HAIX-HFO dosage on Cr(VI) in the presence of sulphate

25 mL aliquots of a standard solution containing 1 mg/L Cr(VI) and 3000 mg/L sulphate at a pH of 4 was added to portions of HAIX-HFO with masses of 0.001 g, 0.002 g, 0.003 g, 0.004 g, 0.005 g, 0.006 g, 0.007 g, 0.008 g, 0.009 g and 0.01 g. After shaking for 360 minutes (200 rpm, 25-26°C) the concentration of Cr(VI) remaining in solution was determined by ICP-OES.

3.4.2 Adsorption studies for Cd(II) by HCIX-HFO

3.4.2.1 Effect of pH on the adsorption of Cd(II) by HCIX-HFO

The effect of pH was investigated by adjusting the pH of 25 mL aliquots of a 1mg/L Cd(II) solution to pH 2, 3, 4 and 5 by the addition of NaOH and HCl. HCIX-HFO (0.05g) was added to each aliquot and shaken for 24 hours (200 rpm, 25-26°C). The concentration of Cd(II) remaining in solution was determined by ICP-OES.

3.4.2.2 Effect of contact time on Cd(II) adsorption by HCIX-HFO

The effect of contact time was investigated by adding 25 mL aliquots of a solution containing 1 mg/L Cd(II) and 3000 mg/L sulphate, adjusted to pH 4 with NaOH and HCl, to 0.005 g of HCIX-HFO. The mixtures were then shaken (200 rpm 25-26°C) for 5, 10, 15, 30, 45, 60, 120, 150, 180, 180, 240 and 360 minutes. After the relevant stirring time, the Cd(II) concentration remaining in solution was determined by ICP-OES.

3.4.2.3 Effect of HCIX-HFO dosage on adsorption of Cd(II)

The effect of HCIX-HFO dosage was investigated by adding 25 mL aliquots of a standard solution with 1 mg/L of Cd(II) and 3000 mg/L of sulphate adjusted to pH 4 to different masses of HCIX-HFO. The masses of HCIX-HFO used were 0.001 g, 0.002 g, 0.003 g, 0.004 g, 0.005 g, 0.006 g, 0.007 g, 0.008 g, 0.009 g and 0.01 g. The mixtures were shaken (200 rpm, 25-26°C) for 360 minutes. The Cd(II) concentration remaining in solution was determined by ICP-OES.

3.4.3 Adsorption studies for Pb(II) by HCIX-HFO

3.4.3.1 Effect of pH on the adsorption of Pb(II) by HCIX-HFO

The effect of pH was investigated by adjusting the pH of 25 mL aliquots of a 1 mg/L of Pb(II) solution to pH 2, 3, 4 and 5 by the addition of NaOH and HCl. HCIX-HFO

(0.05 g) was added to each aliquot and shaken (200 rpm, 25-26°C) for 24 hours. The Cd(II) concentration remaining in solution was determined by ICP-OES.

3.4.3.2 Effect of contact time on Pb(II) adsorption by HCIX-HFO

The effect of contact time was investigated by adding 25 mL aliquots of a solution containing 1 mg/L Pb(II) and 3000 mg/L sulphate, adjusted to pH 4 with NaOH and HCl to 0.005 g portions of HCIX-HFO. The mixtures were then shaken (200 rpm, 25-26°C) for 5, 10, 15, 30, 45, 60, 120, 150, 180, 180, 240 and 360 minutes. After the relevant stirring time, the Pb(II) concentration remaining in solution was determined by ICP-OES.

3.4.3.3 Effect of HCIX-HFO dosage on adsorption of Pb(II)

The effect of HCIX-HFO dosage was investigated by adding 25 mL of a standard solution with 1 mg/L of Pb(II) and 3000 mg/L of sulphate adjusted to pH 4 to different masses of HCIX-HFO. The masses of HCIX-HFO used were 0.001 g, 0.002 g, 0.003 g, 0.004 g, 0.005 g, 0.006 g, 0.007 g, 0.008 g, 0.009 g and 0.01 g. The resulting mixtures were shaken (200 rpm, 25-26°C) for 360 minutes. The Pb(II) concentration remaining in solution was determined by ICP-OES.

3.4.3.4 Competitive adsorption of Pb(II) and Cd(II) by HCIX-HFO

A binary stock solution containing 1 mg L Cd(II), 1 mg/L Pb(II) and 3000 mg/L sulphate was prepared, and the solution pH adjusted to pH 4 by the addition of NaOH and HCL. 25 mL aliquots of the binary solution were added to 0.005 g portions of HCIX-HFO and the mixtures shaken (200 rpm, 25-26°C) for 24 hours.

3.4.3.5 Regeneration studies for HCIX-HFO

The exhausted resin obtained from the competitive Pb(II) and Cd(II) adsorption study was used to evaluate the regeneration of HCIX-HFO by NaCl and NaOH respectively Two solutions of 5% NaCl and 1 M NaOH were prepared by weighing appropriate masses of NaCl and NaOH. Exhausted HCIX-HFO was contacted with

either a 5% NaCl or a 1M NaOH solution and shaken (200 rpm, 25-26°C) for 24 hours. After 24 hours the supernatant solutions were analysed for Cd(II) and Pb(II) concentration by ICP-OES.

3.4.3.6 Adsorption of heavy metals with HCIX-HFO from real AMD

A sample of AMD was collected from the Western Witwatersrand mining basin and before conducting the adsorption study the pH was measured and the identity and quantity of metals in solution was determined in triplicate by ICP-OES.

The competitive adsorption was evaluated by adding 25 mL of the AMD to 0.05 g of HCIX-HFO and shaking (200 rpm, 25-26°C) for 360 minutes. On completion of the experiment the supernatant was filtered and the metal concentrations remaining in solution were determined in triplicate by ICP-OES.

3.4.4   Kinetic Modelling

The adsorption kinetics were studied by fitting the data to the pseudo-first-order and pseudo second order kinetic models as well as the intraparticle diffusion model. The kinetic modelling gave information about the mechanisms and rate controlling steps in the adsorption studies.

3.4.4.1 Pseudo-first order kinetic model

The pseudo first order kinetic model is described by equation 3.2 (Ho and McKay, 1999).

$$\frac{d_{qt}}{d_t} = k_1 (q_e - q_t)$$ (3.2)

The linear form of the equation is given by Equation 3.3

$$\log(q_e - q_t) = log q_e - \frac{k_1}{2.303} t$$ (3.3)

Where

- q_e – Amount of metal ion adsorbed per unit mass of adsorbent at equilibrium (mg g^{-1}).

- q_t – Amount of metal ion adsorbed per unit mass of adsorbent (mg g^{-1}) at time (t).

- k_1 – is the first order rate constant for adsorption (L min^{-1}).

- t - time (min)

From the plot of log (q_e – q_t) vs t (Equation 3.3) linear regression was used to obtain the equation that best fits the data. From the equation of the straight line, the calculated adsorption capacity at equilibrium, q_e and k_1 were determined from the intercept and slope, respectively.

3.4.4.2 Pseudo – second order kinetic model

The equation of the pseudo-second order kinetic model is given in equation 3.4 (Ho and McKay, 1999).

$$\frac{d_{qt}}{d_t} = k_2 \, (q_e - q_t)^2 \tag{3.4}$$

The linear expression of the pseudo second order model is given by equation 3.5

$$\frac{t}{q_t} = \frac{1}{k_2 q_e{}^2} + \frac{t}{q_e} \tag{3.5}$$

Where,

- q_e – Amount of metal ion adsorbed per unit mass of adsorbent at equilibrium (mg.g^{-1}).

- q_t – Amount of metal ion adsorbed per unit mass of adsorbent at time, t (mg.g^{-1}).

- k_2 – the rate constant for second-order model adsorption (g mg^{-1} min^{-1})

- t – time (min)

A straight line was obtained from the plot of $\frac{t}{q_t}$ vs t by linear regression. From the equation of the straight line, the slope and intercept gave the values for q_e and k_2 respectively.

3.4.4.3 Intraparticle diffusion model

The intraparticle diffusion model was used to determine the rate limiting step for adsorption (Worch, 2012).

The intraparticle diffusion kinetic model is described by equation 3.6. From the equation, a plot of qt vs t $^{1/2}$ gives series of straight lines. The initial straight line describes intra-particle diffusion where the slope is used to determine the K_{ID} and the intercept indicates the boundary layer thickness.

$$q_t = K_{ID} \, (t^{0.5})$$
(3.6)

Where,

- q_t - amount of metal ion adsorbed per unit mass of adsorbent at time, t $(mg.g^{-1})$

- K_{ID} – the intraparticle diffusion rate constant $mg.g^{-1}.min^{0.5}$

- t – time (min)

3.4.5   Isotherm studies

Equilibrium isotherm data obtained by contacting the adsorbate with varying masses of adsorbent were fitted to the Freundlich, Langmuir and the Temkin isotherm models.

3.4.5.1 Freundlich isotherm model

The Freundlich isotherm is applicable when the adsorbate interacts with the adsorbent, and the adsorption is not restricted by monolayer formation, and the surface of the adsorbent is heterogeneous. The heterogeneous surface is assumed to consist of sites with different adsorption potentials. The formula for the Freundlich isotherm is given by the equation 3.7 (Foo and Hameed, 2010).

$$q_e = K_f \, C_e^{\frac{1}{n}}$$
(3.7)

Where:

q_e - is the amount of metal ion (mg) adsorbed per unit mass of adsorbent (g) at equilibrium (mg.g^{-1})

C_e - is the concentration of metal remaining in solution at equilibrium (mg.L^{-1})

K$_f$ - is the strength of adsorption (L.g^{-1})

n - is related to the heterogeneity of the adsorbent surface.

The linear equation is expressed as shown equation 3.8

$$\log q_e = \log K_f + \frac{1}{n}\log C_e \qquad (3.8)$$

From the plot of log q$_e$ vs log C$_e$, linear regression is used to obtain the equation of the straight line. The values of K$_f$ and n are determined from the intercept and slope, respectively. The higher the value of K$_f$, the higher the adsorption loading. Mostly n can be any value: when n < 1 shows relatively high adsorbent loadings at low concentrations, when n > 1 the isotherms are unfavourable.

3.4.5.2 Langmuir isotherm model

The Langmuir isotherm model assumes that there is a finite number of active sites which are homogeneously and consistently distributed over the surface of the adsorbent. The Langmuir isotherm is expressed in equation 3.9 (Foo and Hameed, 2010).

$$q_e = \frac{q_{max} \cdot K_L \, C_e}{1 + K_L \, C_e} \qquad (3.9)$$

Where,

- q_e is amount of adsorbate adsorbed per unit mass of adsorbent at equilibrium (mg.g^{-1}).

- C$_e$ is equilibrium concentration (mg.L^{-1}).

- q_{max} is maximum adsorption capacity at monolayer coverage (mg.g^{-1}).

- K_L is the equilibrium constant related to the energy of adsorption L g^{-1}.

The linear form of the Langmuir equation is given by equation 3.10.

$$\frac{C_e}{q_e} = \frac{C_e}{q_{max}} + \frac{1}{K_L\, q_{max}}$$ (3.10)

The plot of $\frac{C_e}{q_e}$ vs C_e provides a straight line, where values of q$_{max}$ and K$_L$ are determined from the slope and intercept, respectively.

3.4.5.3 Temkin isotherm model

The Temkin isotherm is expressed in equation 3.10. It assumes that the adsorption is characterised by uniform binding energy up to a maximum value and the heat of adsorption decreases in a linear manner. The Temkin isotherm model is represented in equation 3.11 (Foo and Hameed, 2010).

$$q_{e\,=}\ \frac{RT}{b}\,Ln(A.\,C_e)$$ (3.11)

Where,

- q_e is mass of metal ion adsorbed per unit mass of adsorbent at equilibrium (mg.g^{-1}).

- C_e is equilibrium concentration (mg.L^{-1}).

- b is the Temkin constant

- R universal constant (8.314 J/mol.K)

- T absolute temperature (K).

The linear form of the Temkin model is given by equation 3.12

$$q_e = \frac{RT}{b}\ln(A) + \frac{RT}{b}\ln C_e$$ (3.12)

The plot of q_e vs $\ln C_e$ gives a straight line where values of the constants, A and b, are determined from the slope and intercept respectively.

3.5   References

Foo, K.Y. and Hameed, B.H., 2010, Insights into the modelling of adsorption isotherm data. Chemical Engineering Journal., 156(1), pp. 2-10.

Ho, Y.S. and McKay, G., 1999. Pseudo-second order model for sorption processes. Process biochemistry, 34(5), pp.451-465

Pan, B., Wu, J., Pan, B., Lv, L., Zhang, W., Xiao, L., Wang, X., Tao, X. and Zheng, S., 2009. Development of polymer-based nanosized hydrated ferric oxides (HFOs) for enhanced phosphate removal from waste effluents. Water Research, 43(17), pp.4421-4429.

Worch, E., 2012. Adsorption technology in water treatment: fundamentals, processes, and modeling. Walter de Gruyter.

CHAPTER 4
RESULTS AND DISCUSSION

This chapter discusses the observations and results obtained for the characterization and application of the hybrid resins. The adsorption trends and mechanism models responsible for the adsorption patterns are also narrated.

4.1   Characterization of hybrid ion exchange resins embedded with hydrous ferric oxide nanoparticles

4.1.1   SEM-EDS characterization of HAIX-HFO

Figure 4.1 a) depicts the SEM image for a cross section of a HAIX-HFO bead (magnification of 14000). The image showed white particles which indicated the HFO nanoparticles to be uniformly dispersed through the interior of the IRA 400 Cl form resin. In the SEM image very little agglomeration of HFO was observed.
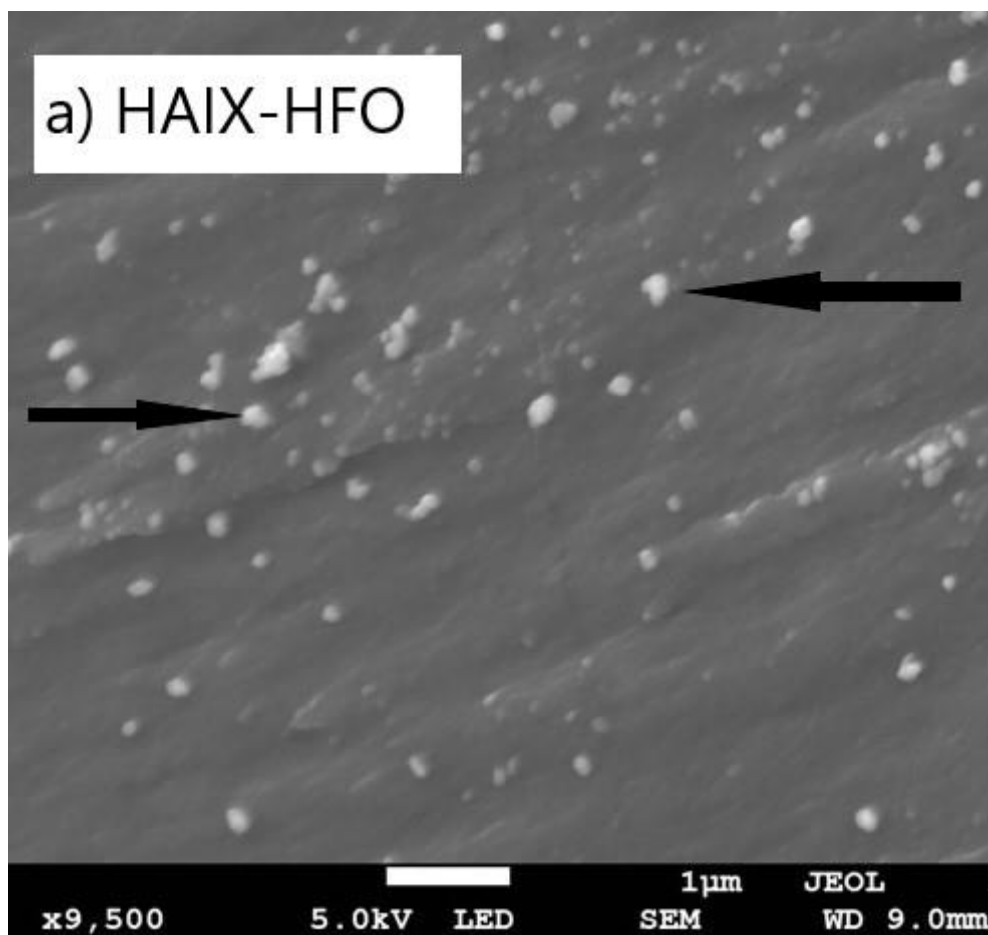
Figure 4.1: a) SEM image for cross section of HAIX-HFO resin bead.

Figure 4.1 b) showed the EDS spectrum of a cross section HAIX-HFO resin bead. In the spectrum bands at approximately 0.7 KeV and at 6.5 KeV are due to Fe, which showed the presence of the incorporated HFO nanoparticles. The presence of Cl indicated that the fixed quaternary ammonium ion exchange sites of the parent resin were in the chloride form. The presence of Au was due to coating of the surface prior to analysis. The EDS also indicated the weight % of Fe to be 4.4%. This was lower than the 14 % reported by De Kock (2015).
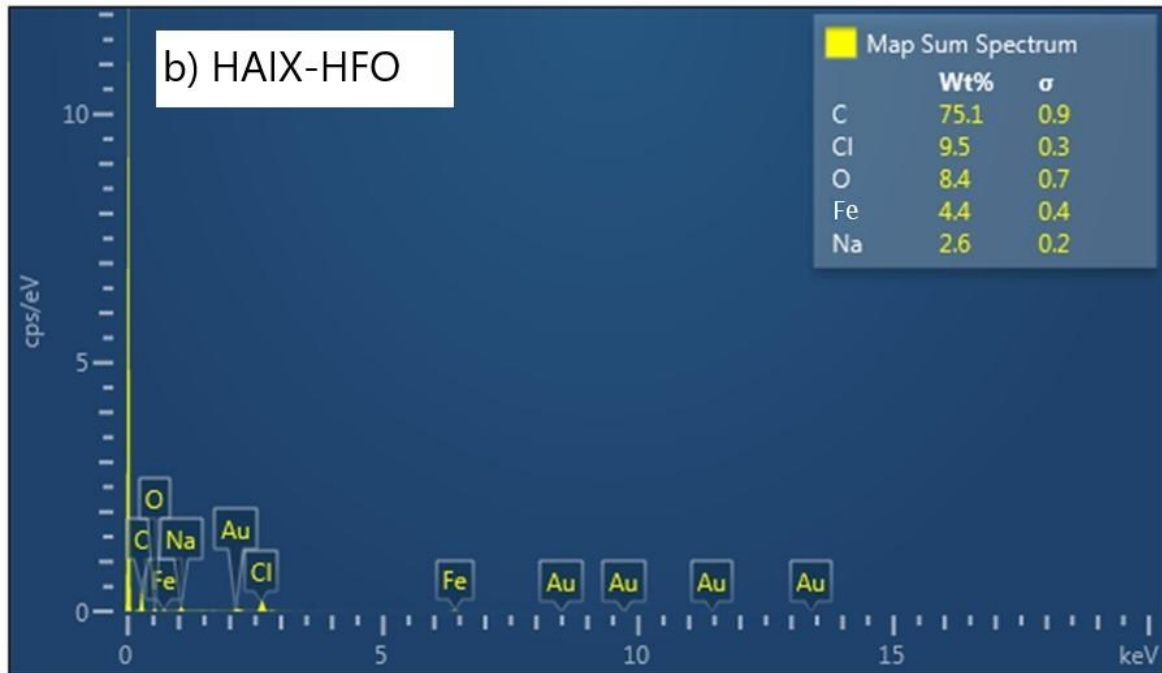
Figure 4.1: b) EDS spectra of cross section HAIX-HFO resin bead.

4.1.2   SEM-EDS characterization of HCIX-HFO

Figure 4.2 shows the HCIX-HFO SEM image in which white particles were observed at a magnification of 9500. The observed white particles were the incorporated hydrous ferric oxide nanoparticles which showed a good dispersion with some agglomeration.
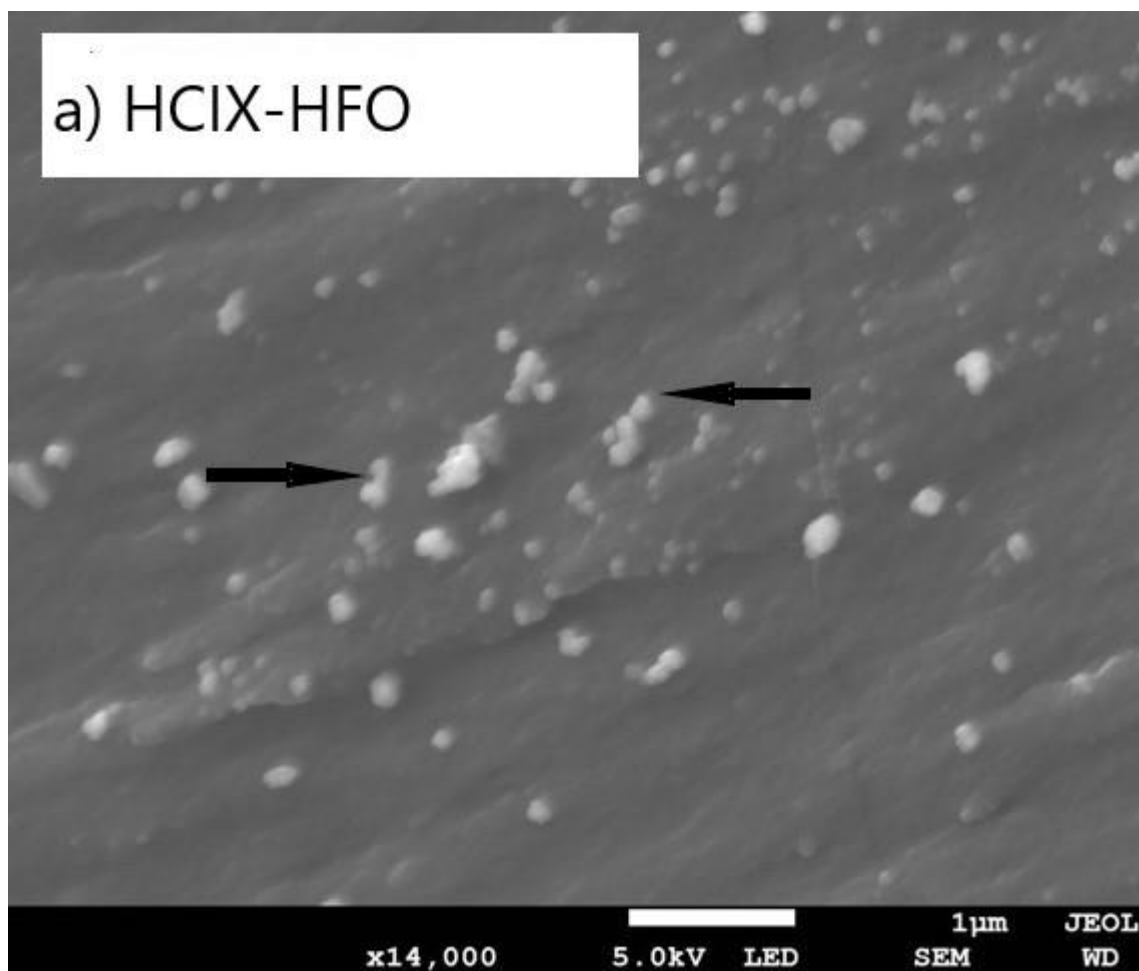
Figure 4.2: a) SEM image for cross section of HCIX-HFO resin bead.

Figure 4.2 b) shows the EDS spectrum of HCIX-HFO. The incorporation of the HFO was proven by the presence of bands at 0.6 KeV and at 6.5 KeV which were due to Fe. The presence of Na indicated that the fixed sulphonates ion exchange sites of the parent resin were in the Na form. The sulphur observed at 2.3 KeV was due to the sulphonates of the parent resin. The weight % of Fe was 14.9. This was found to be comparable with the results reported by De Kock (2015) were Fe was reported to be 14 % for a hybrid anion exchanger.

Figure 4.2: b) EDS spectra of cross section HCIX-HFO resin bead.

4.1.3 Determination of Iron oxide species in HAIX-HFO and HCIX-HFO by Raman spectroscopy

Raman spectroscopy was used to distinguish the types of iron oxide incorporated in the HAIX-HFO and HCIX-HFO. Figure 4.3 shows the Raman spectra for HAIX-HFO, with bands that were positioned at 309 cm^{-1}, 493 cm^{-1}, 576 cm^{-1},720 cm^{-1} and 1727 cm^{-1}. Figure 4.4 shows the Raman spectra for HAIX-HFO, with bands positioned at 309 cm^{-1}, 511 cm^{-1} and 1770 cm^{-1}.
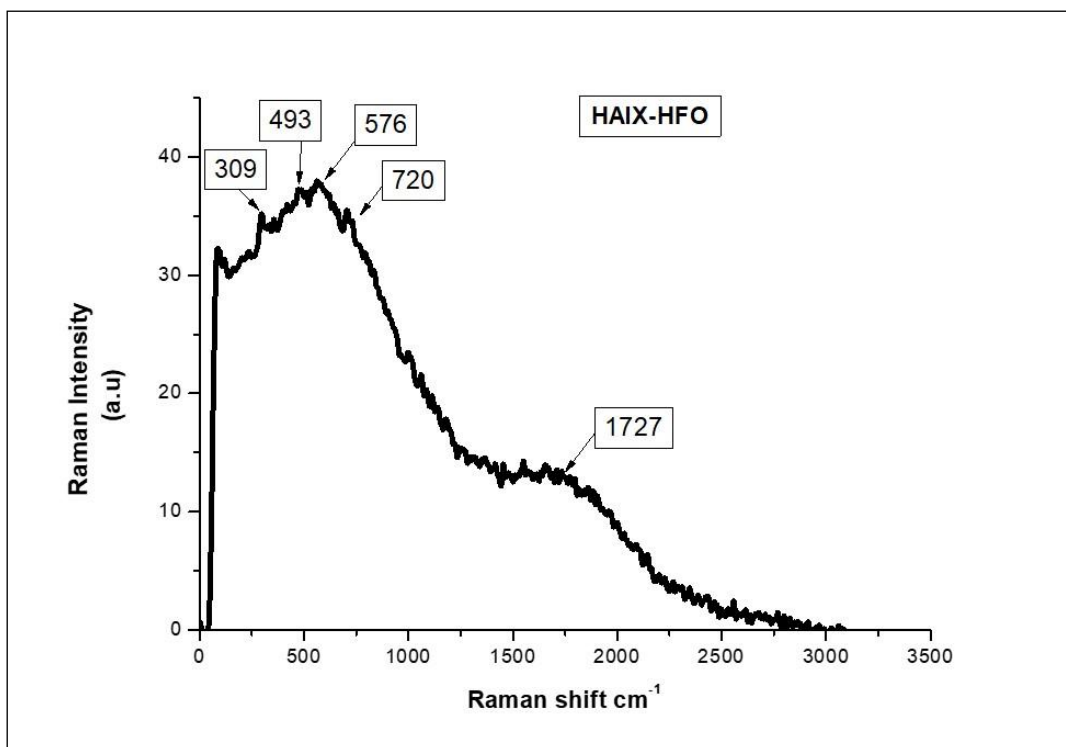
Figure 4.3: Raman spectra for HAIX-HFO.
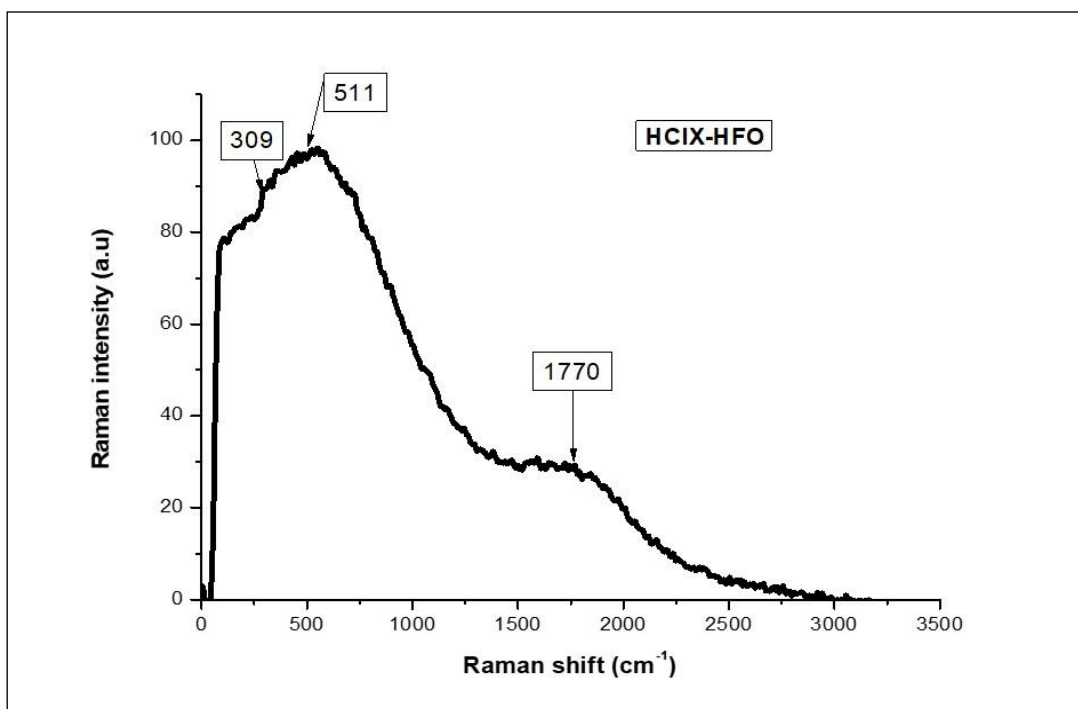
Figure 4.4: Raman spectra for HCIX-HFO.

64

HFO bands reported as being characteristic of ferrihydrite were compared to the bands found for HAIX-HFO (Figure 4.3) and HCIX-HFO (Figure 4.4) (Table 4.1). The Raman bands characteristic of ferrihydrite are found at 370, 510 and 710 cm^{-1} (Cornell and Schwertmann, 2003; Hanesch, 2009). Das and Hendry (2011) reported bands at 361, 508, 707 and 1045 cm^{-1}. The band at 720 cm^{-1} for HAIX-HFO corresponds to the primary diagnostic band for ferrihydrite at 710 cm^{-1}. For HCIX-HFO the band at 511 cm^{-1} corresponds to the ferrihydrite band at 510 cm^{-1}. Both HAIX-HFO and HCIX-HFO consists of a resin matrix made up of an organic backbone, which results in significant fluorescence which largely obscures the Raman bands. This fluorescence makes a definitive determination of the iron oxide phase difficult.

Table 4.1: Characteristics Raman bands.

Iron Oxide	Raman bands (cm^{-1})	Reference
Ferrihydrite	370; 510; 710	Hanesh, 2009 Cornell and Schwertmann, 2003
	361; 508; 707; 1045	Das and Hendry, 2011
HAIX-HFO	309; 493; 576; 720; 1727	This study
HCIX-HFO	309; 511; 1770	This study

4.2 Batch adsorption studies

Batch adsorption studies were conducted to determine the influence of pH, contact time and adsorbent dosage on the adsorption of Cr(VI), Cd(II) and Pb(II). The results from the contact time and adsorbent dosage studies were subjected to kinetic modelling and isotherm modelling. The effect of co-competing sulphate on Cr(VI) adsorption, the competitive adsorption of Cd(II) and Pb(II), adsorption of metals from real AMD as well as the regeneration of exhausted HCIX-HFO are also presented.

4.2.1 Batch adsorption studies for adsorption of Cr(VI) with HAIX-HFO

The choice of HAIX-HFO for the adsorption of Cr(VI) was based on the anionic nature of HAIX-HFO matrix which will reject cationic species and only adsorb anionic species. As Cr(VI) exists predominately as $HCrO_4^-$ and $Cr_2O_7^{-2}$ at pH less 5 (Figure 2.1) it is expected that the anionic hybrid exchanger will adsorb Cr(VI).

4.2.1.1 Effect of pH for adsorption of Cr(VI) by HAIX-HFO

The pH of an aqueous solution affects the adsorption as it impacts the speciation of the adsorbate. The speciation of chromium determines whether it will be adsorbed by anionic or cationic adsorbents. Chromium exist in two oxidation states in aqueous systems, that is Cr(VI) and Cr(III), that have different charges. Cr(VI) only exists in strongly acidic solution as $Cr_2O_7^{2-}$ and $HCrO_4^-$. At lower pH, both species have higher removal efficiency by ion exchange resins (Balasubramanian and Pugalenthi, 1999). Ferric oxides are amphoteric, that is, they are able to react as both an acid or a base. This amphoteric nature is also dependent on the pH. Therefore, it is important to determine the pH at which maximum Cr(VI) removal occurs.

The effect of pH on Cr(VI) adsorption by HAIX-HFO is shown in Figure 4.5. The removal of Cr(VI) increased slightly from pH 2 to 4, with removal increasing from 89 % to 99% respectively. At pH >4, the removal of Cr(VI) decreased. At pH 5, the removal of Cr(VI) was 77%, which is a 23% decrease from the higher capacity at pH 4. The decrease might be due to reduction of Cr(VI) at high pH, in which Cr(VI) was continually being reduced to Cr(III) and anion exchange resins were no longer applicable for its removal (Xiao et al., 2016). Also, the adsorption of Cr(VI) was favoured at acidic conditions because when the pH increases the concentration of OH^- (hydroxyl ion) increases which competes for the adsorption sites on the ferric hydroxide nanoparticle surface (Polowczyk et al., 2016). Therefore, there was competition between OH^- and Cr(VI) ($Cr_2O_7^{2-}$ or $HCrO_4^-$) for adsorption sites. A study by Hua (2017) also reported that adsorption of Cr(VI) with a macroporous anion exchange resin immobilized with nanoscale hydrous ferric oxide was favoured at acidic pH, with adsorption of Cr(VI) decreasing steadily as the pH increased from 3

to 9. It was concluded that hybrid anion exchange resins embedded with HFO nanoparticles was applicable for Cr(VI) adsorption from acidic aqueous media.
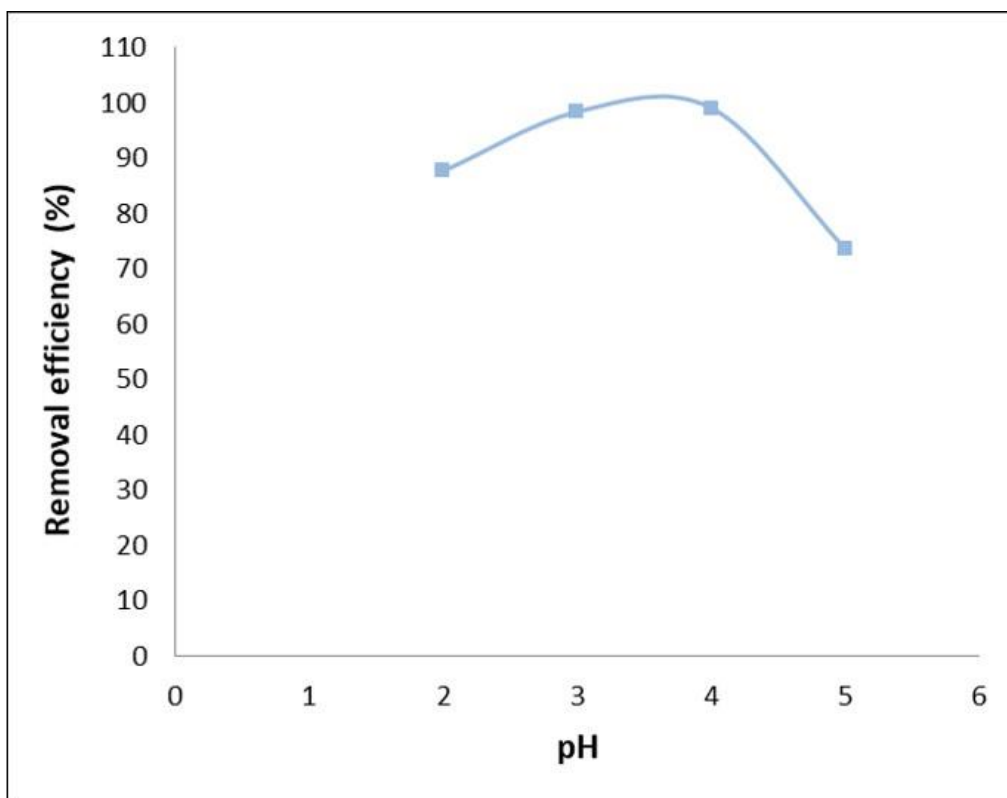
Figure 4.5: Effect of pH on %Cr(VI) removal by HAIX-HFO.

4.2.1.2 Effect of sulphate on Cr(VI) adsorption by HAIX-HFO

In AMD, sulphate is present in concentrations much greater than Cr(VI) (DWA, 2013). It was therefore necessary to look at the competitive adsorption of sulphate with Cr(VI). Sulphate exists as a divalent anion which offers greater competition to Cr(VI) (Blaney et al., 2007). Previous studies (Acelas *et. al.*, 2015) showed that sulphate significantly reduced the adsorption of phosphate by a hybrid anion exchanger with encapsulated ferric oxide. Several reports have included the effect of co-competing sulphate and other anions on the adsorption of Cr(VI) by anion exchangers with encapsulated HFO (Hua *et.al.*, 2017; Kołodyńska *et.al.*, 2015; Kowalczyk *et.al.*, 2013). However, in all of these studies, single fixed concentrations of sulphate (40 – 50 mg/L) were used. It was therefore important to determine what effect increasing sulphate concentration had on Cr(VI) adsorption.

The effect of increasing sulphate concentration on the removal of Cr(VI) by HAIX-HFO given in Figure 4.6. The percentage of Cr(VI) adsorbed decreased rapidly as the sulphate concentration increased from 0 mg/L (100% Cr(VI) adsorbed) to a sulphate concentration of 1000 mg/L (60.8% Cr(VI) adsorbed). At higher sulphate concentrations the decrease in Cr(VI) adsorption levelled off, with a further 3-fold increase of sulphate concentration (to 3000 mg/L) only resulting in a further 10% reduction in Cr(VI) adsorption. As the average sulphate(SO_4^{2-}) concentration of AMD from the Witwatersrand mining basin is approximately 3000 mg/L (DWA, 2013), the results show the applicability of being used at a sulphate concentration of 3000 mg/L as a competitor ion to further investigate the applicability of HAIX-HFO for the adsorption of 1 mg/ L of Cr(VI). The adsorption of Cr(VI) decreased in the presence of sulphate because of enhanced competition for the adsorption sites of the HAIX-HFO. HAIX-HFO consists of two types of adsorption sites with two different adsorption mechanisms. These are the fixed quaternary ammonium ion exchange sites from the ion exchange resin and the ligand exchange sites of the embedded HFO. The mechanism of adsorption of the quaternary ammonium groups occurred through ion exchange where the Cl^- counter ion is exchanged with Cr(VI) or sulphate. The HFO nanoparticles adsorb through ligand exchange mechanism.

When sulphate was present at concentrations ranging from 0 to 1000 mg/L, the adsorption of Cr(VI) decreased because the quaternary ammonium sites were being saturated with sulphate. After 1000 mg/L SO_4^{2-}, Cr(VI) adsorption remained relatively constant because Cr(VI) was being adsorbed by the HFO adsorption sites and were not being replaced by sulphate. Also, sulphate has been reported to be adsorbed through the quaternary ammonium groups as it only forms outer sphere complexes with the embedded HFO (Blaney et al, 2007). At which site the Cr(VI) will be adsorbed depends on the identity of the competitor ion. Cr(VI) has been reported to be adsorbed by the anion exchange sites provided by quaternary ammonium groups in a hybrid anion exchanger (Hua et al., 2017).
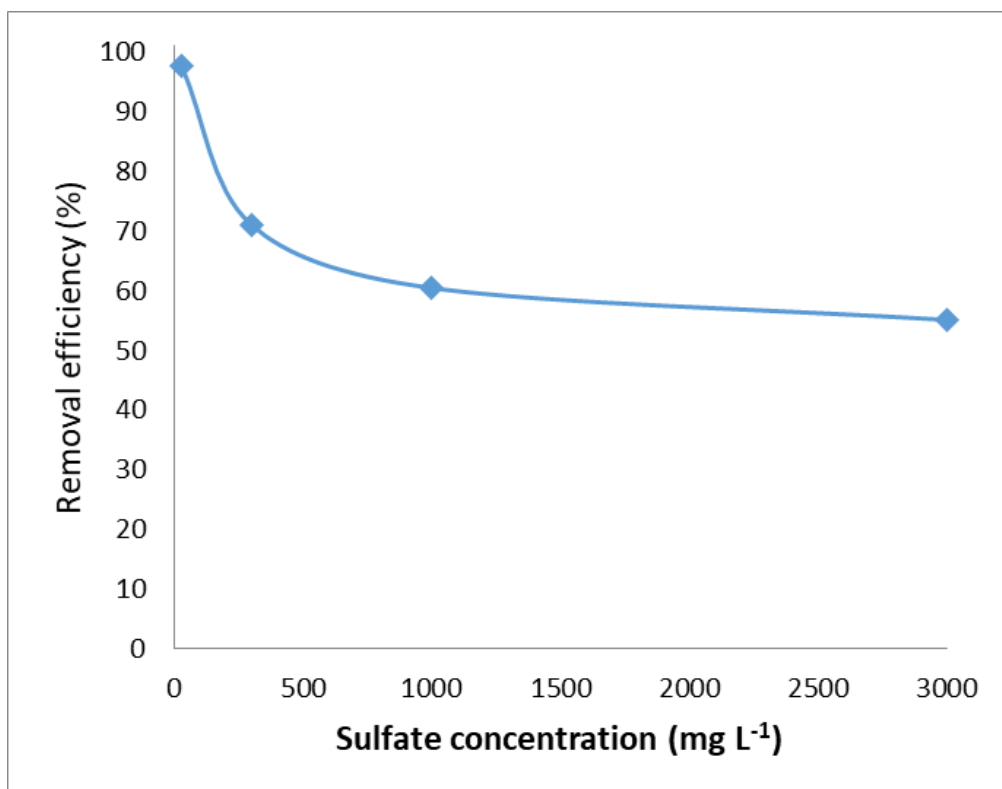
Figure 4.6: Effect of sulphate concentration on the removal of Cr (VI) with HAIX-HFO.

4.2.1.3 Effect of contact time on Cr(VI) adsorption in the absence and presence of sulphate.

The removal of Cr(VI) is affected by time required for the saturation of the adsorption sites of HAIX-HFO. It was therefore important to determine the contact time to reach maximum adsorption of Cr(VI) ions by HAIX-HFO and hence equilibrium.

The effect of contact time on the adsorption of Cr(VI) by HAIX-HFO with and without sulphate is given in Figure 4.7. In the absence of sulphate the initial adsorption of Cr(VI) was rapid until 180 minutes. After 180 minutes' adsorption slowed down significantly but did not reach a constant state. From the data a contact time of 360 minutes was found to be sufficient for equilibrium to be reached. With sulphate present, rapid adsorption only occurred in the first 60 minutes. Between 60 and 180 minutes the rate of adsorption slowed down and equilibrium was reached after 240 minutes.

The shorter time required to reach equilibrium for Cr(VI) removal with co-competing sulphate may have been due to the fast kinetics provided by the HFO nanoparticles (Chattopadhyay et al 2014). When no sulphate was present, Cr(VI) was adsorbed by the quaternary ammonium exchange sites as well as the ion exchange sites. This lead to a higher Cr(VI) removal capacity as there was no competition for either adsorption sites. However, the required contact time was longer for Cr (VI) in the absence of sulphate due to adsorption in the anion exchange sites. The contact time for all further studies was taken to be 360 minutes to ensure complete adsorption.
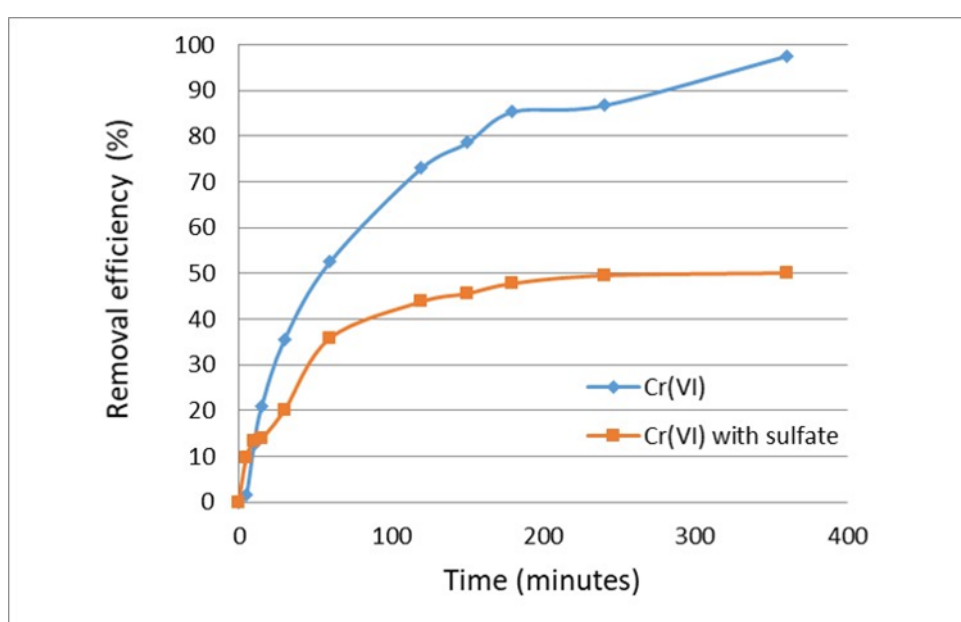
Figure 4.7: Percentage removal efficiency for Cr(VI) with increasing contact time.

4.2.1.4 Effect of HAIX-HFO dosage on Cr(VI) adsorption

There is a dependence between adsorbent dosage and the concentration of the pollutant to be removed. It was therefore important to determine what dosage will provide maximum removal of Cr(VI). The effect of HAIX-HFO dosage on the adsorption of Cr(VI) with and without sulphate is given in Figure 4.8. In both cases the percentage removal of Cr(VI) increased as the dosage of HAIX-HFO increased. For 1 mg/L Cr(VI) without sulphate, 100% adsorption was achieved with a HAIX-HFO dosage of 0.005 g when contacted with 25 mL of Cr(VI) solution. For the adsorption of 1 mg/L Cr(VI) combined with 3000 mg/L sulphate, a much higher mass

of HAIX-HFO was required to reach the maximum Cr(VI) removal. As sulphate competes with Cr(VI) for the adsorption sites, a higher dosage of HAIX-HFO was required. That is, as the dosage of HAIX-HFO increased, the number of available adsorption sites for Cr(VI) adsorption increased. The percentage adsorption reached a point at which 100% adsorption of Cr(VI) was attained. That point was taken as the optimum mass at 0.005 g.
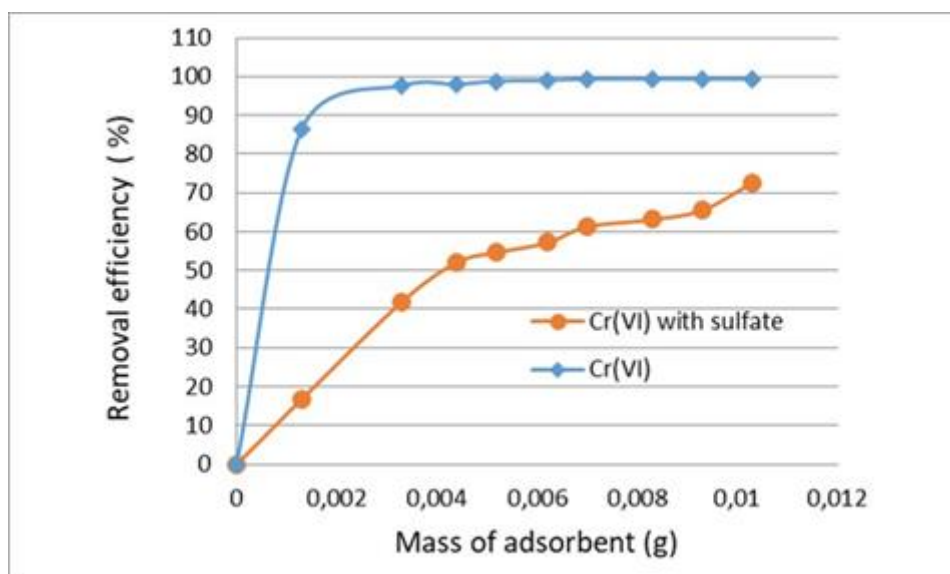
Figure 4.8: Percentage removal efficiency for Cr(VI) with increasing HAIX-HFO dosage.

4.2.1.5 Kinetic modelling of Cr(VI) adsorption with HAIX-HFO

Kinetic modelling was investigated to clarify the mechanism of adsorption as well as the rate limiting mass transfer mechanisms for Cr(VI) adsorption. The parameters obtained from fitting the kinetic data obtained with and without sulphate as a competitor ion to the pseudo-first-order kinetic and pseudo-second-order kinetic models are given in Table 4.2. The pseudo-second-order kinetic model was found to have the highest correlation coefficient (R^2). Both calculated q_e values obtained for Cr(VI) alone and for Cr(VI) with sulphate obtained from the pseudo-second-order kinetic model are a closer match to the experimental q_e than that obtained from fitting the data to the pseudo-first order model. The results agreed with what was reported for Cr(VI) adsorption by a commercial, polystyrene microporous HFO anion exchange resin (Kołodyńa *et.al.*, 2015). However, Kowalczyk (2015) and Hua (2017)

reported that Cr(VI) was described by pseudo-first order kinetics from binary solutions.

As the pseudo-second order model was better at describing the kinetic data obtained from the adsorption of Cr(VI) by HAIX-HFO with and without sulphate, it was concluded that the adsorption mechanism in both cases is chemisorption, where there is a sharing or exchange of valence electrons between Cr(VI) and the exchange groups of HAIX-HFO (Ho and McKay, 1999).

Table 4.2: Modelled pseudo-first order and pseudo-second order kinetic parameters for Cr(VI).

C_o (Cr(VI)) (mg/L)	Sulphate (mg/L)	$q_{e.exp}$ (mg g^{-1})	Pseudo-first-order kinetic model			Pseudo-second-order kinetic model		
			K_1 (min^{-1})	$q_{e1.cal}$ (mg g^{-1})	R^2	K_2 (g min^{-1}mg^{-1})	$q_{e2.cal}$ (mg g^{-1})	R^2
1.00	0	4.91	0.006	2.97	0.5784	0.002	5.79	0.9856
1.00	3000	2.22	0.006	1.02	0.1898	0.013	2.47	0.9929

The kinetic data was fitted to the Intraparticle diffusion model in order to determine the rate limiting mass transfer mechanism. Parameters obtained for the intraparticle diffusion model for adsorption of Cr(VI) alone and with sulphate as a competitive ion are given in Table 4.3. Diffusion can be explained to occur in three stages, the first stage is film diffusion were the sorbate moves from the bulk solution through the boundary layer surrounding the sorbent particle. The second stage was diffusion of the sorbate into the pores of the sorbent. The final stage was a very slow step that occurs when the sorbate is migrating into the micropores of ion exchange resin (Worch, 2012).

Data fitted to the intraparticle diffusion model for Cr(VI) adsorption by HAIX-HFO in the absence of sulphate gave a graph that showed two stages of adsorption. The first stage showed a linear increase in the amount of Cr(VI) removed due to diffusion

into the pores of the exchanger. The next stage, where Cr(VI) removal slows down was probably due to diffusion into the micropores of the exchanger and interaction between Cr(VI) and the exchange sites within the pores.

The intraparticle diffusion for Cr(VI) when sulphate was present also occurred in two stages. The first linear region was attributed to the diffusion of Cr(VI) into the pores and along the pore walls of the sorbent. The second stage was the diffusion into the micropores of the HAIX-HFO and exchange with the ion-exchange sites. The major difference between the two was the decrease in rate of intraparticle diffusion (K_{ID}) when sulphate is present.

In the absence of sulphate, the intraparticle diffusion rate (K_{id} = 0.4323 mg.g^{-1}.min$^{0.5}$) indicated that diffusion occurred at a faster rate compared to that in the presence of sulphate (K_{id} = 0.1524 mg.g^{-1}.min$^{0.5}$). The Boundary Layer Thickness (BLT) value for the adsorption of Cr(VI) in the absence of sulphate was lower (-0.8608 min$^{0.5}$) than that in the presence of sulphate (0.1045 min$^{0.5}$). This was an indication that the contribution of surface adsorption by sulphate to the rate limiting step was greater as compared to that of Cr(VI) only (Koushkbaghi., 2018).

Table 4.3: Intraparticle diffusion model parameters for Cr(VI) adsorption with HAIX-HFO.

Initial Cr(VI) mg/L	Initial sulphate mg/L	K_{ID} (mg g^{-1}.min$^{0.5}$)	BLT	R^2
1.00	0	0.4323	-0.8608	0.9735
1.00	3000	0.1524	0.1045	0.9794

4.2.1.6 Isotherm modelling of Cr(VI) removal by HAIX-HFO

Fitting of the Cr(VI) isotherm data to the three isotherm models was done in order to clarify the mechanism of adsorption. The data was fitted to the linear form of each

model and the closeness of fit determined by least squares regression. The parameters obtained from fitting Cr(VI) isotherm data to the Langmuir, Freundlich and Temkin isotherm models is given in Table 4.4. The closeness of fit for each isotherm model to the experimental data was determined by comparison of the correlation coefficients (R^2). The adsorption isotherm data for Cr(VI) in the absence of sulphate was a fit to the Langmuir isotherm, with R^2 being slightly higher than that obtained for the other two models. The Langmuir model assumes that mono layer adsorption occurs with the sorbate binding with a limited number of adsorption sites that have the same energy (Dada et al., 2012).

Parameters obtained from fitting the data to the isotherm models where then used to calculate adsorption capacities predicted by each model. These calculated capacities from each model were then compared to the experimentally determined capacity data (Figure 4.9 and Figure 4.10). The modelled capacity values that lies closest to the experimental line is assumed to best describe the experiment. For the adsorption of Cr(VI) without sulphate (Figure 4.9) the obtained results corresponded with what was concluded from the correlation coefficients, that the Langmuir isotherm best describes the adsorption of Cr(VI) in the absence of sulphate. From the Langmuir constant (K_L), a dimensionless separation factor (R_L) can be calculated using Equation 4.1

$$R_L = \frac{1}{1+K_L.C_o}$$ (4.1)

Where K_L is the calculated Langmuir constant and C_o is the initial concentration of adsorbate.

The R_L values are interpreted in the following way:

$R_L > 1 \rightarrow$ adsorption is unfavourable

$R_L = 1 \rightarrow$ adsorption is linear

$R_L < 1 \rightarrow$ adsorption is favourable

$R_L = 0 \rightarrow$ adsorption is irreversible

For the adsorption of Cr(VI) in the absence of sulphate, the R_L value is 0.0467, indicating that the adsorption is favourable.

For Cr(VI) adsorption in the presence of sulphate, the isotherm data was best fitted with the Temkin isotherm model. However, this contradicted to what was reported by Kowalczyk (2015) where Cr(VI) adsorption from a complex solution was best described by the Langmuir model. The Temkin model considers adsorbate-adsorbent interactions and uniform binding energies. It also assumes that the heat of adsorption (ΔH_{Ads}) decreases in a linear manner as a consequence of increasing surface coverage (Ayawei *et. al.,* 2017).

Comparison of calculated q_e values obtained by applying the calculated parameters for each model (Figure 4.10) showed that the Temkin and Langmuir models for Cr(VI) adsorption when sulphate was present best describe the experimental data. However, the line that has more points that touch on the experimental line is that of the Langmuir isotherm. This is despite the very low product moment correlation coefficient obtained ($R^2 = 0.4218$). The results suggested that there was possible monolayer coverage of Cr(VI) on the surface of the HAIX-HFO.

Table 4.4: Modelled Freundlich, Langmuir and Temkin parameters for Cr(VI) adsorption.

Initial Cr(VI) (mg/L)	Sulphate (mg/L)	Freundlich			Langmuir			Temkin		
		K_f (L g^{-1})	N	R^2	q_{max} (mg/g)	K_L (L/mg)	R^2	A (L/g)	B (J/mol)	R^2
1.00	0	61.2	1.7	0.9643	25.1	18.14	0.9764	223	494	0.9635
1.00	3000	4.48	1.3	0.8438	8.88	0.83	0.4218	8.9	1357	0.8505
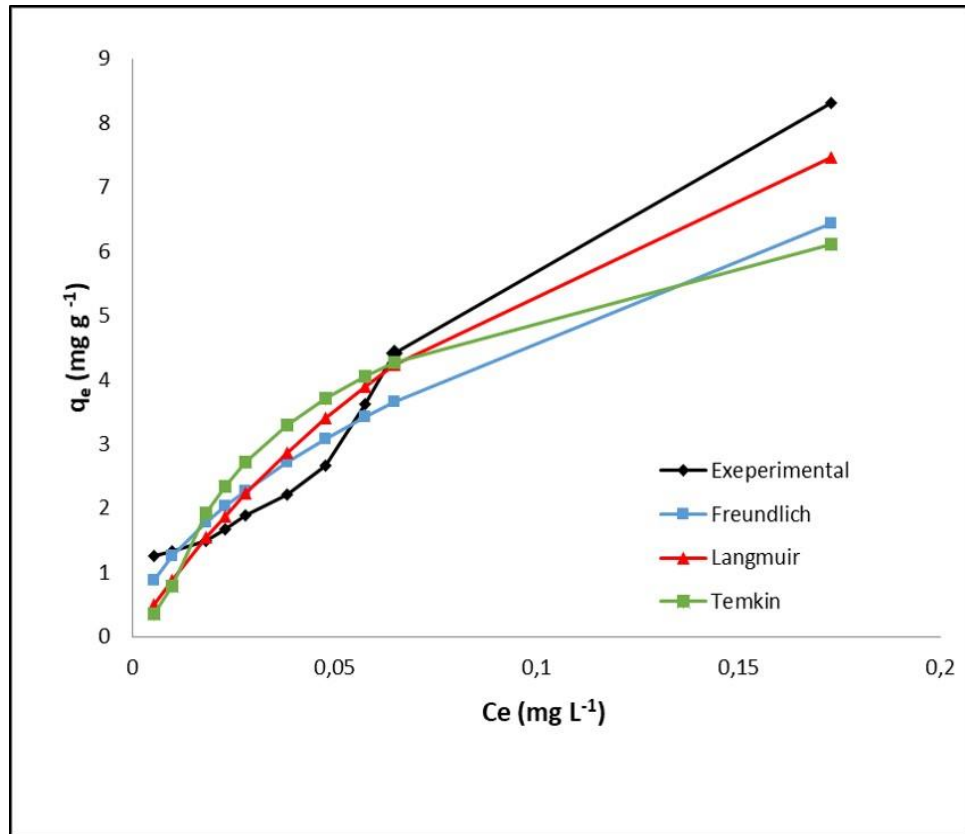
Figure 4.9: Comparison of modelled adsorption capacities from Langmuir, Freundlich and Temkin models and experimental data for Cr(VI) in the absence of sulphate.
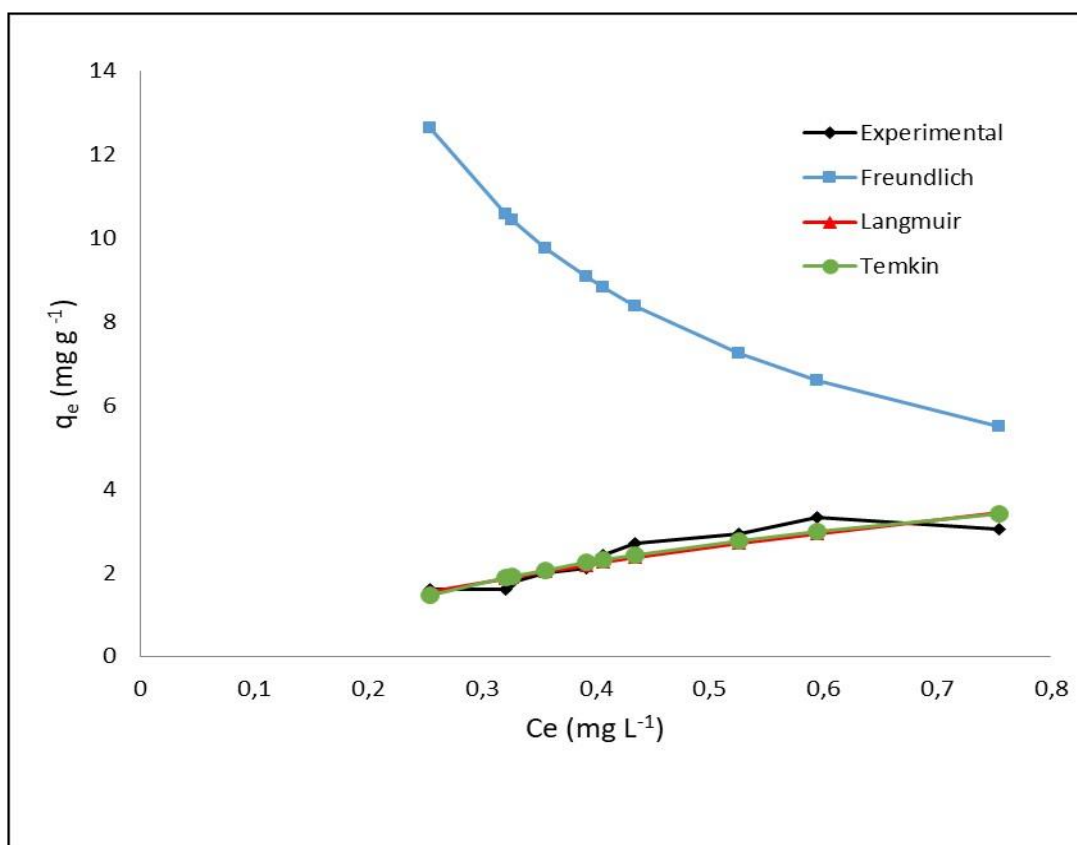
Figure 4.10: Comparison of modelled adsorption capacities from Langmuir, Freundlich and Temkin models and experimental data for Cr(VI) in the presence of sulphate.

4.2.2 Batch adsorption studies for Cd(II) with HCIX-HFO

HCIX-HFO was employed for Cd(II) and Pb(II) adsorption studies as the cationic exchange sites of the strong acid cation exchange resin matrix will result in attraction of the positively charged Cd(II) and Pb(II) ions. Cd(II) adsorption by unmodified cation exchange resins has been reported (Fei *et al.*, 2009; Pehlivan and Altun, 2006; Wong *et al.,* 2014). No report of the adsorption of Cd(II) by a hybrid cation exchange resin was found.

4.2.2.1 Effect of pH on the adsorption of Cd(II) with HCIX-HFO

The effect of pH on Cd(II) adsorption in the absence of sulphate shown in Figure 4.11. The removal efficiency of HCIX-HFO for Cd(II) was found to be at a maximum between pH 3 to 4 with 94% and 98% removal respectively, at pH 5 the removal

was 84%. Reports on the effect of pH on Cd(II) adsorption by cation exchange resins are contradictory. Pehlivan and Altun (2006) found maximum Cd(II) adsorption at a pH 8 to 9, and that minimal adsorption occurred at pH less than 4. Fei (2009) found that a pH between 4 and 5 gave the highest adsorption, which was similar to the maximum adsorption reported by Wong (2014) at a pH of 4.5 – 5.5. Minimal adsorption was observed at pH 2.5. Low adsorption of Cd(II) at pH below 4 was considered to be due to competition by hydrogen ions for the cationic exchange sites.

The drastic decrease in Cd(II) adsorption at pH 5 (Figure 4.11) might be due to the speciation chemistry of Cd. Above pH 5.5, $CdHCO_3^+$ ions are formed and possibly compete with Cd(II) free ions (Mislin and Ravera, 1986). Fei (2009) also reported that Cd(II) adsorption decreased after pH 5 which was considered to be as result of the hydrolysis of Cd(II) at pH 5 and higher. The adsorption of Cd(II) by HFO have been reported. In a study by Streat (2008) HFOs were reported to adsorb Cd(II) at pH range of 4-9 due to the HFO surface being negatively charged.
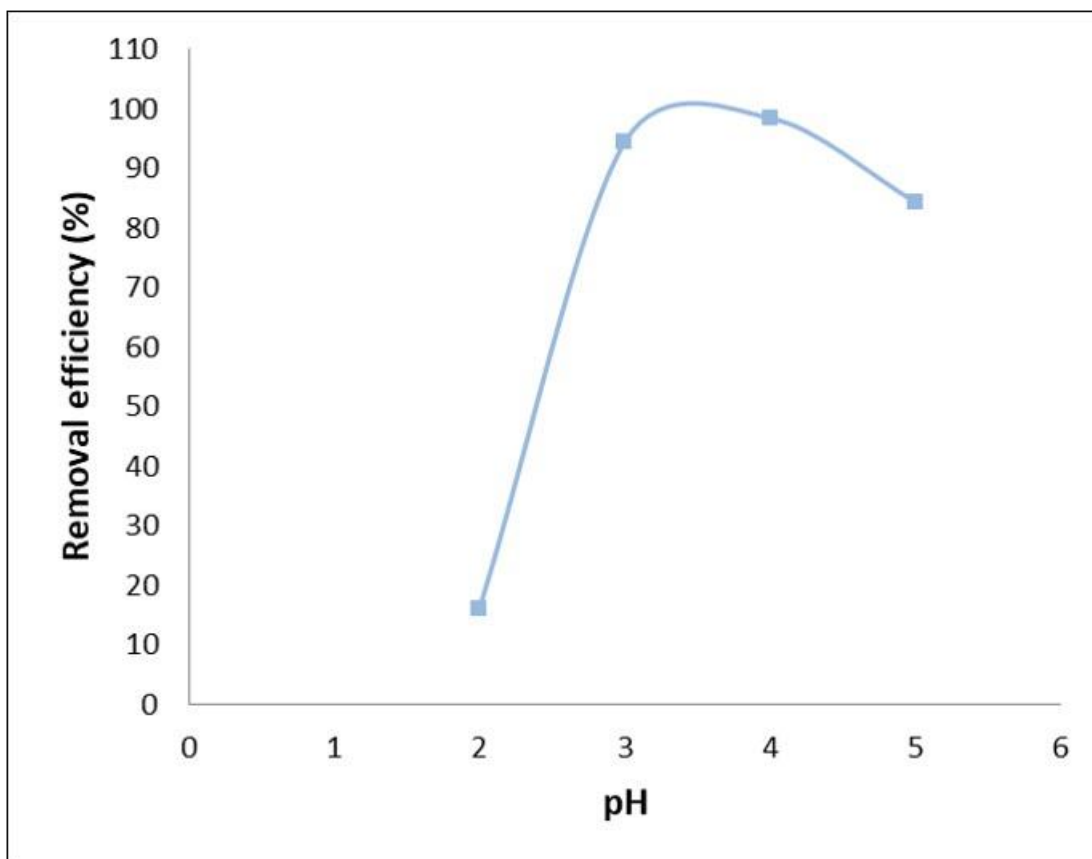
Figure 4.11: Effect of pH on percentage Cd(II) removal with HCIX-HFO.

4.2.2.2 Effect of contact time on adsorption of Cd(II) with HCIX-HFO

The effect of contact time on Cd(II) removal by HCIX-HFO from a 1 mg L^{-1} Cd(II) solution with 3000 mg L^{-1} sulphate at a pH of 4 is shown in Figure 4.12. The removal efficiency of Cd(II) rapidly increased from 0 to 120 minutes, followed by a slower adsorption stage before equilibrium was reached. After 180 minutes the increasing contact time did not result in further Cd(II) adsorption. The maximum removal efficiency was 33% at 360 minutes. It was observed that Cd(II) adsorption was significantly lower when sulphate was present in higher concentrations. There are two possible reasons. The first reason might be due to the use of lower mass for HCIX-HFO compared to the pH study (0.005 g versus 0.05 g). The second possibility being the formation of Cd(II) ternary sulphate complexes (Hoins *et al.,* 1993) that are negatively charged and excluded from the resin matrix by the Donnan membrane effect (SenGuptta, 2017).

The rapid increase in adsorption capacity at the initial contact time was the result of the electrostatic attraction between the metal ions and the oppositely charged exchange sites on the surface of HCIX-HFO. Also the availability of the abundance of active sites on the adsorbent at the start of the adsorption process. As time increases, the rate of removal decreases due to the diffusion into the pores and micropores of HCIX-HFO and as the result of fewer unoccupied binding sites (Wong et al., 2014). After 360 minutes of contact maximum removal was achieved by HCIX-HFO.
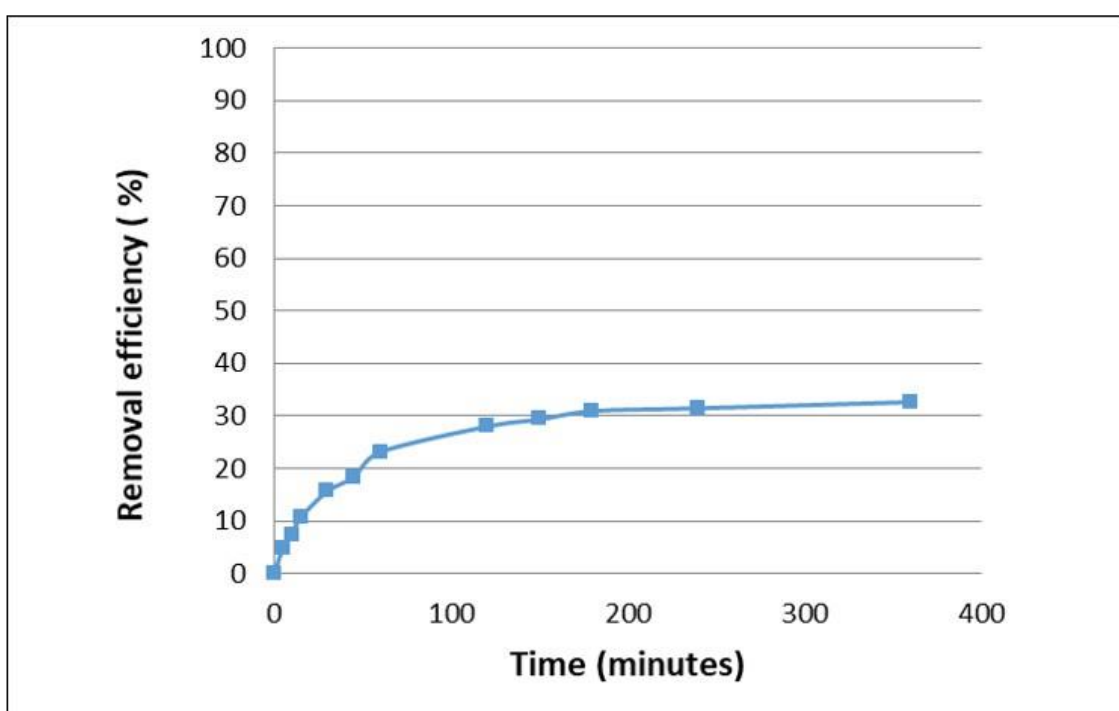
Figure 4.12: Effect of contact time on Cd(II) adsorption by HCIX-HFO.

4.2.2.3 Effect of HCIX-HFO dosage on Cd(II) adsorption.

Figure 4.13 shows the effect of HCIX-HFO dosage on Cd(II) adsorption at a pH of 4 in the presence of 3000 mg/L sulphate. Cd(II) adsorption increased rapidly from 0.01g to 0.04 g then gradually increased. It reached a point where any additional increase in dosage had no substantial change in the removal of Cd(II). This was unexpected because higher dosages should provide additional adsorption sites for Cd(II) adsorption. The lack of Cd(II) adsorption at higher dosages is mostly likely

due to the formation of ternary Cd-sulphate complexes (Hoins *et al.,* 1993) that are negatively charged and excluded from the resin matrix by electrostatic repulsion.
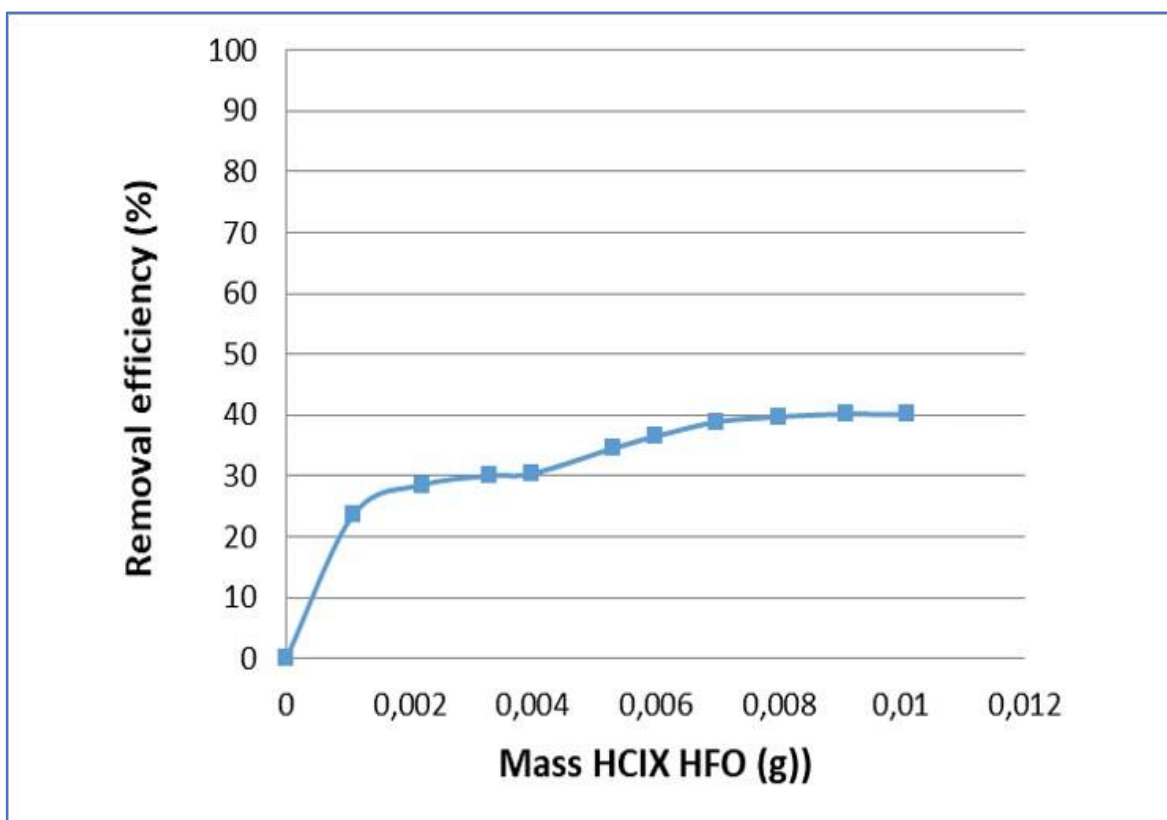
Figure 4.13: Percentage removal efficiency for Cd(II) with increasing HCIX-HFO dosage

4.2.2.4 Kinetic modelling of Cd(II) adsorption with HCIX-HFO in the presence of sulphate

The parameters obtained from fitting of the kinetic data to the linear first-pseudo-order and second-pseudo-order kinetic models given in Table 4.5. The data was a best fit to the pseudo-second order model. This was based on the correlation coefficient value and closeness of the experimentally determined capacity to the capacity calculated by the pseudo-second order model. This implied that the mechanism of adsorption is chemisorption (SenGupta, 2017). Similar observation was reported by Bai and Bartkiewicz (2009) where sulphonates were cation exchange resins were used to adsorb Cd(II). Wong (2014) also Cd(II) to follow the

pseudo-second order model when being adsorbed by cationic iminodiacetate exchange resin.

Table 4.5: Pseudo-first order and pseudo-second order modelling of Cd(II) adsorption by HCIX-HFO in the presence of sulphate.

Cd(II) (mg/L)	Sulphate (mg/L)	$q_{e.exp}$ (mg g^{-1})	Pseudo-first-order			Pseudo-second-order		
			K_1 (min^{-1})	$q_{e.cal}$ (mg g^{-1})	R^2	K_2 (g min^{-1}mg^{-1})	$q_{e.cal}$ (mg g^{-1})	R^2
1.00	3000	1.45	0.006	0.642	0.2249	0.016	1.647	0.9964

The fit of the Cd(II) kinetic data to the Intraparticle diffusion model is shown in Figure 4.14. The parameters obtained from the first linear region of the plot are given in Table 4.6. The adsorption of Cd(II) occurred in two stages. In the first stage, Cd(II) was diffusing into the pores of HCIX-HFO. The second stage was diffusion into the micropores and interaction of Cd(II) ions with the exchange sites within pores of HCIX-HFO. The BLT value is -0.0611 min$^{0.5}$ which shows that there was little contribution of surface adsorption onto HCIX-HFO. The value of the BLT is largely decreased by the high agitation rate employed in the current study. The rate of diffusion, K_{ID} was found to be 0.1282 mg.g^{-1}.min$^{0.5}$.
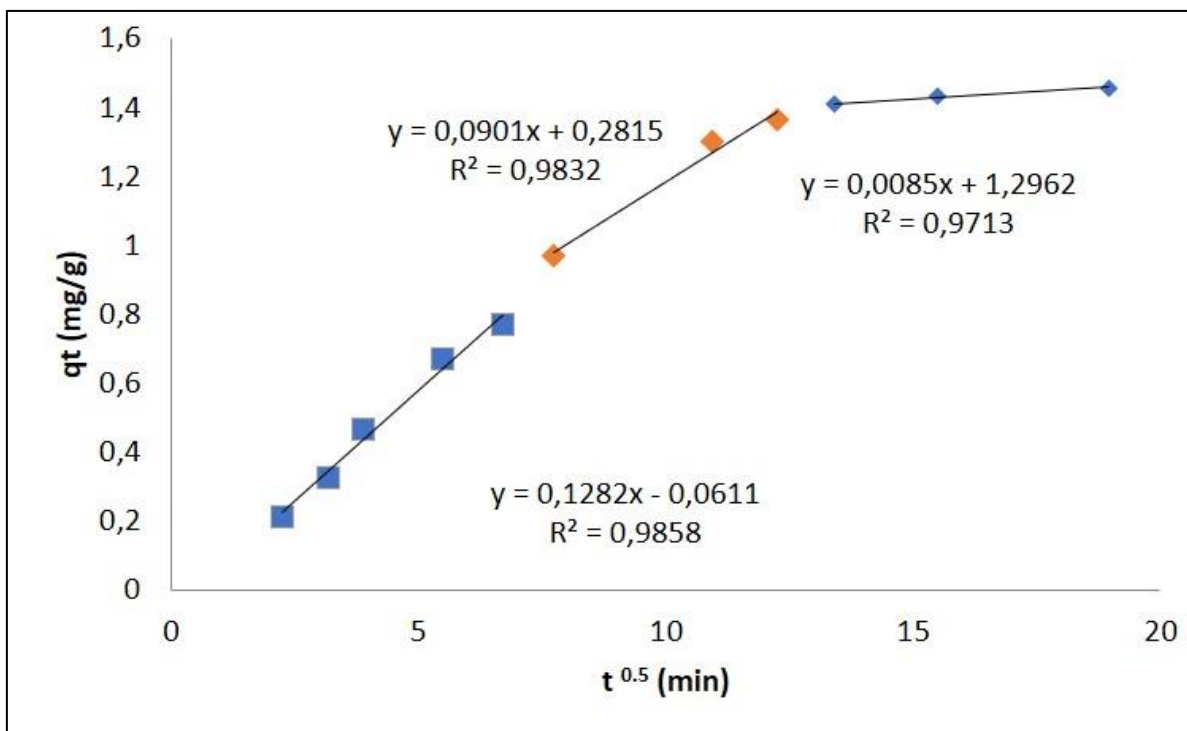
Figure 4.14: Fit of Cd(II) kinetic data to the Intraparticle diffusion model

Table 4.6: Intraparticle diffusion model for Cd(II) adsorption in the presence of sulphate.

Initial Cr(VI) mg/L	Initial sulphate mg/L	K_{ID} (mg g^{-1}.min$^{0.5}$)	BLT	R^2
1.00	3000	0.1282	-0.0611	0.9858

4.2.2.5 Isotherm modelling of Cd(II) adsorption in the presence of sulphate

The parameters obtained from fitting the experimental isotherm data for Cd(II) adsorption to the Langmuir, Freundlich and Temkin isotherm models are given Table 4.7. In this study, the Freundlich model had the highest correlation coefficient of 0.8472. The experimental capacity data was also plotted together with capacity data calculated using the parameters obtained from fitting the experimental data to each of the models (Figure 4.15). The models show that none of the models chosen were able to accurately predict the experimental data, however, the Freundlich and

Langmuir models were closest in predicting the experimental data. In addition, the n value obtained from the Freundlich model is 0.35. The n value is an indicator for favourability of adsorption (SenGupta, 2017). When the value of n is between 1 and 10 the adsorption is considered to be favourable (Bai and Bartkiewicz, 2009). The adsorption of Cd(II) with HCIX-HFO was found not to be favourable due to the n value being less than 1 (n = 0.35). This was also confirmed by the low adsorption capacity of Cd(II) by HCIX-HFO.

Table 4.7: Parameters for Freundlich, Langmuir and Temkin isotherm modelling of Cd(II) adsorption in presence of sulphate.

Initial Cd(II) (mg/L)	Sulphate (mg/L)	Freundlich			Langmuir			Temkin		
		K_f L g^{-1}	N	R^2	q_{max} mg/g	K_L L/mg	R^2	A L/g	B J/mol	R^2
1.00	3000	94	0.35	0.8472	-1.79	-2.0	0.8385	4.52	208	0.6472
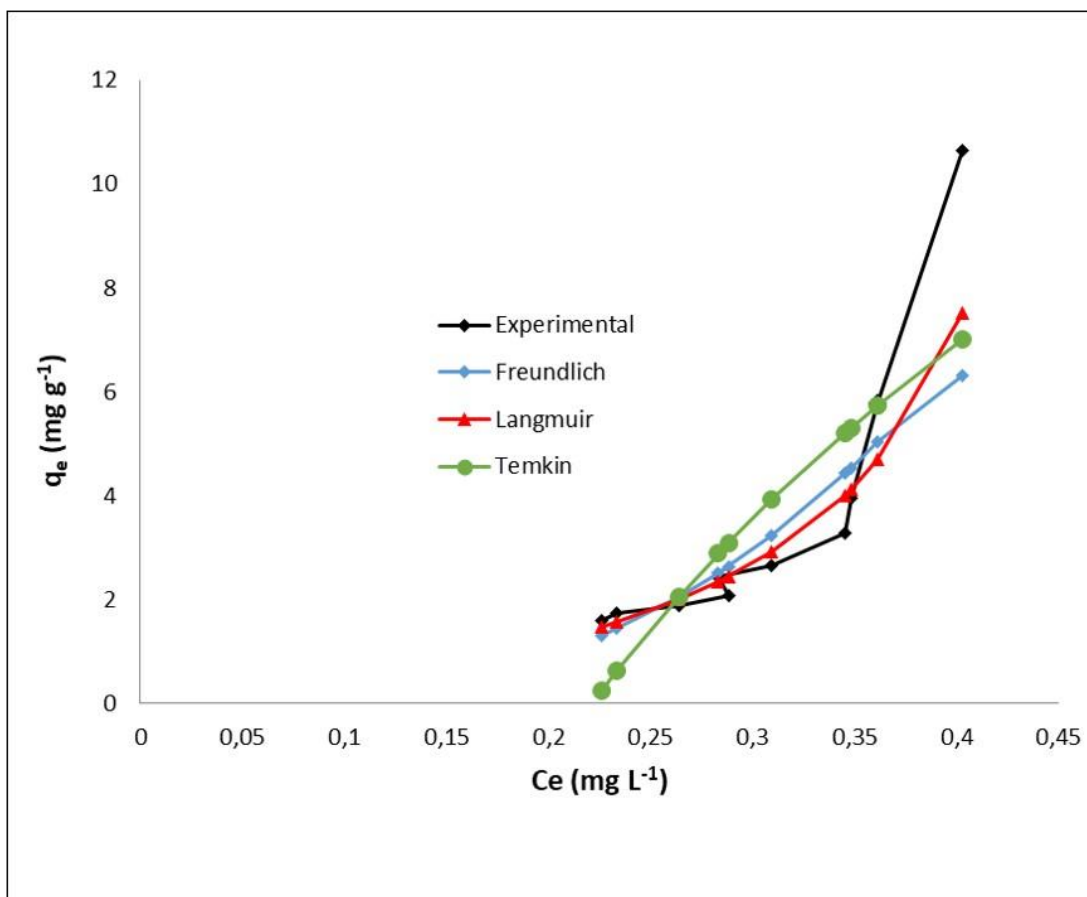
Figure 4.15: Comparison of modelled adsorption capacities and experimental data for Cd(II) adsorption in the presence of sulphate by HCIX-HFO

4.2.3   Adsorption studies for Pb(II) by HCIX-HFO

Only one report of the adsorption of Pb(II) by a hybrid iron cationic exchange resin has been found (Chanthapon *et al.,* 2018). Chanthapon used commercial cationic polystyrene based cation resins with sulfonic functional that had nano particle zero valent iron embedded in the polymer matrix. In this study a similar commercial cation exchange resin with embedded nanoparticle hydrated ferric oxide (HCIX-HFO) was used for Pb(II) adsorption together with a high sulphate concentration so as to mimic the conditions found in AMD.

4.2.3.1 Effect of pH on adsorption of Pb(II) with HCIX-HFO

The effect of pH on Pb(II) adsorption by HCIX-HFO is given in Figure 4.16. Adsorption increased as pH increased from 2 to 4, followed by a slight decrease at pH 5. These results concur with results reported by Ahmetli (2011) that show that Pb mostly exists as Pb(II) in acidic solution. The results indicate that Pb(II) adsorption is favoured in acidic solution. The decreased adsorption of Pb(II) at pH 5 is possibly due to hydroxylation of Pb(II) resulting in the formation of $Pb(OH)_2$ (Koushkbaghi et al., 2017). In a study by Chanthapon (2018) the adsorption of Cd(II) was conducted at pH of 5. In the current work, a pH 4 was chosen for further Pb(II) adsorption studies.
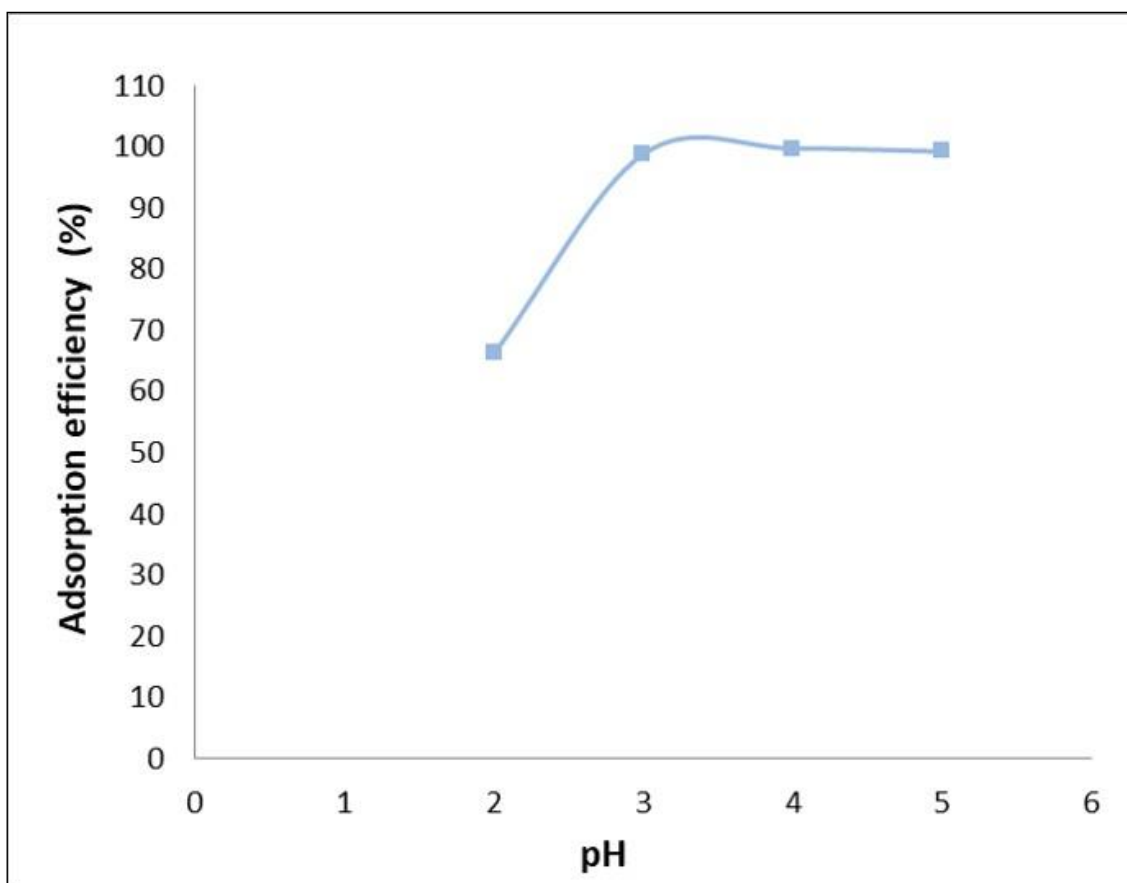
Figure 4.16: Effect of pH on percentage Pb(II) removal with HCIX-HFO.

4.2.3.2 Effect of contact time on adsorption of Pb(II) with HCIX-HFO

Figure 4.17 shows the relationship between Pb(II) removal and the contact time for HCIX-HFO. There was a rapid increase in percentage Pb(II) removed in the first 180 minutes. After 180 minutes the rate of adsorption slowed down significantly. Unfortunately, Chanthapon (2018) did not report kinetic data for Pb(II) adsorption by a zero valent iron cation exchanger. The equilibration time for Pb(II) adsorption of by a cation exchange resin was reported as 90 minutes (Demirbas *et al.,* 2005) contact time of 360 minutes was chosen for further studies
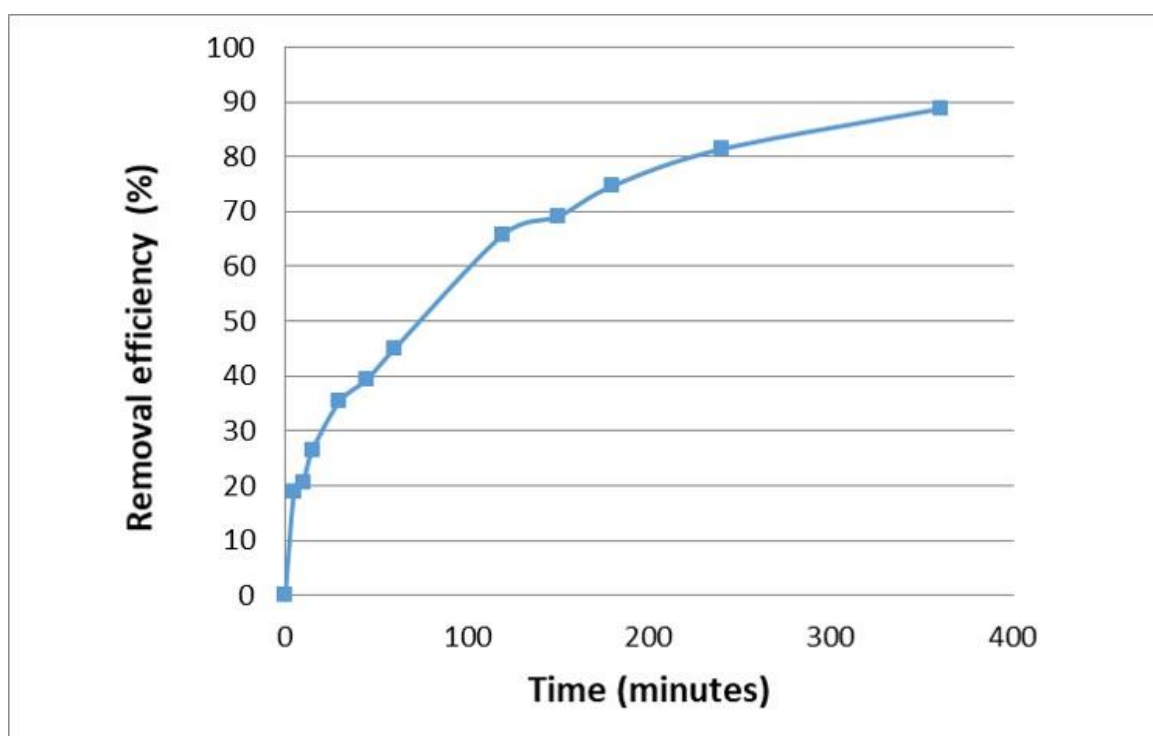
Figure 4.17: Effect of contact time on adsorption of Pb(II) with HCIX-HFO.

4.2.3.3 Effect of HCIX-HFO dosage on Pb(II) adsorption

The effect of HCIX-HFO dosage on Pb(II) adsorption at pH 4 in the presence of 3000 mg/L sulphate is given in Figure 4.18. Adsorption increased as mass of adsorbent increased until a plateau is reached at a mass of 0.003 g. The increase adsorption as mass increased from 0.001 g to 0.003 g was due to the additional adsorption sites. As the mass increases above 0.003 g approximately 90% of the

Pb(II) had been removed from solution. The remaining Pb(II) concentration was too low to provide a sufficient concentration gradient to maintain the diffusion of Pb(II) ions into the pores of the adsorbent. A similar trend for adsorbent dosage was also observed and discuss in some studies related to adsorption processes using ion exchange resins (Chanthapon *et al.,* 2018).

HCIX-HFO dosage on Pb(II) adsorption at pH 4 in the presence of 3000 mg/L sulphate is given in Figure 4.18. Adsorption increased as mass of adsorbent increased until a plateau is reached at a mass of 0.003 g. The increase adsorption as mass increased from 0.001 g to 0.003 g was due to the additional adsorption sites. As the mass increases above 0.003 g approximately 90% of the Pb(II) had been removed from solution. The remaining Pb(II) concentration was too low to provide a sufficient concentration gradient to maintain the diffusion of Pb(II) ions into the pores of the adsorbent. A similar trend for adsorbent dosage was also observed and discuss in some studies related to adsorption processes using ion exchange resins (Chanthapon *et al.,* 2018).

Figure 4.18: Effect of HCIX-HFO dosage on Pb(II) adsorption.

4.2.3.4 Kinetic modelling Pb(II) adsorption in the presence of sulphate by HCIX-HFO

The kinetic data for Pb(II) adsorption was fitted to the pseudo-first order and pseudo-second-order kinetic models (Table 4.8). The pseudo-second-order model was had the highest correlation coefficient (0.9773) and the calculated capacity (q_{e2}) value (2.54 mg.g^{-1}) closer to that of the experimentally determined value (2.27 mg.g^{-1}) than that of the pseudo-first order model (1.2 mg.g^{-1}). This implied that the adsorption kinetics for Pb(II) by HCIX-HFO occurred through chemisorption.

Table 4.8: Pseudo-first order and pseudo-second order kinetic modelling of Pb(II) adsorption in the presence of sulphate.

Pb(II) (mg/L)	Sulphate (mg/L)	$q_{e.exp}$ (mg.g^{-1})	Pseudo-first-order			Pseudo-second-order		
			K_1 (min^{-1})	$q_{e.cal}$ (mg.g^{-1})	R^2	K_2 (g min^{-1}mg^{-1})	$q_{e.cal}$ (mg.g^{-1})	R^2
1.00	3000	2.27	0.004	1.2	0.3749	0.0079	2.54	0.9773

The results from fitting the kinetic data for Pb(II) adsorption to the intraparticle diffusion model are given in Table 4.9. The data showed two distinct linear regions which show that diffusion of Pb(II) involved two stages (Figure 4.19). The first process was the stage in which Pb(II) diffuses through the pores of HCIX-HFO. In the second stage Pb(II) ions are being diffused into the micropores and interacting with the adsorption sites of HCIX-HFO. The BLT value was low (0.2606 min$^{0.5}$) indicating that surface adsorption had very little impact
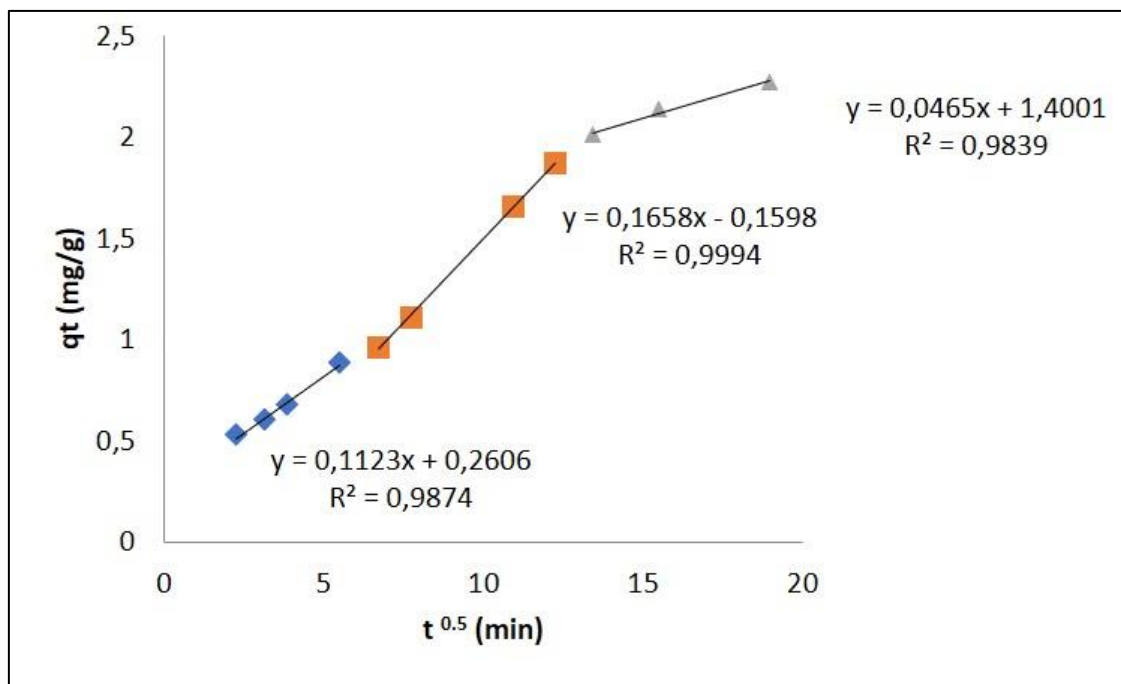
Figure 4.19: Fit of Pb(II) kinetic data to the Intraparticle diffusion model

Table 4.9: Intraparticle diffusion parameters for the adsorption of Pb(II) in the presence of sulphate

Initial Pb(II) Concentration (mg/L)	Initial sulphate concentration (mg/L)	K_{ID} (mg g^{-1}.min$^{0.5}$)	BLT (min$^{0.5}$)	R^2
1.00	3000	0.1123	0.2606	0.9874

4.2.3.5 Isotherm modelling of Pb(II) adsorption in the presence of sulphate by HCIX-HFO

The isotherm data for Pb(II) adsorption by HCIX-HFO obtained at a pH of 4 in the presence of sulphate was fitted to the Freundlich, Langmuir and Temkin isotherm models (Table 4.10). The Freundlich isotherm had the highest correlation coefficient. The obtained parameters from the Freundlich isotherm, K_f and n, were

graphically determined to be 17.6 L g^{-1}, and 1.73 respectively. The K_f value expresses the strength of adsorption. The n value gives the adsorption intensity or degree of favourability. When n is greater than 1 the adsorption is favourable. Based on the n value of 1.73, the adsorption of Pb(II) by HCIX-HFO was obtained to be favourable. A similar finding was reported by Chanthapon (2018) for a cationic exchanger that contained nanoparticulate zero valent iron.

The comparison between experimental determined adsorption capacities and those calculated by the Freundlich, Langmuir, Temkin isotherm models are shown in Figure 4.20. It was observed that the Freundlich model best represents the experimental data at low Pb(II) equilibrium concentrations and that at higher Pb(II) equilibrium concentrations the Langmuir model provides a better representation of the experimental data. One possible explanation for the observation was the hybrid, HCIX-HFO contains two types of adsorption sites. These are the fixed, sulfonate cation exchange sites of the host ion exchange resin and the ligand exchange sites of the embedded ferric oxide nanoparticles. The assumptions of the Langmuir model are that adsorption occurs through a monolayer, and that all adsorption sites are homogeneous in terms of their energy (Worch, 2015). At higher adsorbent dosages there were sufficient exchanges sites that are preferred by Pb(II) and there was no need for exchange onto the less preferred site. At lower concentrations there were insufficient preferred exchange sites and both types of sites were utilized by Pb(II). This corresponded to adsorption by sites that have heterogeneous energies and would therefore be described by the Freundlich model.

Table 4.10: Modelled Freundlich, Langmuir and Temkin isotherm parameters for the Pb(II) adsorption with HCIX-HFO in presence of sulphate.

Initial Cd(II) (mg/L)	Sulphate (mg/L)	Freundlich			Langmuir			Temkin		
		K_f L g^{-1}	n	R^2	q_{max} mg/g	K_L L/mg	R^2	A L/g	B J/mol	R^2
1.00	3000	17.6	1.73	0.8801	13.76	6.86	0.5158	152	1305	0.7261
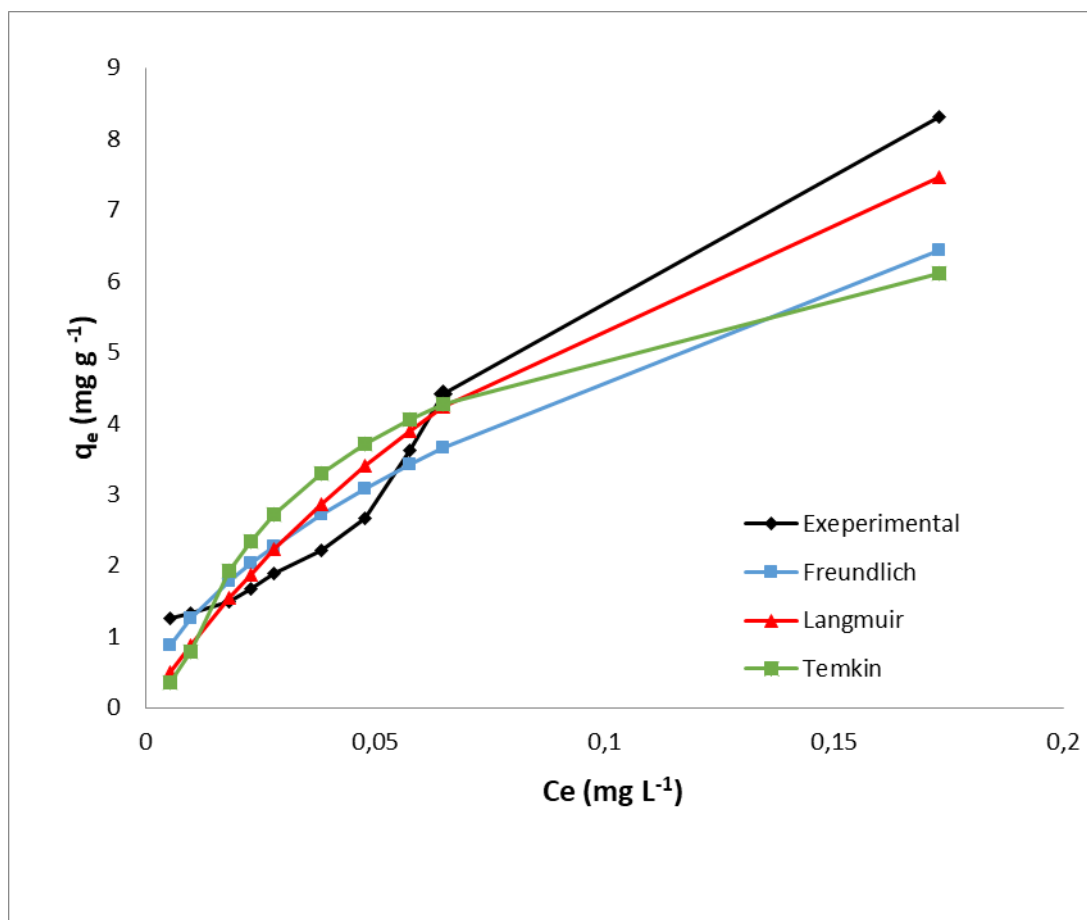
Figure 4.20: Comparison of experimentally determined adsorption capacities with adsorption capacities calculated from the Langmuir, Freundlich and Temkin isotherm models.

4.2.3.6 Competitive adsorption of Cd(II) and Pb(II) from a binary solution by HCIX-HFO

As Cd(II) and Pb(II) are likely to co-exist in AMD together with high concentrations of sulphate, batch adsorption studies at pH of 4 were done to determine the competitive adsorption of Cd(II) and Pb(II) sulphate is present. From the previous findings (Section 4.2.1 and 4.2.2), it was expected that Cd(II) would have a small impact on Pb(II) adsorption. The competitive adsorption capacities are given in Table 4.11.

The percentage of Pb(II) adsorbed (99.67%) higher than that of Cd(II) (30.54%). It was clear from the high percentage removal of Pb(II) that the presence of Cd(II) has

no effect on the adsorption of Pb(II). Also, the competitive adsorption capacities were similar to those obtained for both Pb(II) and Cd(II) alone. Based on the limited studies done, the implication was that either there was no selective adsorption for the metals or, more likely, the metals preferentially adsorb onto one of the two adsorption sites within HCIX-HFO. Macanás (2011) reported that ions with the same charge, but with a smaller ionic radius, are more strongly bound to cation exchange resins. The ionic radius changes in the order of Ni(II) <Cu(II) <Zn(II) <Cd(II) <Pb(II). The suggestion being that Cd(II) preferentially binds to the cationic exchanges sites of the parent resin rather than the ligand exchange site of the HFO.

HCIX-HFO showed a higher affinity for Pb(II) which may be due to Lewis acid interactions that result to the formation of stable innersphere complexes with HFO (Chanthapon et al., 2018).

Table 4.11: Percentage removal of Cd and Pb with HCIX-HFO.

Metal	Mean removal efficiency(%)	Adsorption capacity q_e (mg g^{-1})
Pb	99.67 (±0.032)	2.5 (±0.011)
Cd	30.54 (±0.029)	1.54 (±0.05)

4.2.3.7 Regeneration of HCIX-HFO exhausted with Cd(II) and Pb(II).

The manufacturer of the cation exchange resin used for the synthesis of HCIX-HFO recommends that NaCl, HCl or H_2SO_4 be used to regenerate the resin after adsorption. On the other hand, Kunaschk (2015) has reported the regeneration of HFO using NaOH. Regeneration of the cation exchange matrix will return the sulfonate exchange sites back to the Na$^+$ form. The use of HCl or H_2SO_4 will return the exchange sites to the H$^+$ form. Regeneration of HFO with NaOH will result in the hydroxyl groups replacing the species adsorbed on HFO. HCIX-HFO that had been exhausted with a binary Cd(II) and Pb(II) solution was regenerated using 1M NaCl

and 2 M NaOH in two separate steps. It was expected that the use of different regenerating solutions would help elucidate which type of adsorption site was responsible for the respective adsorption of Pb(II) and Cd(II).

Table 4.12 gives the percentage recovery of Pb(II) and Cd(II) after regenerating with NaCl and NaOH. Only NaCl resulted in the recovery of Cd(II) and Pb(II). As the percentage recovery for both metal ions were close to 100%, giving a confidence that both metals were adsorbed on to the same adsorption sites, that is the sulfonate ion exchange site and not the HFO sites. The percentage recovery of Cd(II) was slightly higher than that of Pb(II) due to their lower affinity for the exchange sites and being desorbed by NaCl easily. It was unexpected that NaOH did not desorb any metals. Even if the OH$^-$ group was prevented from diffusing into the HCIX-HFO beads by Donnan exclusion (Sengupta, 2017) it would be expected that the Na$^+$ would be able to regenerate the sulfonate exchange sites.

Table 4.12: Percentage Cd(II) and Pb(II) desorbed from HCIX-HFO during regeneration.

Metal	% recovery with NaCl	% recovery with NaOH
Cd	99.9 (±0.062)	0
Pb	98.8 (±0.383)	0

4.2.3.8 Adsorption of metal ions from real AMD by HCIX-HFO

AMD was obtained from the Western region of the Witwatersrand mining basin. The sample was characterised in terms of pH and concentration of metal ions (Table 4.13). The sample was found to be highly acidic with a pH of 2.62 which was below the optimal pH for Cd(II) and Pb(II) adsorption as determined previously (4.2.1.1 and 4.2.2.1 respectively).

Table 4.13: Characteristics of AMD sample from western basin of Witwatersrand mining region.

Metal	Mean concentration of metal in AMD before adsorption (mg/L)
Cd	$0.021(\pm1.21\times10^{-6})$
Co	$3.147(\pm0.027)$
Cr	$0.188(\pm4.22\times10^{-6})$
Cu	$1.4206(\pm3.59\times10^{-5})$
Fe	$0.9095(\pm0.0002)$
Ni	$16.1(\pm0.052)$
Pb	$0.031\ (\pm2.85\times10^{-6})$
Ti	$20.53\ (\pm1.75)$
Zn	$14.7\ (\pm0.055)$
Mg	$31.2\ (\pm0.041)$

After contacting 0.005 g of HCIX-HFO with 25 mL of AMD sample for 360 minutes, the concentrations of the metal ions remaining in solution were determined by ICP-OES (Table 4.14).

Among the present metals in AMD, only Cu, Ni and Pb were adsorbed. The concentration of the other metals remained unchanged. HCIX-HFO showed a maximum percentage removal for Cu(II) and Ni(II)of 7.5 and 7.4% respectively. The percentage removal of Pb(II) was 45.98%.

Table 4.14: Adsorption of metal ions from real AMD sample.

Metal	Raw AMD (mg/L)	AMD after adsorption (mg/L)	Removal (%)	Adsorption capacity mg/g
Cu	$1.4206(\pm 3.59 \times 10^{-5})$	$0.1065 (\pm 7.58 \times 10^{-6})$	$7.5 (\pm 0.194)$	$0.5220(\pm 0.0135)$
Ni	$16.1(\pm 0.052)$	$1.1916 (\pm 3.33 \times 10^{-5})$	$7.4(\pm 0.036)$	$5.86(\pm 0.0283)$
Pb	$0.031 (\pm 2.85 \times 10^{-6})$	$0.0165 (\pm 1.23 \times 10^{-11})$	$45.98(\pm 0.011)$	$0.069(\pm 1.72 \times 10^{-5})$

4.2.4   References

Acelas NY, Martin BD, López D, Jefferson B, 2015, Selective removal of phosphate from wastewater using hydrated metal oxides dispersed within anionic exchange media, Chemosphere, 119: 1353-1360.

Ahmetli, G., Yel, E., Deveci, H., Bravo, Y. and Bravo, Z., 2012. Investigation of Pb (II) adsorption onto natural and synthetic polymers. Journal of Applied Polymer Science, 125(1), pp.716-724.

Ayawei, N., Ebelegi, A.N., Wankasi, D., 2017, Modelling and Interpretation of Adsorption Isotherm., Hindawi Journal of Chemistry., https://doi.org/10.1155/2017/3039817.

Balasubramanian, S. and Pugalenthi, V., 1999. Determination of total chromium in tannery wastewater by inductively coupled plasma-atomic emission spectrometry, flame atomic absorption spectrometry and UV–visible spectrophotometric methods. Talanta, 50(3), pp.457-467.

Bai, Y. and Bartkiewicz, B., 2009. Removal of Cadmium from Wastewater Using Ion Exchange Resin Amberjet 1200H Columns. Polish Journal of Environmental Studies, 18(6).

Blaney, L.M., Cinar, S. and SenGupta, A.K., 2007. Hybrid anion exchanger for trace phosphate removal from water and wastewater. Water research, 41(7), pp.1603-1613.

Chanthapon, N., Sarkar, S., Kidkhunthod, P. and Padungthon, S., 2018. Lead removal by a reusable gel cation exchange resin containing nano-scale zero valent iron. Chemical Engineering Journal, 331, pp.545-555.

Chattopadhyaya, M.C., Soares, M.G., Campos, M.T.D.J.S., Ismadji, S., Lofrano, G., Barakat, M.A., Ikehata, K., Yin, X.B., Chowdhury, P., Sharma, S.K. and Carotenuto, M., 2014. Heavy metals in water: presence, removal and safety. Royal Society of Chemistry.

Cornell, R.M. and Schwertmann, U., 2003. The iron oxides: structure, properties, reactions, occurrences and uses. John Wiley & Sons.

Das, S. and Hendry, M.J., 2011, Application of Raman spectroscopy to identify iron minerals commonly found in mine wastes., Chemical Geology, 290 (3-4), pp. 101-108.

Dada, A.O., Olalekan, A.P., Olatunya, A.M. and Dada, O.J.I.J.C., 2012. Langmuir, Freundlich, Temkin and Dubinin–Radushkevich isotherms studies of equilibrium sorption of Zn2+ unto phosphoric acid modified rice husk. IOSR Journal of Applied Chemistry, 3(1), pp.38-45.

De Kock, L.A., 2015, Hybrid ion exchanger supported metal hydroxides for the removal of phosphate from wastewater. PhD (Chemistry).[Unpublished]: University of Johannesburg. Retrieved from: https://ujdigispace.uj.ac.za. (Accessed: 07/09/2017)

Demirbas, A., Pehlivan, E., Gode, F., Altun, T. and Arslan, G., 2005. Adsorption of Cu (II), Zn (II), Ni (II), Pb (II), and Cd (II) from aqueous solution on Amberlite IR-120 synthetic resin. Journal of Colloid and Interface Science, 282(1), pp.20-25.

Department of Water Affairs (DWA), 2013: Feasibility Study for a Long-term Solution to address the Acid Mine Drainage associated with the East, Central and West Rand underground mining basins. Study Report No. 5.4: Treatment Technology Options –DWA Report No.: P RSA 000/00/16512/4

Fei, W., Wang, L.J., Li, J.S., Sun, X.Y. and Han, W.Q., 2009. Adsorption behavior and mechanism of cadmium on strong-acid cation exchange resin. Transactions of Nonferrous Metals Society of China, 19(3), pp.740-744.

Hanesch, M., 2009. Raman spectroscopy of iron oxides and (oxy) hydroxides at low laser power and possible applications in environmental magnetic studies. Geophysical Journal International, 177(3), pp.941-948.

Ho, Y.S. and McKay, G., 1999. Pseudo-second order model for sorption processes. Process biochemistry, 34(5), pp.451-465.

Hoins, U., Charlet, L., Sticher, H., 1993, Ligand effect on the adsorption of heavy metals: The sulphate-Cadmium-Goethite case. Water, Air, and Soil Pollution, 68, (1-2), pp. 241-255.

Hua, M., Yang, B., Shan, C., Zhang, W., He, S., Lv, L. and Pan, B., 2017. Simultaneous removal of As (V) and Cr (VI) from water by macroporous anion exchanger supported nanoscale hydrous ferric oxide composite. Chemosphere, 171, pp.126-133.

Kołodyńska, D., Kowalczyk, M., Hubicki, Z., Shvets, V., Golub, V., 2015, Effect of accompanying ions and ethylenediaminedisuccinic acid on heavy metals sorption using hybrid materials Lewatit FO36 and Purolite Arsen X. Chemical Engineering Journal, 276, pp. 376-387.

Kowalczyk M., Hubicki Z., Kołodyńska D., 2013. Modern hybrid sorbents – New ways of heavy metal removal from waters. Chemical Engineering and Processing: Process Intensification. 70, pp. 55-56.

Koushkbaghi, Shahnaz, Amirabbas Zakialamdari, Mohammad Pishnamazi, Hossein Fasih Ramandi, Majid Aliabadi, and Mohammad Irani. "Aminated-Fe3O4 nanoparticles filled chitosan/PVA/PES dual layers nanofibrous membrane for the removal of Cr (VI) and Pb (II) ions from aqueous solutions in adsorption and membrane processes." Chemical Engineering Journal 337 (2018): 169-182.

Kunaschk, M., Schmalz, V., Dietrich, N., Dittmar, T., Worch, E., 2015. Novel regeneration method for phosphate loaded granular ferric (hydr)oxide – A contribution to phosphorous recycling. Water Research, 71, pp. 219-226.

Macanás, J., Ruiz, P., Alonso, A., Muñoz, M. and Muraviev, D.N., 2011. Ion-exchange assisted synthesis of polymer-stabilized metal nanoparticles. Solvent Extraction and Ion Exchange: A Series of Advances, 20.

Mislin, H., O. Ravera, O., (Eds.),Cadmium in the Environment, Birkhäuser Verlag, Basel (1986), pp. 28-40

Pehlivan, E. and Altun, T., 2006, The study of various parameters affecting the ion exchange of Cu^{2+}, Zn^{2+}, Ni^{2+}, Cd^{2+}, and Pb^{2+} from aqueous solution on Dowex 50W synthetic resin. Journal of Hazardous Materials, 134(1-3), pp. 149-156.Aya

Polowczyk, I., Urbano, B.F., Rivas, B.L., Bryjak, M. and Kabay, N., 2016. Equilibrium and kinetic study of chromium sorption on resins with quaternary ammonium and N-methyl-D-glucamine groups. Chemical Engineering Journal, 284, pp.395-404.

SenGupta, A.K., 2017. Ion Exchange in Environmental Processes: Fundamentals, Applications and Sustainable Technology. John Wiley & Sons.

Streat, M., Hellgardt, K. and Newton, N.L.R., 2008. Hydrous ferric oxide as an adsorbent in water treatment: Part 3: Batch and mini-column adsorption of arsenic, phosphorus, fluorine and cadmium ions. Process safety and environmental protection, 86(1), pp.21-30.

Wong, C.W., Barford, J.P., Chen, G. and McKay, G., 2014. Kinetics and equilibrium studies for the removal of cadmium ions by ion exchange resin. Journal of Environmental Chemical Engineering, 2(1), pp.698-707.

Worch, E., 2012. Adsorption technology in water treatment: fundamentals, processes, and modeling. Walter de Gruyter.

Xiao, K., Xu, F., Jiang, L., Duan, N. and Zheng, S., 2016. Resin oxidization phenomenon and its influence factor during chromium (VI) removal from wastewater using gel-type anion exchangers. Chemical Engineering Journal, 283, pp.1349-1356.

CHAPTER 5

CONCLUSIONS AND RECOMMENDATIONS

This chapter summarizes the findings of the study. It also provides recommendations for future work.

5.1   Conclusions

HAIX-HFO and HCIX-HFO were synthesized using an *in-situ* method whereby the HFO nanoparticles were formed inside the pores of commercially available anionic (Amberlite IRA 400) and cationic (IMAC HP1110) exchange resins respectively. Characterization of the hybrid resins by SEM showed that the HFO nanoparticles were uniformly distributed throughout the interior of the resin beads. For both HAIX-HFO and HCIX-HFO the HFO nanoparticles appeared as white discrete particles that showed very little agglomeration. EDS spectra confirmed that Fe was present in the interior of the beads. From EDS, the weight percentage of Fe in HAIX-HFO was 4.4%, while in HCIX-HFO it was 14.9%. The difference in the amount of Fe incorporated into the anionic and cationic resins can be attributed to the differences in the fixed functional exchange groups of the resins which resulted in more Fe being incorporated into the cationic exchange resin beads. Raman spectroscopy was used to tentatively assign the iron compound as ferrihydrite based on the peaks at 511 cm^{-1} (HCIX-HFO) and 720 cm^{-1} (HAIX-HFO). A significant amount of fluorescence was observed in both spectra which was attributed to the organic matrix of the ion exchange resins. This fluorescence made a more definitive determination difficult.

HAIX-HFO was used for the adsorption of Cr(VI). The adsorption of Cr(VI) was carried out from pH 2 to 5. At pH 2, 89% of the Cr(VI) was removed from solution. This increased to 99% at pH 4. The adsorption of Cr(VI) decreased as the pH increased, with only 77% Cr(VI) being removed at pH. All further studies were conducted at an initial pH of 4. Sulphate as a co-competitor ion had a significant impact on the adsorption of Cr(VI). Cr(VI) adsorption decreased as the concentration of sulphate increased from 0 mg/L to 1000 mg/L (39.2% decrease).

101

As the sulphate concentration increased from 1000 mg/L to 3000 mg/L, the impact on Cr(VI) adsorption lessened considerably. Thus, it can be concluded that Cr(VI) is selectively adsorbed by HAIX-HFO even in the presence of very high sulphate concentrations. This was attributed to the presence of two different types of adsorption sites, fixed quaternary ammonium ion exchange sites of the resin and hydrated ferric oxide ligand exchange sites, that preferentially adsorb either Cr(VI) or sulphate by two different adsorption mechanisms.

The adsorption of Cr(VI) with and without sulphate (3000 mg/L) was found to follow the pseudo-second order which implies that the adsorption of Cr(VI) was by chemisorption with sharing or exchange of valence electrons for both cases. The best fitting kinetic model was determined on the basis of the R^2 value as well as the closeness of the experimentally determined capacity (q_e) to the capacity calculated by the pseudo-first order and pseudo-second order models. The experimentally determined equilibrium capacity for Cr(VI) was 4.91 mg.g^{-1} and the capacity from the pseudo-second order model was 5.79 mg.g^{-1}. For the adsorption of Cr(VI) in the presence of sulphate the closeness of the experimentally determined q_e value (2.22 mg.g^{-1}) was an even better fit to that predicted by the pseudo-second order model ($q_{e2\ cal}$ = 2.47 mg.g^{-1}) The isotherm models that best fitted the adsorption differed depending whether sulphate was present as a co-competing ion or not. Fitting of the kinetic data to the Intra-particle Diffusion model showed that intra-particle diffusion was the rate limiting mass transfer mechanism. In addition the intra-particle diffusion rate constant (K_{ID}) was significantly smaller when sulphate was present as a co-competing ion (Cr(VI): K_{ID} = 0.4323 mg.g^{-1}.min$^{0.5}$; Cr(VI)/SO$_4^{2-}$: K_{ID} = 0.1524 mg.g^{-1}.min$^{0.5}$). Thus, the presence of sulphate significantly slowed down the diffusion of Cr(VI) into the pores of the hybrid resin.

The adsorption of Cr(VI) without sulphate was best described by the Langmuir isotherm with a calculate capacity, $q_{e.cal,}$ of 25.1 mg.g^{-1}. Calculation of R_L from the Langmuir constant, K_L, showed that the adsorption of Cr(VI) in the absence of sulphate was favourable (R_L = 0.0467). In the presence of sulphate, the adsorption of Cr(VI) was found to be best described by the Temkin isotherm model.

Adsorption of Pb(II) and Cd(II) by HCIX-HFO was investigated. For both Pb(II) and Cd(II) maximum adsorption occurred at a pH of 4 in the absence of sulphate. The kinetics of Pb(II) and Cd(II) adsorption was investigate with sulphate present in solution at a concentration of 3000 mg/L. Both Pb(II) and Cd(II) was best described by pseudo-second order kinetics, which implied that the mechanism of adsorption was chemisorption. The experimentally determined capacity for Cd(II) adsorption was found to be 1.45 mg.g^{-1}. The experimentally calculated capacity for Pb(II) was 2.27 mg.g^{-1}. For both Pb(II) and Cd(II), the mass transport mechanism was found to be Intra-particle diffusion with similar intra-particle diffusion rate constants. The adsorption of Pb(II) was best described by the Freundlich isotherm model and with n = 1.73 which means that the adsorption was favourable. For Cd(II) both the Freundlich and Langmuir models were a good fit for the data. The n value from the Freundlich model was 0.35 which implies that HCIX-HFO was not a good adsorbent for Cd(II).

For the competitive adsorption study with Pb(II) and Cd(II) it was found that HCIX-HFO had a higher adsorption capacity for Pb(II) (2.5 mg.g^{-1}) than Cd(II) (1.54 mg.g^{-1}).

The HCIX-HFO ion exchange resin that was exhausted with Pb(II) and Cd(II) was regenerated with NaCl and NaOH. Regeneration with NaCl was successful with 99.9% and 98.8% of Cd(II) and Pb(II) being desorbed. NaOH did not desorb either of the metal ions. Adsorption of metals from a real AMD sample was conducted. The AMD sample was characterized for pH and metal identity and concentration prior to the adsorption study with HCIX-HFO. Of the 10 metals identified within the AMD sample, only Pb(II), Ni(II) and Cu(II) were adsorbed with capacities of 46.8%, 92.6% and 92.5% respectively. In conclusion, HCIX-HFO can be used to adsorb metals from real AMD, with Ni(II) and Cu(II) being preferentially adsorbed.

5.2   Recommendation for future work

- Further characterization of the prepared hybrid ion exchange material for the remediation of AMD needs to be done. These include XRD, XPS and FTIR. This would enable further characterization of the HFO nanoparticles and elucidate interactions between the resin matrix and HFO as well as between HFO, resin matrix and adsorbed metal ions.

- Regeneration of the HAIX-HFO exhausted with Cr(VI) and sulphate in order to determine at which sites Cr(VI) and sulphate are adsorbed.

- Determine isotherm and kinetic models that describe the adsorption of sulphate by HAIX-HFO.

- Carry out selectivity studies for Ni and Cu adsorption by HCIX-HFO.

- Expand the desorption studies for HCIX-HFO including regeneration-adsorption cycles to evaluate the reusability of the hybrid resin.

- The extension of the application of the synthesized material to other pollutant water with high metals such as Pb(II) concentration is highly recommended.

- Simulation, modelling and design of prototype for the adsorption processes.

- Investigation of the efficiency of the resin for continuous processes by carrying out fixed bed pilot scale studies for metal ion adsorption from AMD from different sources.

- Conduct a cost benefit analysis based on the results from the continuous fixed bed processes.